BRNO UNIVERSITY OF TECHNOLOGY

VYSOKÉ UČENÍ TECHNICKÉ V BRNĚ

FACULTY OF CHEMISTRY

FAKULTA CHEMICKÁ

INSTITUTE OF MATERIALS SCIENCE

ÚSTAV CHEMIE MATERIÁLŮ

POLY(3-HYDROXYBUTYRATE) BASED MATERIALS FOR 3D PRINTING IN MEDICAL APPLICATIONS

MATERIÁLY NA BÁZI P3HB PRO 3D TISK MEDICÍNSKÝCH APLIKACÍ

MASTER'S THESIS

DIPLOMOVÁ PRÁCE

AUTHOR

AUTOR PRÁCE

Bc. Štěpán Krobot

SUPERVISOR

VEDOUCÍ PRÁCE

Mgr. Radek Přikryl, Ph.D.

BRNO 2022

BRNO UNIVERSITY OF TECHNOLOGY
FACULTY OF CHEMISTRY

Assignment Master's Thesis

Project no.:	FCH-DIP1750/2021	Academic year: 2021/22
Department:	Institute of Materials Science	
Student:	**Bc. Štěpán Krobot**	
Study programme:	Chemistry, Technology and Properties of Materials	
Study field:	Chemistry, Technology and Properties of Materials	
Head of thesis:	**Mgr. Radek Přikryl, Ph.D.**	

Title of Master's Thesis:

Poly(3–hydroxybutyrate) based materials for 3D printing in medical applications

Master's Thesis:

The aims of this work are following. To do a research on 3D printing of polymeric materials used for bone tissue replacement. Design and preparation of FDM 3D printing filaments from composite materials. Characterisation of surface tension, mechanical and thermal properties of such materials. Optimisation of surface properties of printed specimen with respect to roughness in order to achieve optimal cell response, adhesion and proliferation. Arrangement of biological testing and its evaluation.

Deadline for Master's Thesis delivery: 13.5.2022:

Master's Thesis should be submitted to the institute's secretariat in a number of copies as set by the dean This specification is part of Master's Thesis

Bc. Štěpán Krobot student	Mgr. Radek Přikryl, Ph.D. Head of thesis	doc. Ing. František Šoukal, Ph.D. Head of department

In Brno dated 1.2.2022

prof. Ing. Michal Veselý, CSc.
Dean

ABSTRACT

This master's thesis deals with the preparation and testing of 3D printed scaffolds for bone tissue engineering. The aim of the thesis is laboratory preparation of polymer blends on the basis of poly(3-hydroxybutyrate), poly(lactic acid) and polycaprolactone and their processing into the form of 3D printing filaments. Three polymeric blends were prepared and processed into the form of 3D printing filaments. Differential scanning calorimetry was conducted to evaluate the thermal properties, followed by temperature tower test and warping test to determine the processing conditions for 3D printing. The lowest warping coefficient was 1.26 for a blend of poly(3-hydroxybutyrate) with polycaprolactone and plasticizer. Tensile test, three-point flexural test and compression test were used to study the mechanical properties of materials. Scaffolds with different surfaces for bone tissue engineering were 3D printed from prepared filaments to determine the most optimal surface for cell proliferation. To determine the surface properties and their influence on cell adhesion, optical contact angle measurement with the use of OWRK method to calculate surface energy was conducted. 3D printed surfaces were also subjected to roughness analysis by confocal microscopy to determine their roughness and its effect on contact angle with water and cell growth. Finally, in the last part, in vitro tests on scaffolds were conducted in collaboration with the Institute of Experimental Medicine (Czech Academy of Sciences) to find out whether the prepared materials are non-cytotoxic and how the surface of scaffold affects the cell growth and proliferation. In the end, two out of three materials were proven to be non-cytotoxic (both blends of poly(3-hydroxybutyrate) with polycaprolactone) and that their mechanical properties were comparable with human trabecular bone. The most optimal surface for cell growth is probably grid diameter 50 μm with roughness along the perimeter 1.9 μm, which corresponds with water contact angle 74.1°.

ABSTRAKT

Tato diplomová práce se zabývá přípravou a testováním 3D tištěných skafoldů pro kostní tkáňové inženýrství. Cílem práce je laboratorní příprava polymerních směsí na bázi poly(3-hydroxybutyrátu), polymléčné kyseliny a polykaprolaktonu a jejich zpracování do podoby 3D tiskových strun. Byly připraveny tři polymerní směsi, které byly zpracovány do podoby 3D tiskových strun. Pro vyhodnocení termických vlastností byla provedena diferenciální skenovací kalorimetrie, následně teplotní věžový test a test „warpingu“ pro stanovení zpracovatelských podmínek při 3D tisku. Nejnižší naměřený „warping“ koeficient byl 1,26 u směsi poly(3-hydroxybutyrátu) s polykaprolaktonem a změkčovadlem. Ke studiu mechanických vlastností materiálů byla použita tahová zkouška, tříbodová ohybová zkouška a tlaková zkouška. Skafoldy s různými povrchy pro kostní tkáňové inženýrství byly 3D tisknuty z připravených strun s cílem určit nejoptimálnější povrch pro proliferaci buněk. Pro stanovení povrchových vlastností a jejich vlivu na adhezi buněk bylo provedeno měření optického kontaktního úhlu s využitím metody OWRK pro výpočet povrchové energie. 3D vytištěné povrchy byly také podrobeny analýze drsnosti pomocí konfokálního mikroskopu, aby byla určena jejich drsnost a její vliv na kontaktní úhel s vodou a růst buněk. Nakonec v poslední části byly ve spolupráci s Ústavem experimentální medicíny AV ČR provedeny in vitro testy na skafoldech s cílem zjistit, zda jsou připravené materiály necytotoxické, a jak povrch skafoldu ovlivňuje růst a proliferaci buněk. Bylo zjištěno, že dva ze tří materiálů nejsou cytotoxické (obě směsi poly(3-hydroxybutyrátu) s polykaprolaktonem) a že jejich mechanické vlastnosti jsou srovnatelné s lidskou trabekulární kostí. Nejoptimálnějším povrchem pro růst buněk je pravděpodobně mřížka o průměru 50 μm s drsností podél perimetru 1,9 μm, což odpovídá kontaktnímu úhlu s vodou 74,1°.

KEYWORDS

3D printing, FDM, poly(3-hydroxybutyrate), biocompatibility, tissue engineering, scaffolds

KLÍČOVÁ SLOVA

3D tisk, FDM, poly(3-hydroxybutyrát), biokompatibilita, tkáňové inženýrství, skafoldy

BIBLIOGRAPHIC CITATION

KROBOT, Štěpán. *Materiály na bázi P3HB pro 3D tisk medicínských aplikací* [online]. Brno, 2022 [cit. 2022-05-10]. Dostupné také z: https://www.vutbr.cz/studenti/zav-prace/detail/137436. Diplomová práce. Vysoké učení technické v Brně, Fakulta chemická, Ústav chemie materiálů. Vedoucí práce Radek Přikryl.

ACKNOWLEDGEMENTS

At this point I would like to thank especially my supervisor Mgr. Radek Přikryl, Ph.D. for all the advice provided regarding the preparation of this thesis and also for his help and willingness to consult all my questions. Furthermore, I would like to thank Ing. Veronika Melčová for all the advice and consultation, help with the evaluation of the results and practical training on many laboratory instruments. Without her help and never-ending support not even a half of this thesis would see the light of day. I would also like to thank Ing. Přemysl Menčík Ph.D. for practical training on the 3D printer and help with the preparation of files for 3D printing, their optimization and for continuous supply of beverage stimulants, which were essential to keep me vigilant and productive for the time necessary to complete this thesis, and to Mgr. Michala Rampichová, Ph.D. from the Department of Tissue Engineering (Institute of Experimental Medicine, Czech Academy of Sciences) for willingness to perform biological tests necessary for the elaboration of this work. However, gratitude is due to the whole team of the End-of-life laboratory and not only to the three members mentioned above, for their warm approach and for creating great working conditions where it was a pleasure to work with them. Last but not least, of course, I thank my family for their helpfulness, dedication, understanding, and above all, for the necessary time and peace of mind they afforded me to produce this thesis.

DECLARATION OF AUTHENTICITY

I declare that I have prepared the master's thesis independently, under the supervision of Mgr. Radek Přikryl, Ph.D. I also declare that all the sources of visual information and literary sources from which I have drawn are duly cited in the list of sources. The master's thesis is the property of the Faculty of Chemistry, Brno University of Technology. It can be used for commercial purposes only with the consent of the thesis supervisor and the dean of the Faculty of Chemistry of the Brno University of Technology.

……

Author's signature

CONTENTS

1 INTRODUCTION

In recent years, a great attention concerning bioplastics and especially those which are also biodegradable has been established. Intensive research has been carried out around the field of biodegradable materials, as they possess many properties, which they can provide us and which we can benefit from in our daily lives.

Over the past few decades, concerns about the state of the environment, climate change and limited fossil resources have led to intensive research into alternatives to fossil polymers. The increasing use of synthetic polymers as a result of rising human populations and living standards will lead to higher oil production requirements in the coming decades and will contribute to the possible depletion of oil before the end of the 21st century, resulting in the emission of hundreds of millions of tonnes of CO_2 into the atmosphere. As CO_2 is the main anthropogenic gas thought to affect the Earth's radiative balance, there is an opinion that there is a close correlation between the concentration of CO_2 in the atmosphere and the change in the Earth's temperature. This is the reason why there is so much effort given to try to replace standard fossil-based plastics with more ecological alternatives. Interestingly, biobased plastics often show similar properties and have an equal performance as the alternatives based on fossil fuels.

Some bioplastics as well as biodegradable polymers also get attention for their biocompatibility, which means that they can be implanted into the human body, where they cause no harm and later they can be absorbed and fully disintegrated. Due to this fact they are being used in medicine to improve regeneration and restore damaged tissues and also to shorten healing time. One of the most advanced approaches used in contemporary regenerative medicine is tissue engineering. The key role in tissue engineering is played by a porous structure called scaffold which serves as a support for various cells and is then integrated in the human body. There are various techniques to create scaffolds, such as solution or melt casting into moulds, lyophilisation, foaming, porogen leaching, or various softening techniques. A relatively new method of 3D printing or additive manufacturing, in which the product is created according to a precise digital 3D model, is being used with success, allowing complex structures, including porous internal structures, to be produced in a time and cost-effective manner. Furthermore, freedom of design, mass customisation and waste minimisation are other main benefits of 3D printing. Recently with progress made in the field of additive manufacturing techniques, tissue engineering has started using 3D printing methods to produce scaffolds, from biocompatible polymer materials, with specific structure to enhance their properties. This theme is presented via this thesis as it focuses on a research on 3D printing of P3HB biodegradable polymeric blends for bone tissue engineering.

2 THEORETICAL PART

2.1 3D printing in medicine and medical applications

2.1.1 Reasons for using 3D printing in medicine

Advances in 3D printing, also called additive manufacturing, in recent years are capturing attention in the medicine and medical applications because of their potential to improve treatment for certain medical conditions. A radiologist, for instance, might create an exact replica of a patient's spine to help plan a surgery; a dentist could scan a broken tooth to make a crown that fits precisely into the patient's mouth. In both instances, the doctors can use 3D printing to make patient-based products that specifically match a patient's anatomy. 3D printing offers significant promise in the healthcare field, particularly because this type of manufacturing does not rely on moulds or multiple pieces of specialised equipment and designs can rapidly be modified.

3D printing has enabled the production of customised prosthetic limbs, cranial implants, or orthopaedic implants such as hips and knees. Also in the case of bone fractures, there is a possibility to prepare a 3D printed scaffold, which can be seeded with bone cells or even combined with growth factors and/or stem cells to further enhance the healing potential. The scaffold is then transplanted into the affected area, where it stimulates bone cells (osteocytes and osteoblasts) so the treatment is more specific. If the scaffold is made of a biodegradable material (for example PLA, PHB, collagen, chitosan etc.) or their blends, it is absorbed after time and does not stay in the body.

A variety of 3D printers are available on the market, ranging from inexpensive models aimed at consumers and capable of printing small, simple parts, to commercial grade printers that produce significantly larger and more complex products. To date, most products developed via 3D printing have been medical devices such as orthopaedic implants; more than 100 have been reviewed. Such a manufacturing approach offers several clinical advantages. For example, manufacturers have used 3D printing technologies to create devices with complex geometries such as knee replacements with a porous structure as shown in the *Figure 1*, which can facilitate tissue growth and integration. 3D printing also provides the ability to create a whole product or device component at once while other manufacturing techniques may require several parts to be fabricated separately and screwed or welded together. [1]

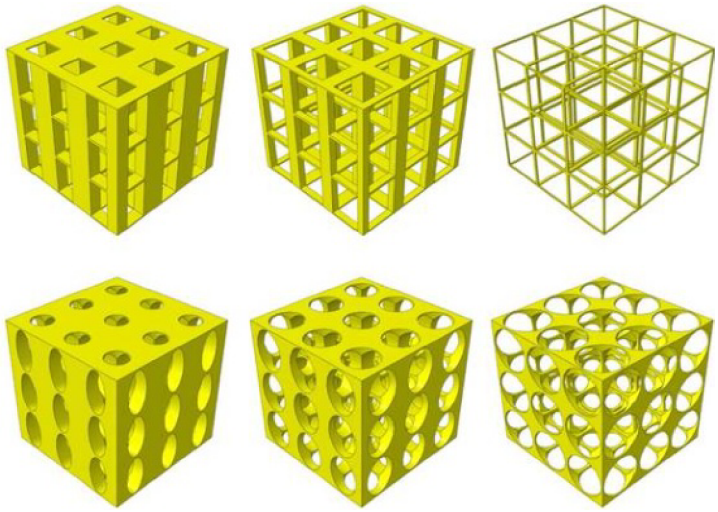

Figure 1: *Scaffolds with different internal structure and porosity [2]*

While some large-scale manufacturers are creating and marketing these products, this level of customization is also being used at the site of patient care in what is called point-of-care manufacturing. This on-demand creation of 3D-printed medical products is based on a patient's imaging data. Medical devices that are printed at the point of care include patient-matched anatomical models, prosthetics, and surgical guides, which are tools that help guide surgeons on where to cut during an operation. The number of U.S. hospitals with a centralised 3D printing facility has grown rapidly in the past decade, from just three in 2010 to more than 100 by 2019. As the technology evolves, this point-of-care model may become even more widespread. [1]

3D printing also has potential applications in other product areas. For example, research is underway to use 3D printing to manufacture pharmaceuticals with the potential for unique dosage forms or formulations, including those that might enable slower or faster absorption. Additionally, researchers are using bioprinters to create cellular and tissue constructs, such as skin grafts and organs, but these applications are still in experimental phases. [1]

2.1.2 Methods of 3D printing

3D printing is a process done using a machine that produces three-dimensional objects by adding consecutive layers on each other. This machine is called a 3D printer and for the printing it uses a code (G-code) which is based on the 3D model of an object we want to print. For this purpose computer-aided design drawing (CAD), which allows the manufacturer to easily make changes or adapt the product as desired as many times as it is needed, is usually used. Using 3D printing a man can produce shapes that are extremely complex yet still very light and reliable. Unlike traditional methods, in which products are created by shaping raw material into a final form through carving, grinding, or moulding, 3D printing is an additive manufacturing technique that creates 3D objects by building successive layers of raw material (metals, plastics, and ceramics). [3] Polymers are considered as the most suitable materials in the 3D printing industry and thus are the most common ones due to their diversity and ease of adoption to different 3D printing processes. Polymers for additive manufacturing are found in the form of thermoplastic filaments, reactive monomers, resins or powders. However, not all thermoplastics or composite filaments are usable or ideal for 3D printing, as opposed to injection moulding production. [4]

The most commonly used materials (polymers) are PLA, ABS and currently also PETG. ABS exhibits good mechanical properties but emits unpleasant odour during processing whereas PLA is environmentally friendly but in terms of mechanical and thermal properties does not reach the same qualities as ABS. [4] So far, the efforts of many researchers have been geared towards developing the viability of additive manufacturing for modern biodegradable and compostable filaments for printing. By using new materials such as biodegradable polymers, products can also be more environmentally friendly. The most commonly used polymers, including only biodegradable, are polylactic acid, poly(3-hydroxybutyrate), polyvinylalcohol and others. [3]

Some advantages of 3D printing methods over the conventional manufacturing processes include the customization of medicines with individually adjusted doses, the ability to fabricate the sophisticated and complex solid dosage forms, on-demand manufacturing, and cost-effectiveness. Furthermore, recent years have seen an increasing interest in applying 3D printing technology to the pharmaceutical manufacturing of drug products and development of various drug delivery systems. [5]

3D printing approaches can differ in terms of how the layers are deposited and in the type of materials used. At room temperature, the primary forms of materials used for 3D printing are solidifiable fluid (SLA, DLP), non-brittle filament (FDM), and fine powder (SLS). Each form is specific for a certain 3D printing process (abbreviations are explained in the next chapters). [6] Various 3D printing methods have been developed by varying also its energy source and other mechanical characters. Among them, the common 3D printing technologies applicable for pharmaceutical areas include these main categories: printing-based inkjet (IJ) systems, nozzle-based deposition systems, and laser-based writing systems, which can be further divided into several subtypes, depending on the materials and energy sources. An illustration of the subtypes is depicted in *Figure 2*. [3]

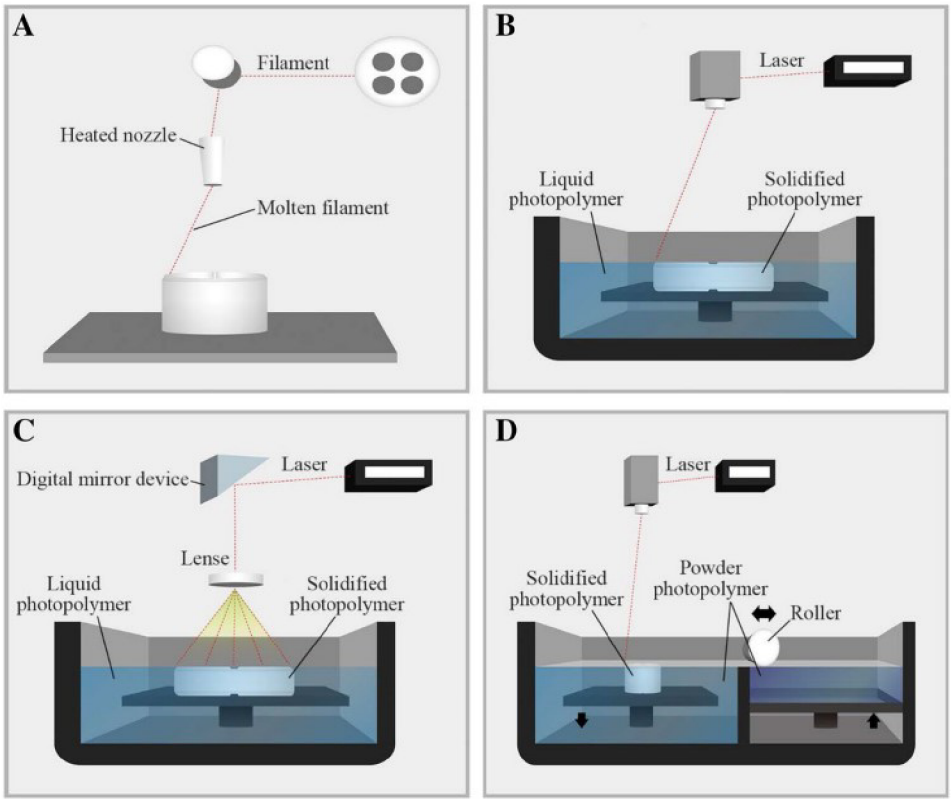

Figure 2: *Examples of 3D printing methods. A) FDM, B) SLA, C) DLP, D) SLS [1]*

2.1.2.1 Printing-based inkjet (IJ) systems

IJ systems comprise two types of technologies, namely, continuous inkjet printing (CIJ) and drop-on-demand printing (DOD) – presented in *Figure 3*. CIJ technology creates a continuous stream of ink through an orifice of 50–80 μm diameter, by using a high-pressure pump, whereas, DOD technology produces droplets of 10–50 μm with a volume of 1–70 pL. Both IJ systems possess a printer head and need to control the speed, size, and interval of drop formations and also fluid viscosity.

The DOD system can use two types of printer head: a thermal head or a piezoelectric crystal. In thermal DOD, also called bubble jet printing, the ink is heated locally and forms bubbles that eject ink. In piezoelectric DOD, the rapid change in the shape of piezoelectric crystal results in a sudden volume change, producing an acoustic pulse sufficient for the ejection of ink. This piezoelectric DOD method can be used with a diverse range of liquids, while the thermal DOD method is limited to volatile liquids. Considered that the thermal method reaches temperatures of up to 300 °C, which may cause the degradation of drugs and the piezoelectric DOD method, can be operated at room temperature with less volatile and more biocompatible liquids, the piezoelectric DOD method may be more suitable for pharmaceutical applications. Considering the main advantages and drawbacks following the DOD method, for the purposes of 3D printing for tissue engineering it is a preferable method than CIJ. [1]

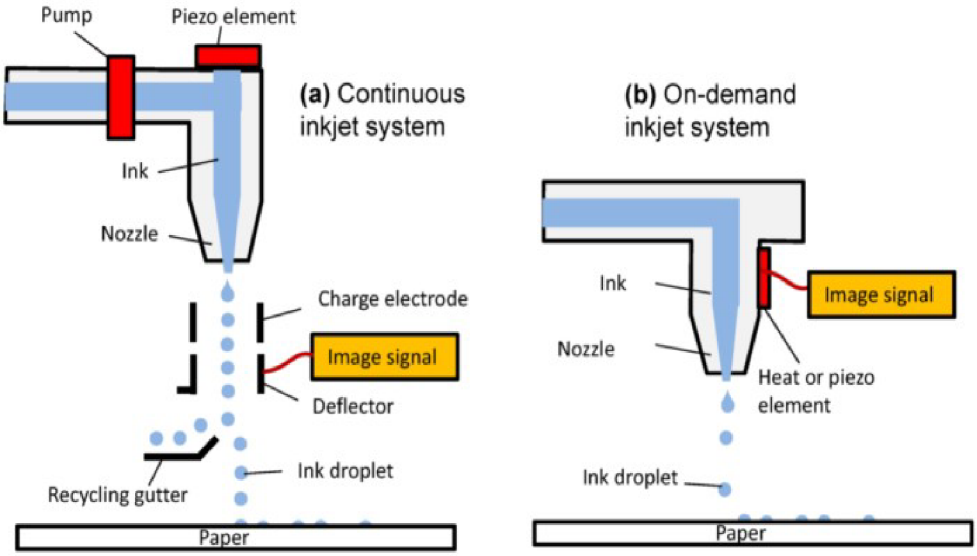

Figure 3: *Two main types of inkjet (IJ) systems [7]*

The DOD technology can be further divided into two subtypes, termed drop-on-drop deposition and drop-on solid deposition. In drop-on-drop deposition, the printer head ejects the droplets onto each other to produce a solid layer, resulting in a high resolution 3D structure. This direct writing IJ-printing method is capable of fabricating microscopic drug delivery systems having diverse geometries, where droplet size is about 100 μm in diameter and layer thicknesses are smaller than the droplet size probably due to surface wetting, solvent evaporation, or shrinkage. The physical properties of the printable fluid, such as viscosity and volatility, are also important to prevent fluid leaking, and nozzle clogging. Compared to drop-on-drop deposition, drop-on-solid deposition seems to be more applicable for the printing of a wide range of drugs, from chemical entities to biomolecules. Drop-on-solid deposition is also termed drop-on-powder or drop-on-bed deposition, binder jetting, plaster printing, or powder bed 3D printing, since it spreads the solid materials (powder) on the top of a platform and sprays the binder (a liquid ink) on the powders selectively. The platform is then lowered, and a new powder layer is spread again, repeating the process until a 3D structure is generated. The powder bed that is generally of 200 μm in height and particle size ranges from 50 to 100 μm is adhered to each other by the binder ink to create a 3D object. The reactivity of the powder bed with the binder ink and the topological characteristics of the powder are critical factors affecting the quality of the final products. [3]

2.1.2.2 Nozzle-based deposition systems

Probably the most common type of 3D printing is the so-called "fused deposition modelling" (FDM), which consists in melting a filament of polymer material slightly above its melting temperature and then extruding it with a nozzle onto a substrate, on which it solidifies again. The individual layers of the printed product are formed by repeatedly moving the head (*Figure 2*). [2]

Considering that the drawbacks of the most common printing-based IJ method are insufficient hardness, a rough surface, and low drug loadings, nozzle-based deposition systems would be a suitable alternative to overcome those limitations. Instead of dropping the binder solution on a powder bed, nozzle-based deposition systems mix the solid components with the binder prior to 3D printing and directly deposit the mixture through a nozzle to create a 3D object. This method can be divided into two subtypes, named fused deposition modelling (FDM) and pressure-assisted microsyringes (PAM), according to the process with or without material melting, respectively.

FDM is one of the most commonly used 3D printing techniques and has been well-studied in many fields, including pharmaceuticals, foods, bioengineering etc. FDM, which is also called fused filament fabrication, defines a process in which a molten thermoplastic polymer filament is extruded through a high-temperature nozzle and deposited layer-by-layer with immediate solidification onto a build plate (*Figure 4*). FDM printing resolution can range from about 10 to 300 μm depending on a nozzle diameter, width of printed layer, perimeter printing speed etc. [8] For example, scaffolds printed from ABS using nozzle with diameter 0.2 mm showed resolution of 100 μm. [9]

FDM manufacturing process exhibits many advantages since it allows the production of highly complex drug carriers with difficult geometries and offers good mechanical strength, as well as options to modify the drug release profiles. The 3D structures fabricated by FDM usually have good mechanical properties such as those made up of PLA and PCL. Furthermore, the control over porosity and properties can be achieved by adjusting the printing speed. FDM is a well-known technique which is easy to use, safe and reliable with a low purchase price. A wide range of thermoplastic polymers such as PLA, PCL, and recently their composites with ceramics like hydroxyapatite (HAp) can be made in quite complex structures and superior chemical and physical functionality. [10] However, there are also some drawbacks that limit its pharmaceutical applications, such as high operation temperatures, and still very limited options regarding biodegradable thermoplastic polymers with good melt viscosity properties for extrusion.

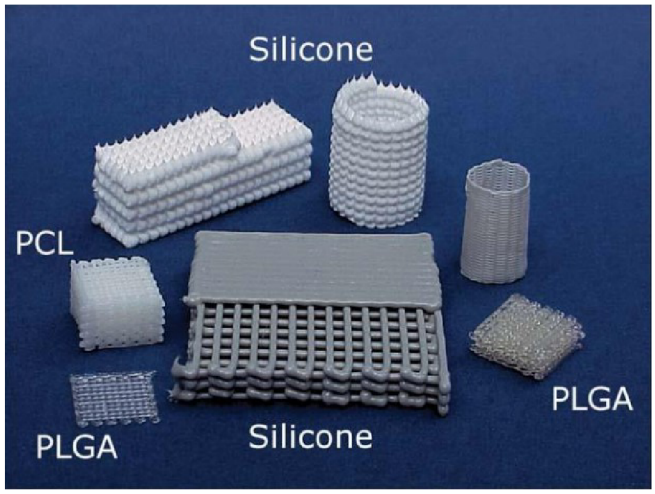

Figure 4: *Various materials processed by the FDM [11]*

PAM is another type of nozzle-based deposition systems. In PAM, viscous and semi-liquid materials are extruded from a microsyringe. This syringe can move like an IJ printer head, and the semi-liquid material is released by compressed air. PAM technology is able to create complex drug delivery systems with microstructure of 5–10 μm or less and is advantageous over other methods since it can be operated in a continuous flow at room temperatures. However, the use of solvents may lead to safety and stability issues during the manufacturing and drying steps. [3]

2.1.2.3 Laser-based deposition systems

Stereolithography (SLA) is a laser-based printing method that was the first commercially available solid freeform fabrication technique. The fabrication of a 3D object by SLA is based on the controlled solidification of a liquid resin by photo-polymerization. A movable platform is located in the vessel filled with liquid photopolymer. First, the lifting platform starts near the surface of the liquid photopolymer, and after the proper laser is applied, the platform is lowered into a vessel to a depth equivalent to the thickness of the new polymerized layer. This process is repeated until a solid 3D product is obtained (*Figure 5*). SLA has high resolution which allows creating a complex structure, and it also minimises the heating during the printing process, and thereby it is highly applicable to thermo-labile drug carriers. The choice of photopolymer is essential, as it should be a liquid that quickly solidifies upon illumination with ultraviolet (UV) light and, also, it must be approved for human use. Approved photosensitive polymers and the low drug loading significantly limit the pharmaceutical applications of SLA, although it is widely used in tissue engineering.

Digital light projection (DLP) is an emerging 3D printing technique similar to SLA, which also uses liquid photopolymer resins and a laser beam to solidify and build an object. The difference between DLP and SLA is the use of a digital mirror device, allowing for the curing of a single layer at once. The simultaneous control of the millions of mirrors allows an entire layer to be cured at once, resulting in substantially reducing the layer production time. Accordingly, DLP offers a comparatively faster building and easy adjustment of the layer thickness. [3]

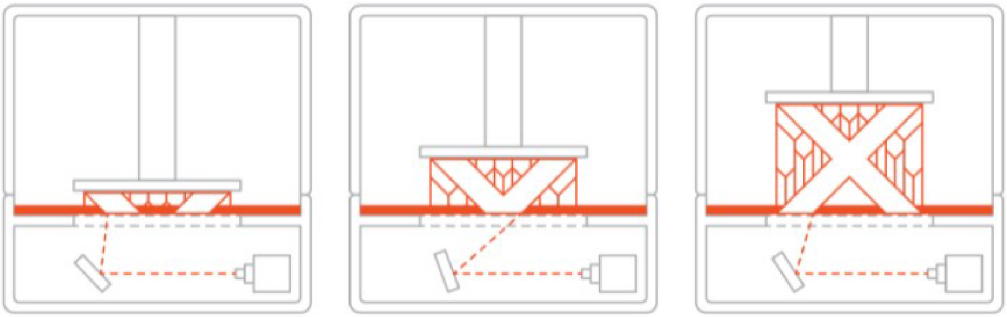

Figure 5: *SLA printing process in time (left to right) [12]*

Another laser-based system is selective laser sintering (SLS). SLS uses a high-power laser as an energy source to sinter a powder material. Once the laser selectively fuses the powder material, the platform supporting polymer lowers to refill with powder. High-strength, chemical resistance, and speed are advantages acquired by SLS technology. SLS can be applied to a wide range of materials, including polymers, metals, and ceramics. Electron beam melting (EBM) and selective laser melting (SLM) are also similar techniques to SLS. However, unlike sintering technology, both EBM and SLM completely melt metal powders during the layer-by-layer process. The SLM method uses energy from a laser beam to fuse the powder particles by heating it beyond the melting point, while EBM uses a high-power electron beam in a vacuum. EBM can provide higher throughput and more uniform thermal field distribution than SLS, but its accuracy and surface quality are lower. SLS, EBM and SLM are widely used mainly in drug-loaded implants. [3]

In addition to the 3D printing techniques described above, there are many others, including multi-jet modelling, selective heat sintering, and laminated object manufacturing. These are not currently used for pharmaceutical manufacturing, but some of them have a high potential for pharmaceutical applications in the future. Therefore, a great advance in material sciences and the emergence of new adequate materials will facilitate more broad applications of various 3D printing systems.

2.2 Biomaterials used in 3D printing systems

With advances in the 3D printing field, it is increasingly being used in tissue engineering for the scaffold manufacturing process. This puts a pressure on materials suitable for this purpose. They have to fulfil the requirement of biocompatibility which according to Williams Dictionary of Biomaterials means:

1. The ability of a material to perform with an appropriate host response in a specific application
2. The quality of not having toxic or injurious effects on biological systems [13]

Biopolymers are the group that exhibits most of the needed properties at reasonable cost, especially those which are also biodegradable. However, some biopolymers, which also fall into a category of biodegradable polymers, are not available in nature (or not available in sufficient quantities) but can be produced by human intervention from naturally occurring biological sources. Today, most biobased bioplastics are sourced from plant-based raw materials coming from traditional crops like corn and sugarcane. However, efforts have been made to move to second and third generation feedstocks including agricultural, forest, and municipal waste, as well as algae and other non-food biobased feedstocks.

The most important representatives in the category of thermoplastic biopolymers are biodegradable polyesters – polylactic acid (PLA), polyhydroxyalkanoates (PHA) – especially poly(3-hydroxybutyrate), and polycaprolactone (PCL). They have received intense research interest over the past two decades and are finding increasing use in a wide variety of industries and applications due to their unique combinations of properties. 3D printing for medical applications is one of such fields. [14]

This work focuses on the blends of poly(3-hydroxybutyrate) (P3HB) with polylactic acid and polycaprolactone. Blending is a common way to overcome drawbacks that these polymers exhibit, limiting their utilisation. For polylactic acid it is low heat distortion temperature, whereas for polyhydroxybutyrate it is its brittleness and low melt viscosity.

2.2.1 Poly(3-hydroxybutyrate) - P3HB

Unlike PLA, whose production involves precisely designed and ordered chemical reactions, polyhydroxyalkanoates (PHAs) in general are naturally occurring biodegradable polyesters produced directly by bacterial metabolism. In response to conditions of physiological stress, mainly those when nutrients are limited, and in the excess of carbon source, PHAs are synthesised and accumulated by bacteria as a carbon and energy store. More than 250 species of bacteria (*Cupriavidus necator, Methylobacterium rhodesianum, Bacillus megaterium* etc.) capable of producing PHAs have been described. These polymers are then deposited in cytoplasm in cells as water-insoluble continuous granules between 0.2–0.5 mm in size (*Figure 6*). The stored PHAs are degraded by depolymerases and metabolised as a source of carbon and energy as soon as the source of any of the nutrients is limited. Depending on the bacterial species and their growth conditions, the number-average molecular weight of purified PHAs ranges from 3,000 up to 994,000 $g \cdot mol^{-1}$.

For production and use on a large scale it is necessary to extract PHA granules out of the bacteria cells. Currently several methods related to this topic are reported, however most of them are based on the dissolution of the polymer in toxic solvents such as chloroform 1,4-dioxane, dichloromethane and others for the process. Unfortunately these solvents have a negative effect on environmental friendliness which is a very unpleasant fact and also causing additional issues, since the whole manufacturing cycle is targeting to be sustainable and as low-polluting as possible. For this reason new chloroform-free extraction processes, e.g. using fatty acid salts (soaps) made from waste cooking oil thus serving as an alternative surfactant for the isolation of PHB from bacterial biomass, are emerging. [15–17]

Chemically, PHAs include a group of polyesters with different side groups and different numbers of carbon atoms in repeating units. The most studied polyhydroxyalkanoates are poly(3-hydroxybutyrate) P3HB, poly(4-hydroxybutyrate) P4HB and copolymer consisting of P3HB and poly(3-hydroxyvalerate) – polyhydroxybutyrate-co-valerate (PHBV). Chemical structure of the most common polymers of the PHA group is shown in *Figure 7*. [18]

The mechanical behaviour of PHAs in general depends on both the length of the pendant groups and the distance between ester linkages. PHAs with short pendant groups are prone to crystallisation but exhibit stiff and brittle behaviour, while PHAs with longer pendant groups are ductile.

The first PHA to be identified was P3HB. This homopolymer is the most abundant bacteria synthesised polyester and its 3-hydroxybutyrate monomer was thought to be the unique PHA constituent in bacteria. Further research reported heteropolymers in chloroform extracts of activated sewage sludge, like 3-hydroxyvalerate (3HV) among others.

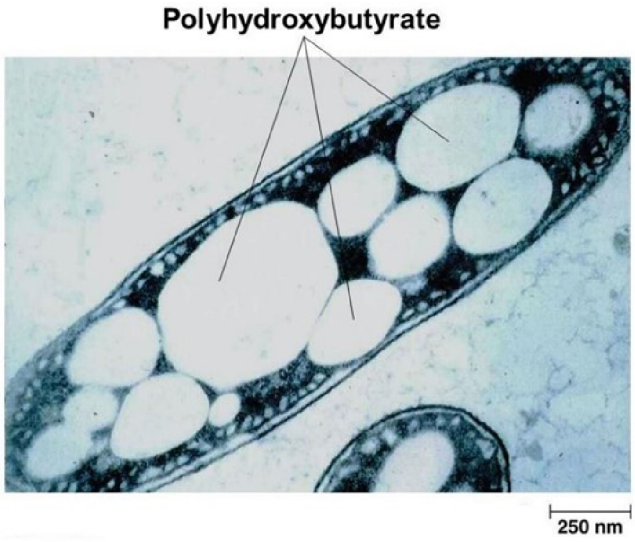

Figure 6: *PHB granules stored in Azotobacter chroococcum bacteria species [19]*

The homopolymer P3HB is a highly crystalline thermoplastic with a melting temperature (T_m) of approximately 175 °C. Some of its physical properties such as T_m, T_g (around 5 °C), crystallinity (80 %) and tensile strength (40 MPa) are very similar to those of polypropylene. However, P3HB is significantly more brittle than PP, with elongation at break of 6–7 % compared to 400 % for PP. The homopolymer of P3HB is a brittle material, while the introduction of other units in the P3HB chain has a significant effect on the mechanical behaviour of polyester. When 3-hydroxyvalerate (3HV) units are incorporated into the polymer chain of P3HB, its regular structure is disturbed and therefore the crystallinity, rate of crystallisation, T_g and T_m decrease in direct proportion to the increase in the number of 3HV units in the chain. As a result, the PHBV copolymer becomes tougher and more flexible with a higher percentage of 3HV units as we can see in *Figure 8*. [20]

PHAs have been blended with many biodegradable and non-biodegradable polymers in order to improve their properties and reduce the cost of material production. P3HB has been found to be miscible with polyethylene oxide (PEO), polyvinyl acetate (PVAc), polyvinylidene fluoride (PVDF) and polymethyl methacrylate (PMMA) at different component ratios and temperatures. P3HB is not miscible or only partially miscible with polyvinyl acetate-co-vinyl alcohol, PCL, PLA and polyoxymethylene. However, reports on the mechanical properties of these blends are limited. [14]

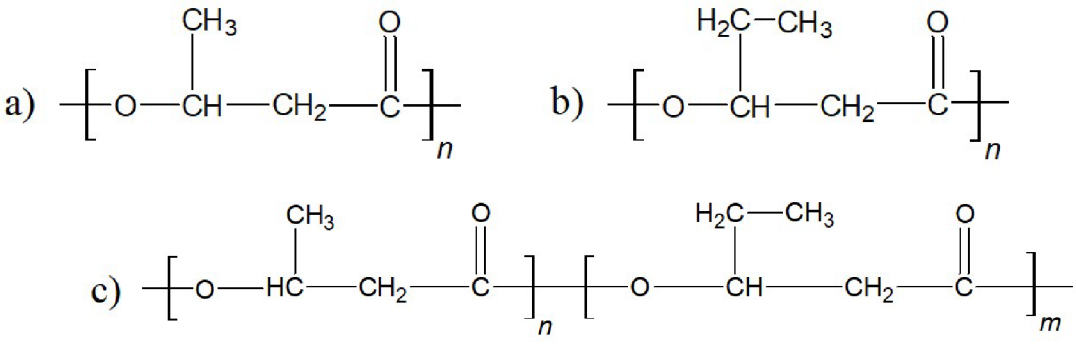

Figure 7: *Chemical structure of the most common polyhydroxyalkanoates: a) P3HB, b) PHV, c) PHBV [21]*

The properties of PHA were also modified by the use of natural fibres. The addition of natural fibres was shown to increase the tensile modulus, T_g and heat distortion temperature (HDT) of the P3HB (or PHBV) composites. PHAs were also graded into fibres for textile applications, with strengths comparable to those of conventional polymer fibres such as polyethylene (PE) or polyethylene terephthalate (PET). [22]

Many factors affect the degradation rate of P3HB, which include surface area, microbial activity, pH, temperature and humidity. The end products of P3HB degradation in aerobic environments are carbon dioxide and water, while under anaerobic conditions methane is also produced. Depending on the environmental conditions, PHBV degrades completely after 6, 75 and 350 weeks in anaerobic wastewater, soil and seawater, respectively. P3HB shows in vivo degradation rate comparable to that of high molecular weight polylactide (approximately six months to a year). The degradation products of PHB are intrinsic to the body and do not cause an inflammatory reaction, which is a problem with some other polyester-based materials. In addition, PHB has mechanical properties that are more suitable for the preparation of rigid tissue substitutes than other polymers used, such as collagen, PLA, PLGA, or PCL. Under standard storage conditions, however, P3HB and PHAs in general do not degrade at all. [23, 24]

Polymer	T_g (°C)	T_m (°C)	Modulus (GPa)	Strength (MPa)	Strain at Break (%)
PHB	9	175	3.8	45	4
PHBV (11% HV)	2	157	3.7	38	5
PHBV (20% HV)	−5	114	1.9	26	27
PHBV (28% HV)	−8	102	1.5	21	700
PHBV (34% HV)	−9	97	1.2	18	970

Figure 8: *The effect of 3HV units contain in PHBV copolymer on its properties [25]*

Due to their inherent biocompatibility and biodegradability, PHAs have found significant applications in medical and pharmaceutical fields (e.g. bone tissue engineering) and applications, (scaffolds for tissue engineering, sutures, staples and skin substitutes), vascular materials (heart valves, cardiovascular fabrics and vascular grafts), orthopaedics (bone graft substitutes and internal fixation devices) and drug delivery systems. Regarding these applications, P3HB has been processed by selective laser sintering (SLS) and fused deposition modelling (FDM) methods. [26, 27] PHAs are also finding increasing use as disposable packaging and disposable items, adhesives, coatings, in appliances, electronics, agriculture and as automotive components. In the United States, PHAs are commercially produced by Danimer, Kaneka, TianAn or Tepha by fermenting enzymatic starch, plant sugars and oils using microbial "biofactories".

A variety of different PHAs, including homopolymers, copolymers and terpolymers has enabled the diversity of properties of polymers belonging to the PHA group, from rigid thermoplastics to thermoplastic elastomers and adhesives. [22] In the Czech Republic, a completely unique biotechnology called HYDAL patented by Nafigate Corporation was introduced in 2018 and is the only one in the world so far that can industrially process used frying oil and convert it into a high-quality P3HB-type biopolymer.

The wide performance range of PHAs and their copolymers justified additional scientific and industrial interest, which led to the discovery of further bacterial PHAs. The wide range of mechanical properties coupled with the biodegradable and the biocompatible behaviours of PHAs makes them potential biomedical candidates including drug delivery and tissue engineering applications.The biocompatibility assessment of PHAs has indicated that cell response also depends on the type of polyester. Several studies reported the investigation of PHAs and P3HB as potential scaffold materials in a diverse range of tissue engineering applications. Other studies have focused on the assessment of P3HB scaffolds for bone and cartilage tissue engineering. Furthermore, polarity of the P3HB on the scaffold seems to play an important role on what concerns cell morphology. [28]

In the work by Kovalcik et al. poly(3-hydroxybutyrate (PHB), poly(3-hydroxybutyrate-co-3-hydroxyvalerate) (PHBV) and poly(3-hydroxybutyrate-co-3-hydroxyhexanoate) (PHBH) were tested for FDM. Properties were compared with PLA. PHBH scaffolds prepared by FDM exhibited excellent mechanical properties, no cytotoxicity and large proliferation of mouse embryonic fibroblast cells within 96 h. The hydrolytic degradation of PHBH and PLA scaffolds tested in synthetic gastric juice for 52 days confirmed a faster degradation of PHBH than PLA. The incorporation of PHB to PLA accelerated the crystallisation and improved the processability of PLA by FDM printing. In addition to PHB, other types of PHA were also blended with PLA to improve the impact properties of the material. Among the different PHAs studied, it has been found that poly(hydroxybutyrate-co-hydroxyhexanoate) has adequate thermal stability and rheological properties to be used in FDM. The assessment of PHB and PHBV thermal degradation showed that these polymers are susceptible and markedly degrade during repeated melt processing. The rheological and mechanical properties of the filaments prepared from PHBH confirmed that they are sufficient for fused deposition modelling.

Scaffolds prepared from PHBH by FDM have shown good mechanical and viscoelastic properties. These scaffolds showed no cytotoxicity. The cytocompatibility in terms of cell proliferation showed significant differences as PLA scaffolds do not allow the cells to proliferate on their surfaces, while the PHBH scaffold surface allowed the cell proliferation comparable to tissue culture plastic. Compared to PLA scaffolds, PHBH promoted much higher cell proliferation. [27]

2.2.2 Polylactic acid – PLA

Polylactic acid (PLA) is a synthetic biodegradable polyester derived from lactic acid monomer obtained from natural plant sources. Lactic acid is commonly found in nature in the form of two enantiomers, which are shown in *Figure 9*. Lactic acid is most commonly produced by bacterial fermentation of carbohydrates from corn, sugar cane, potatoes and biomass. PLA can be synthesised via three different routes: direct condensation polymerization, azeotropic dehydration condensation, and ring-opening polymerization of lactide, which can yield PLA with high molecular weight. The chemical structure of a polylactic acid formed by polymerization of one of its enantiomers is shown in *Figure 10.* Direct condensation polymerization is the least expensive method, but only low molecular weight PLA can be obtained via this route, as it is very difficult to completely remove water from the reaction mixture. The ring-opening polymerization method was patented by the US company Cargill in 1992 and is nowadays the most commonly used method. The process of PLA production by ring-opening polymerization is shown in *Figure 11*. [29]

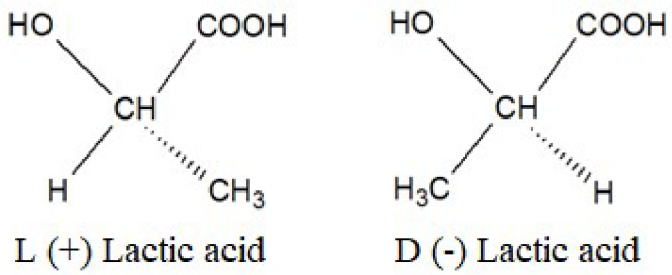

Figure 9: *Enantiomers of lactic acid [21]*

In terms of properties, PLA is well known for its biocompatibility and compostability. In addition, PLA is a thermoplastic polymer and can therefore be easily processed using existing equipment and techniques for processing conventional synthetic polymers and is soluble in most organic solvents, namely methylene chloride and chloroform. The properties of PLA can vary considerably due to the formation of chiral carbon atom and two enantiomers of lactic acid depending on a position of an attached methyl group on the alpha carbon (*Figure 9*). In addition there is also DL-lactic acid which is a racemic mixture of D-lactic acid and L-lactic acid. All three of them (L, D and DL-lactic acid) are produced in nature by microorganisms. [30]

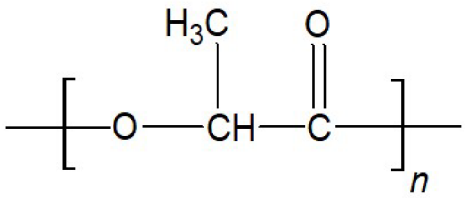

Figure 10: *Chemical structure of polylactic acid [31]*

Poly(L-lactic acid) (PLLA) and poly(D-lactic acid) (PDLA) are semicrystalline polymers, though incorporation of more than 15 % D-lactic acid into PLLA makes the polymer amorphous. Typical melting temperature (T_m) of L-lactic acid homopolymer (PLLA) is around 160–180 °C and glass transition temperature (T_g) around 55–65 °C. Its crystallinity depends strongly on the processing conditions – in particular on the cooling rate. It is characterised by high tensile strength, tensile modulus and low elongation, which makes it more than suitable for load-bearing applications such as orthopaedic fixation and sutures. PLLA exhibits much higher tensile strength (~60 MPa) and tensile modulus (~3 GPa) than many other conventional petroleum-based synthetic plastics. HDPE, for example, has a tensile strength of 20 MPa and a tensile modulus of 1 GPa. Furthermore, polypropylene (PP) also exhibits a similar tensile strength of 30 MPa and tensile modulus of 1.5 GPa as it is shown in *Table 1*. PLA, on the other hand, is a brittle polymer that exhibits a tensile strain at break of less than 6 %. For this reason, intense research interests have been focused on the toughening of PLA plastics and several effective strategies have since been developed. [32]

Table 1: *Comparison of mechanical properties of PLLA versus HDPE and PP*

Material	Tensile strength (MPa)	Tensile modulus (GPa)
PLLA	60	3
HDPE	20	1
PP	30	1.5

The first option for curing PLA is the copolymerization of lactides with other monomers. The second option is to lower the glass transition temperature (T_g) by adding thermodynamically miscible plasticizers such as lactide monomer and oligomer or polyethylene glycol (PEG) and triethyl citrate, the addition of which has increased elongation at break in the resulting products. A third option is to blend PLA with tough polymers, which is probably the simplest choice and therefore the most studied route for toughening PLA. To ensure the biodegradability of the final blends and products, biodegradable tough polymers are often also used for blending with PLA. Of this group of polymers, the greatest research interest has been focused on PCL, which is a biodegradable polymer that is flexible even at room temperature due to its low T_g (−60 °C). Mixing PLA with PCL has led to significant improvements in toughness and tensile strength. PLA has also been cured with other biodegradable polymers such as PBAT and PBS. However, here the results were not as satisfactory as when blended with PCL. The three methods of curing PLA mentioned above – copolymerisation, plasticisation and blending – can significantly increase the ductility of PLA, but at the cost of reducing the tensile strength and modulus. [33]

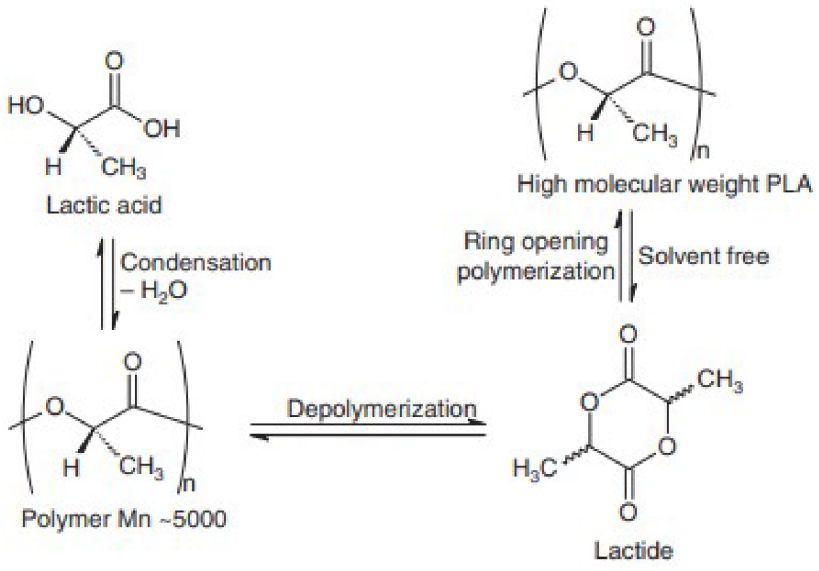

Figure 11: *High molecular weight PLA manufacturing process [21]*

Poly(DL-lactic acid) (PDLLA) is an amorphous statistical copolymer of L-lactic acid and D-lactic acid. It has lower tensile strength, higher elongation and a much higher degradation rate, which in turn makes it more attractive for use as a drug delivery system. [34] PDLLA also exhibits a lower tensile strength, higher elongation at break, and a faster degradation rate than either lactide homopolymer – PLLA and PDLA.

Poly(lactide-co-glycolide) (PLGA) is a copolymer of PLA and PGA used to modify the mechanical and degradation properties of the two homopolymers. [35]

PLA is up to now the most widely used material for 3D printing by FDM method speaking in terms of biodegradable and nonbiodegradable as well. It is also the most used bioplastic for 3D printing by FDM in the regenerative medicine for the production of bioresorbable implants and devices (mostly as scaffolds suitable for cell proliferation for tissue engineering). [36] Why is it that PLA enjoys such popularity compared to other highly used materials? The main reasons are most probably, because PLA can be printed at relatively low temperatures in comparison to other materials used for 3D printing (starting around 180 °C), it is eco-friendly (as it is produced or at least can be produced from renewable bioresources and recycled resources), and is very user-friendly and suitable even for beginner printers who are new to 3D printing and are yet to learn how to operate with more demanding materials. Also 3D printing from PLA filament is less time consuming, because there is no need to sit nearby and to control what is happening while printing since there is less chance of something going wrong. An example of commercially available PLA filaments used for 3D printing is depicted in *Figure 12*.

Figure 12: *PLA filaments for 3D printing of different colours [37]*

Most of the PLA in biomedical applications is produced from L-lactic acid. The implants made of PLLA can be easily degraded and resorbed by the body through the action of enzymes. When broken down via hydrolytic mechanisms, lactic acid is absorbed into the body. Unfortunately, the stereoisomer D-lactic acid is not degraded by the body's enzymes. However, prolonged hydrolysis in body fluids eventually breaks down the bulk of PDLA.

A considerable amount of PLA copolymer is synthesised for tissue engineering. Scaffold made from PLA homopolymer and prepared by FDM 3D printing method as a part of a bone tissue replacement study is shown in *Figure 13*. The main objective during the synthesis of such copolymers is to fine-tune the period of degradation from weeks to years. Commonly, the monomers of glycolide acid and ε-caprolactone are copolymerized with lactide. This is very important for the fabrication of scaffolds for tissue engineering and for wound dressings. The degradation of the copolymer is designed to couple with the growth of tissue and the loss of mass and strength of the prescribed implants. Eventually, the scaffold structure is substituted by the permanent tissue of the patient.

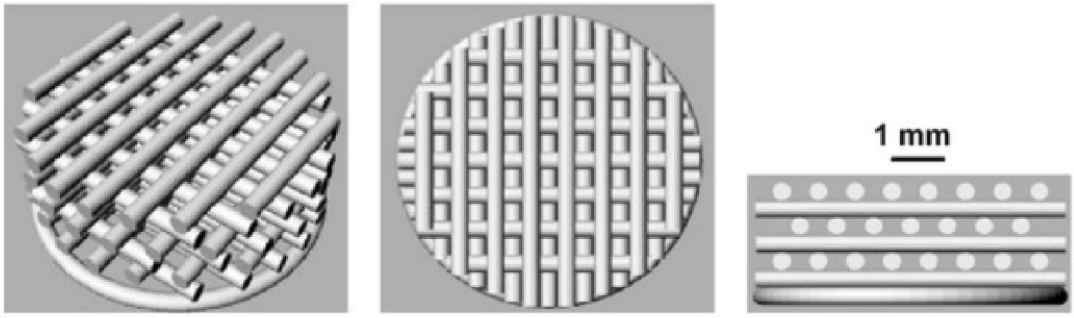

Figure 13: *3D printed scaffolds from PLA used in tissue engineering [38]*

PLA and its copolymers can be used for a wide range of biomedical applications such as sutures, anchors, screws, and scaffolds. They have uses in oral, orthopaedic, auricular, and craniofacial augmentations in plastic surgery. Screws and anchors are produced by the injection moulding method, and sutures are manufactured using a fibre spinning process. Bioresorbable scaffolds are prepared using a range of techniques, including phase separation, solvent evaporation, casting/salt leaching, and 3D printing. PLA copolymers are also widely used as a drug carrier medium. Such drug carriers contain active drugs, which can be efficiently delivered to the target cells and subsequently released at a controlled rate. When the polymer is exposed to aqueous media or tissue the degradation of PLA takes place primarily through hydrolysis in two stages. First, the ester linkages in the PLA polymer chain react with the absorbed water through a hydrolysis reaction and random cleavage begins. Over time, the long polymer chains are broken into shorter ones reducing its molecular weight and forming water-soluble fragments. The rate of cleavage depends on the pH, temperature and moisture level of the environment in which it takes place. This results in embrittlement of the polymer and the products made from it. Eventually, in a second step, the low molecular weight water-soluble PLA fragments diffuse away from the initial polymer structure and finally is metabolised by microorganisms, releasing carbon dioxide, water and humic substances. Generally, the rate of degradation is higher at low molecular weights and for higher glycolide content in the case of PLGA copolymer. [39] [40]

2.2.3 Polycaprolactone – PCL

Poly(ε-caprolactone) (PCL) is a semicrystalline linear aliphatic polyester with a degree of crystallinity around 50 %. It has a rather low glass transition temperature (−60 °C) and melting point (59–64 °C). PCL was one of the earliest polymers synthesised in the early 1930s. It can be manufactured either by hydrolytic, cationic, anionic or coordination polymerization of 6-aminocaproic acid depending on the type of initiator used or by ring opening polymerization (ROP) of a seven-membered lactone ring of ε-caprolactone *Figure 14*. Recently, enzymatic catalysed polymerization of ε-caprolactone has also been reported.

The rate of polymerization depends on the type of initiator used, while the setting equilibrium between polymer and monomer at the usual initiator concentrations depends primarily on the reaction temperature so that the equilibrium polymer concentration decreases with temperature. Catalysts such as stannous octoate are used to catalyse the polymerization and low-molecular-weight alcohols can be used to control the molecular weight of the polymer. The hydrolytic polymerization takes place in the presence of water or substances releasing water. It is characterised by a slower rate of polymerization as opposed to activated anionic polymerization. Acceleration of polymerization can be achieved by the addition of strong acids, e.g. phosphoric acid. [25]

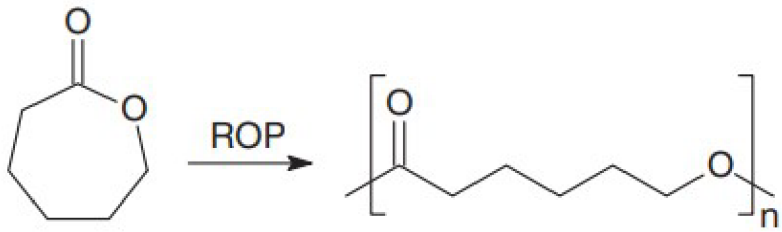

Figure 14: *Scheme of ROP of ε-caprolactone [21]*

PCL is nontoxic and completely degradable through enzyme activities. High molecular weight PCL polymers have mechanical properties similar to PE, possessing a tensile stress of 12–30 MPa and a break extension of 400–900 %. All the properties of PCL are strongly molecular weight dependent. PCL shows high-molecular-chain flexibility and outstanding processability. It can be spun into fibres or blown films under 200 °C without thermal degradation. The processing drawback of PCL is its low melting point and low glass transition temperature, which prohibits its application at elevated temperatures. Therefore, PCL is often blended with other polymers, such as PP, polycarbonate (PC), polyethylene oxide (PEO), and starch or copolymerized with many other lactones, such as glycolide, lactide, δ-valerolactone, ε-decalactone, and alkyl-substituted ε-caprolactone to produce composites with desired properties. PCL is extensively used in food packaging and tissue engineering. For instance, microcellular PCL foams are used for tissue regeneration and cell transplantations. [21]

PCL has a slow degradation rate (up to 2 years) and a high permeability; therefore, it is well-suited for long-term controlled release applications and implants, especially for long term drug delivery systems. Due to its slow degradation rate, copolymers of ε-caprolactone and D,L-lactide are also synthesised to yield materials with more rapid degradation rates. The superior rheological and viscoelastic properties over many of its aliphatic polyester counterparts render PCL easy to manufacture and manipulate into a large range of implants and devices.

The application of PCL as a biomaterial was over the last two decades focusing on medical devices, drug delivery, and tissue engineering. [35] It is widely used in tissue engineering to manufacture different types of stents due to its good biocompatibility and shape retention properties. However, when used for bone tissue engineering, the new bone tissue cannot be tightly bound to the polymer surface due to insufficient bioactivity of the PCL. Hydroxyapatite (HAp) has high bioactivity and has been used as a bone substitute material. Therefore, HAp/PCL composites, in combination with the biocompatibility of the two materials, are expected to apply to bone tissue engineering scaffolds.

Guo et al. used HAp and PCL as raw materials to prepare pure PCL scaffolds and HAp/PCL scaffolds with HAp mass fractions of 5% and 10% respectively by selective laser sintering technology, and analysed the macro- and micro-structure of the scaffolds, compressive strength, porosity and hydrophilicity. [41]

Ein et al. [42] and Cao et al. [43] used PCL silks as raw material to prepare biological tissue scaffolds by fused deposition modelling (FDM) process. This printing method shows advantages in the simple preparation process of the composite material, higher degree of freedom in material selection, simple printing process, and shorter preparation cycle of tissue engineering scaffolds. However, the bioactivity of pure PCL material was insufficient, and FDM fuses were very limited in the degree of freedom in material selection.

Zhao et al. successfully prepared HAp/PCL biological tissue scaffolds by impregnation method, but the strength was only 0.57 ± 0.09 MPa. On the whole, the existing tissue engineering scaffold preparation process has problems of low HA content, easy agglomeration, low stent strength, and single printing material. [44]

In the work by Du et al., porous PCL/HAp composites were obtained by microsphere-based selective laser sintering. The scaffolds exhibited a controlled microstructure and porosity, excellent histocompatibility, and enhanced proliferation and differentiation of mesenchymal stem cells (MSCs) in vitro. This work proved that the micropores created by the microspheres of about 100 μm provide appropriate surfaces for cell adhesion, spread and ingrowth. [45]

2.3 Tissue engineering

2.3.1 The introduction to tissue engineering and important facts

Tissue engineering (TE) is a multidisciplinary field aimed at the development of biological substitutes that restore, maintain, or improve tissue function. Tissue engineering uses for this purpose a carrier (scaffold – *Figure 15*) which is a 3D biomaterial that provides a suitable environment for the attachment and growth of cells. It can be also used as a drug carrier, containing controlled release active agents for long term treatments, including for cancer. 3D scaffolds appeared to be promising constructs for cartilage tissue engineering applications as they possessed good surface properties, proper mechanical strength, and capability of stimulating cell proliferation. [46] The prepared scaffold is then seeded with cells and/or possibly other supporting substances (growth factors, drugs, stem cells etc.). The aim is to produce scaffolds that are able to provide regenerative signals to the cells that direct cell proliferation and differentiation.

Incorporation of growth factors into the scaffold may improve osteogenesis and angiogenesis. Fibroblast growth factor (FGF), platelet-derived growth factor (PDGF), insulin-like growth factor (IGF), epidermal growth factor (EPG), transforming growth factor beta (TGF-β), and bone morphogenetic protein (BMP) are among the known growth factors used for scaffolds in TE to promote bone regeneration. In addition, human mesenchymal stem cells (MSCs) can be used. Multipotent MSCs can be found in several tissues. MSC isolated from bone marrow are able to differentiate into specialised cells from the mesoderm. Human MSCs can be isolated not only from bone marrow, but also from many other tissues such as adipose tissue, dental tissue, placenta, skin or foreskin. Except for MSCs from bone marrow, non-invasive methods are used to obtain MSCs from other tissues directly from the patient. [47]

The seeded scaffold is used as an implant to help to start or accelerate regeneration of the tissue damaged by disease or trauma and, in some cases, to create new tissues or even to replace failing of malfunctioning organs. Typically, this is achieved through the use of degradable biomaterials to either induce surrounding tissue and cell ingrowth or to serve as temporary scaffolds for transplanted cells to attach, grow, and maintain differentiated functions. In any case, the role of the scaffold is temporary as it is then completely absorbed within the host body during the healing process. However, its proper functioning is still crucial for the success of the whole procedure. Therefore, the design and production of an appropriate scaffold material is the first, and one of the most important stages, in tissue engineering strategies. [28]

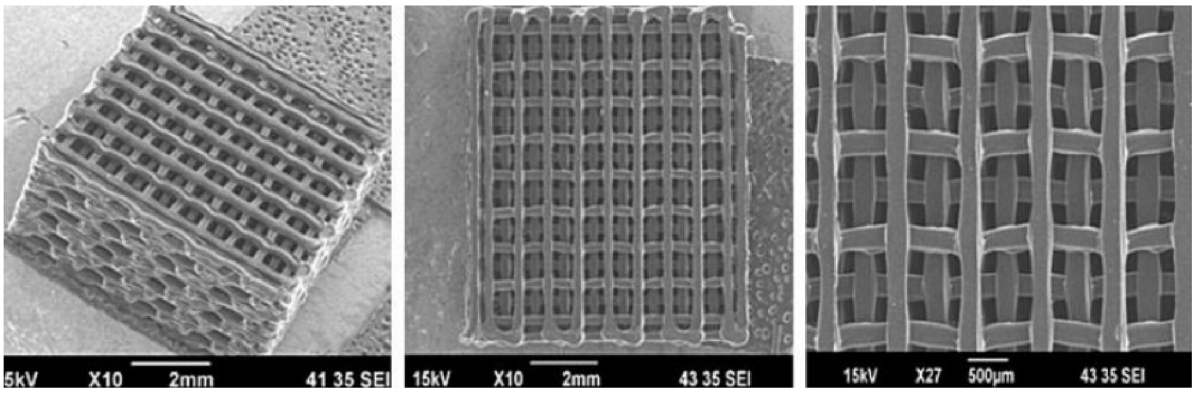

Figure 15: *SEM picture of PCL/PLGA scaffold [48]*

There are three basic tissue engineering strategies that are used to restore, maintain, or improve tissue function.

1. Cell transplantation
2. Scaffold-guided regeneration
3. Cell-loaded scaffold implantation

Cell transplantation involves the removal of healthy cells from a biopsy or donor tissue and then injecting the healthy cells directly into the diseased or damaged tissue. However, this technique does not guarantee tissue formation and generally has less than 10% efficiency. [28]

Scaffold-guided regeneration involves the use of a biodegradable scaffold implanted directly into the damaged area to promote tissue growth. An example of this technique involves a defect in bone where a 3D printed biodegradable scaffold in the shape of the defect is implanted.

Cell-loaded scaffold implantation involves at first the isolation of cells (e.g. stem cells) from a patient. As the example given can be again used a 3D printed biodegradable scaffold that is in this case seeded with cells and then implanted into the bone defect location. Prior to implantation, the cells can be multiplied in a bioreactor (*in vitro*) that mimics the real tissue environment (*in vivo*). An example of cell-loaded scaffold implantation strategy is presented in *Figure 16*.

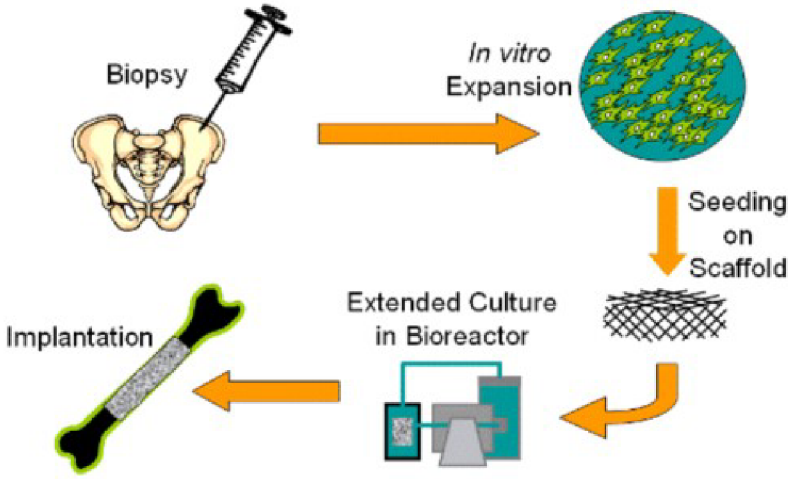

Figure 16: *Basic scheme of cell-loaded scaffold implantation [49]*

Looking back to the 1980s, researchers were already studying an approach to regenerate skin wounds, which resulted in a paper published in Science in 1982. This paper described the prompt and long term closure of full-thickness skin wounds in guinea pigs and humans, achieved by applying a bilayer polymeric membrane, composed of a top silicone layer and a bottom layer of a porous crosslinked network of collagen and glycosaminoglycan (GAG), seeded with a small number of autologous basal cells before grafting. This study was conducted following three main stages, today recognized by many researchers as the three main stages of tissue engineering approach which are as follows.

1. The development of the matrix (scaffold)
2. Seeding the matrix with cells, signals, growth factors etc.
3. Grafting the cell seeded matrix onto the tissue defect

As the result of the study it was demonstrated that, although the acellular matrices can also be used to regenerate skin defects, the cell-seeded ones provided a means for closing the largest full-thickness skin wounds in a shorter period of time. This system, based on a polymeric matrix obtained from two natural origin polymers, clearly opened the way to the concept of tissue engineering and further research in this field – to the regeneration of tissues using cells seeded onto a 3D matrix. [28]

2.3.2 Materials for scaffold fabrication

Several scaffolds based on natural origin polymers have been widely studied for tissue engineering application. Natural polymers have frequently been used in tissue engineering applications because they are either components of, or have properties similar to, the natural extracellular matrix (ECM). Tissue engineering scaffolds comprised of naturally derived macromolecules also exhibit unique advantageous features concerning biocompatibility, cell-controlled degradability and intrinsic cellular interaction. However, these materials do also exhibit some disadvantages that limit their widespread use. In many cases they exhibit a narrow and limited range of mechanical properties. No one material alone will satisfy all design parameters in all applications within the tissue engineering field, but a wide range of materials can be tailored for discrete applications.

Although extensive research has been performed with both types of polymers, synthetic polymers overall offer several advantages over natural polymers such as collagen and fibrin. They can be prepared in a reproducible manner in almost unlimited quantities, and their physical, chemical, and mechanical properties may be easily altered by chemical modifications. In addition, they can be easily processed with conventional polymer processing equipment. Dozens of synthetic biodegradable polymers have been used and developed for use as tissue engineering scaffold materials. It is mainly about materials that undergo surface hydrolysis (or erosion), because they tend to maintain their mechanical properties for an extended time span while they gradually degrade. In contrast, materials that undergo bulk hydrolysis (or erosion) absorb water and then break down abruptly and unanticipatedly, causing a rapid decrease in mechanical properties. The difference between bulk and surface erosion regarding the time-property dependences is presented in *Figure 17*.

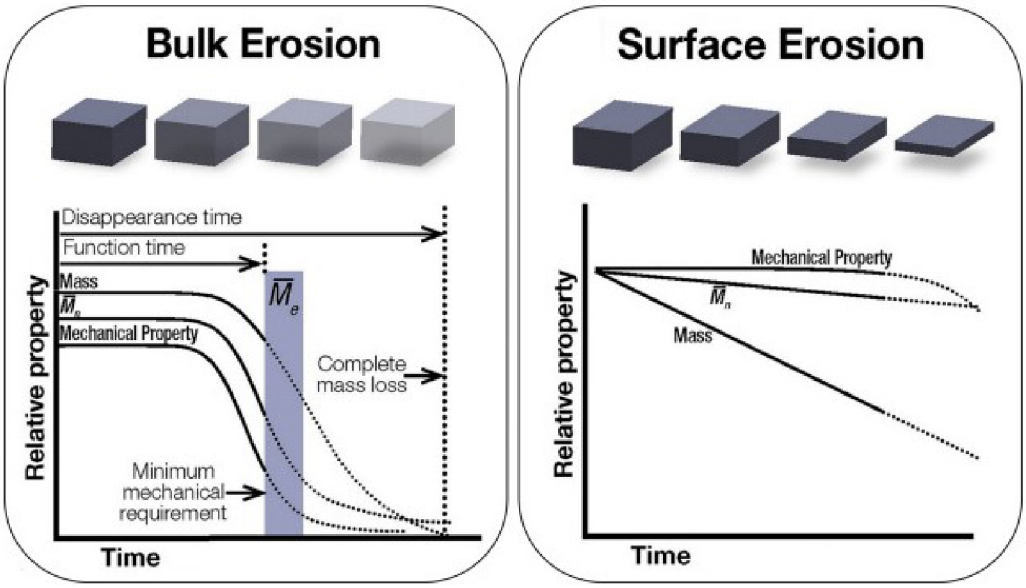

Figure 17: *Comparison of bulk and surface erosion [50]*

Synthetic biodegradable polymers that have traditionally been used as scaffolding materials for tissue engineering include polylactide (PLA), polyglycolide (PGA), and their copolymers, and polycaprolactone (PCL). All of these materials undergo bulk erosion, whereas materials like polyanhydrides (PAs) or polyhydroxyalkanoates (PHAs) undergo surface erosion. Although in general, the optimal degradation rate depends primarily on the specific application in TE so it is hard to assess if surface or bulk erosion is "better". The only important aspect regarding scaffolds is that the selected synthetic polymer should degrade at the same rate as the tissue forms. [35]

The material used for the polymeric scaffold must also exhibit good biocompatibility, meaning that it must not elicit an unresolved inflammatory response nor demonstrate extreme immunogenicity or cytotoxicity. For example, PLA hydrolyzes to lactic acid, which is a normal by-product of muscle contractions in animals. Although higher concentrations of lactic acid in the body can lead to lactic acidosis causing muscle ache, cramps or nausea. The lactic acid is then further metabolised through the tricarboxylic acid cycle and excreted as carbon dioxide (CO_2) and water. Nowadays synthetic biodegradable polymers may be even purposefully tailored to have specific degradation rates based on their composition (e.g., PLGA).

2.3.3 Scaffold properties

The demands placed on the material of the scaffold are high. The basic requirement is a suitable cellular response, but equally important are the mechanical and surface properties and structure. In the case of bone tissue, the material must also be osteoconductive, i.e. stimulating bone growth at the implant site, and osteoinductive, i.e. inducing osteogenic differentiation of local stem cells that are present in the bone marrow.

In order for the cells to grow through the entire volume of the scaffold and form new tissue, the scaffold must have a suitable 3D structure. Such properties include their general biocompatibility and biodegradability. The biocompatibility of natural polymers, e.g., allows for cell infiltration into the matrix. The biodegradability of the matrices may also assist the release of gene transfer agents into the surrounding environment and thus affect nearby cells.

Preferably, a scaffold should have the following characteristics:

(1) 3D and highly porous structure with an interconnected pore network

(2) biocompatible and bioresorbable with a controllable degradation and resorption rate

(3) suitable surface chemistry for cell attachment, proliferation, and differentiation

(4) mechanical properties to match those of the tissues at the site of implantation

(5) be able to be mass produced with consistent quality and without the use of organic solvents

Ideally, highly porous scaffolds are required to allow for cells to infiltrate and attach to the scaffold, to provide a high surface area-to-volume ratio with well-interconnected pore networks for polymer cell interactions, and to obtain minimal diffusion constraints during cell culture. When studying bone cells, it was found that bone cell growth increases with increasing porosity. Past research has stated that a scaffold porosity of greater than 90 % is important for tissue engineering applications. However, in fact, researchers have used scaffolds with porosities ranging from 30 % to 74 % for bone TE due to increased mechanical properties at lower porosities. The optimal pore size for tissue regeneration is dependent on the type of tissue. However, even for bone regeneration, no

consensus regarding the optimal pore size in scaffolds has been determined. Pore sizes ranging from 50 to 710 μm have been suggested for bone regeneration, with many studies stating macropores in the range of 200–350 μm are ideal. [38] Therefore, macropores on the order of hundreds of micrometres with an interconnecting network on the order of tens of micrometres have been deemed suitable for tissue regeneration.

At the same time, the effects of surface chemistry, mechanical properties, and degradation rate play a large role in tissue formation. The nature of the polymer surface can affect the ability of cells and proteins to attach to its surface, proliferate, and differentiate. Polymers like PLA, PGA and P3HB are relatively hydrophobic, and it is difficult to efficiently and evenly seed cells into porous matrices fabricated from these polymers.

The mechanical properties of the scaffold fabricated should closely match the mechanical properties of the tissues to be generated in order to provide support during the initial stages of tissue growth. If the mechanical properties such as compressive strength are too low, the scaffold could be deformed or crushed, leading to deformed tissue growth, or no tissue growth at all. On the other hand, if the compressive strength is too high, the cells may not be subjected to the proper *in vivo* conditions needed to support cell growth. Additionally, in load bearing instances, scaffold mechanical properties that exceed the surrounding bone may lead to "stress shielding," which is a condition where the surrounding bone experiences a decrease in density. Another parameter also important to consider is the elastic modulus of the scaffolds. Differences in elastic moduli between the scaffold and natural bone tissue can result in different amounts of strain at the same stress levels. This can cause delamination of the scaffold from the surrounding tissue.

The mechanical properties as well as the biodegradation process can be modified by crosslinking or by combination with inorganic compounds, e.g. hydroxyapatite (HAp). Collagen-HAp scaffolds were prepared with 99% cross-linking and excellent cell adhesion. HAp stimulates growth factors (e.g. bone morphogenetic protein). Furthermore, tricalcium phosphate (TCP) can be used to promote *in vivo* osteogenic differentiation of mesenchymal stem cells (MSCs). [51–54]

In order to produce affordable scaffolds for TE routinely, a complex manufacturing process must be developed. It is vital that the scaffolds can be fabricated in a consistent and cost-effective fashion so that researchers, surgeons, and patients alike will receive continuous supply of scaffolds with known properties and proven performance. [35]

2.3.4 Methods of scaffold fabrication

The properties and characteristics of the scaffolds used in TE are dependent not only on the type of materials used but also on the fabrication techniques. Each technique offers advantages and disadvantages in the form of control over pore morphology, ability to incorporate bioactive molecules, mechanical properties, and cost. Techniques that involve operating with heat, pressure and organic solvents significantly inhibit the use of incorporating cells and bioactive molecules. On the other hand, techniques that do not utilise heat or organic solvents may not be ideal for mass production of complex geometries and may not be cost-efficient.

A number of conventional manufacturing techniques for fabrication of porous 3D scaffolds were invented. These techniques include fibre bonding, phase separation, solvent casting, particulate leaching, membrane lamination, moulding, and foaming. However, all these methods share a common and unfortunate major drawback: they do not permit enough control of scaffold architecture, pore network, and pore size, producing inconsistent and "non-ideal" 3D scaffolds. While these techniques may be adequate and essential for studying the effects of the substrate material, porosity, pore size, interconnectivity of the pores, mechanical and chemical properties, they do not meet the requirement for cost-effective manufacturing and consistent continuous processes to meet patient needs.

To overcome these issues and to meet the demands of TE, various 3D printing methods for fabrication of customised scaffolds with controlled pore size and pore structure were introduced. Out of many different 3D printing techniques, fused deposition modelling (FDM), stereolithography (SLA), selective laser sintering (SLS), appeared to be the most popular. First of all, FDM 3D printing based on a computer-aided design (CAD) has allowed the production of complex 3D scaffolds with a controllable architecture and fully interconnected porous structure. It offers versatile fabrication inlay-down pattern and good structural integrity for production of 3D constructs with good mechanical and biological properties. [46] [6]

2.3.5 Bone tissue engineering

Bone damage is one of the most common health problems, and although human bones have a certain regenerative and self-healing ability, they are powerless for large bone defects as they are never completely reinstated, because their size is beyond the limit up to which they can repair. In these instances modern medicine is required. The treatment of large bone defects is still one of the challenges of orthopaedic surgery and there has been an increase in the incidence of major fractures in patients over 50 years of age in the European Union, with over 3 million fractures. [55]

The reconstruction of tissue generally involves the replacement of the damaged tissue with an autologous tissue of a different type. In the case of surgical repair, a second surgery is often needed to remove the fixation device, increasing costs and lengthening the recovery time. If new tissue could be created from the patient's own cells, it would alleviate the organ donor shortage problem, as well as reduce the chance of immune rejection and the introduction of foreign pathogens. Additionally, if the tissue or organ could be created from only a handful of cells, issues associated with donor site morbidity could also be addressed. Therefore, one of the most advanced approaches used to overcome the problems, bone tissue engineering was proposed. Bone tissue engineering aims to induce new tissue repairing and regeneration by the synergy of cells, signals and carriers (scaffolds).

In order for the cells to grow through the entire volume of the scaffold and form new tissue, the scaffold must have a suitable 3D structure. Currently, a relatively new method of FDM 3D printing, in which the product is created according to a precise digital 3D model, is being used with success, allowing complex shapes including porous internal structures to be produced in a time- and cost-effective manner. [52]

3 EXPERIMENTAL PART

The experimental part and the aim of this thesis can be divided into two subparts. The aim of the first subpart was the preparation of new composite materials and processing them into the form of filaments for 3D printing, optimisation of the printability conditions and their thermal and mechanical characterization. Finally, these materials underwent cytotoxicity testing in order to determine their usability for 3D printing in bone tissue engineering as scaffolds. The aim of the second subpart was to use the materials prepared in the previous research with the knowledge of their non-cytotoxic behaviour, to print scaffolds from them with different surfaces and then to evaluate the effect of the surface roughness and contact angle with water in order to achieve optimal cell adhesion and proliferation.

3.1 Preparation of materials

Five composite materials, in total, were used in the experimental part. Three materials were newly prepared and two materials were used from previous research. Two of the new materials were based on a plasticized blend of poly(3-hydroxybutyrate) (PHB) EDW 2394 from TianAn and polycaprolactone (PCL) Capa® 6500 from Perstorp. The third material was based on poly(3-hydroxybutyrate) produced by chloroform-free soap route (abbreviated as PHB-soap) [17] and amorphous poly(D,L-lactide) (PLA) Ingeo 4060D from NatureWorks. Syncroflex TM 3114 (oligomeric adipate ester, abbreviated as SF) from Croda was used as a plasticizer in the case of all three materials. Tricalcium phosphate blend (αTCP = 7 %, βTCP = 93 %, abbreviated as TCP) from CN Lab Nutrition was added to the matrix as a bioactive filler. The mean particle size of TCP was 10.8 μm measured by laser diffraction using HELOS analyzer by Sympatec GmbH. The composition of prepared biocomposites is given in *Table 2*. All samples were compounded using the corotating meshing twin screw extruder, from Labtech Engineering Company (D = 16 mm, and L/D = 40). The temperature setting of individual zones of the extruder was 80–180–180–180–180–175–170–160–160–160 °C from a hopper to a nozzle and the rotational speed of screw was set to 150 rev.·min^{-1}. The total weight of each sample for extrusion was 500 g.

The last two composite materials prepared in previous research were newly compounded, processed into the form of 3D printing filament and used for printing of specimens for the surface study and for comparison of corresponding mechanical properties with three newly prepared materials. It includes mechanical testing, optical contact angle measurement and surface roughness analysis by confocal microscopy. These materials are PHB/PLA-SF and PHB/PLA-SF-TCP. For in vitro tests, scaffolds were printed and moulded from the same two materials, but from the granulates and filaments prepared in 2020 (abbreviated as PHB/PLA-SF_2020 and PHB/PLA-SF-TCP_2020). These were chosen for printing of testing specimens with different surfaces (grid diameters), because they have already been proven not to be cytotoxic, thus non-affecting the ability of cells to proliferate in a negative way. [56]

Table 2: *The composition of prepared and used materials: the basic mixture was composed of 12 % of plasticizer and the remaining 88 % is PHB/PLA, PHB-soap/PLA or PHB/PCL in the ratio of 70/30. For filled samples, 15 wt. % of TCP was added to the mixture.*

	Amount (wt. %)				
Material	**PHB or PHB-soap**	**PLA**	**PCL**	**SF**	**TCP**
PHB/PLA-SF	62	26	0	12	0
PHB/PLA-SF-TCP	54	23	0	10	13
PHB-soap/PLA-SF	62	26	0	12	0
PHB/PCL-SF	62	0	26	12	0
PHB/PCL-SF-TCP	54	0	23	10	13

3.2 Preparation of 3D printing filaments

Granules of PHB-soap/PLA-SF, PHB/PCL-SF and PHB/PCL-SF-TCP prepared in the first step in Chapter 3.1 were processed using the HAAKE™ Rheomex OS single screw extruder (Haake Technik GmbH) into the form of 3D printing filaments. The chamber temperature profile from a hopper to a nozzle was set to 185–175–170–160 °C and the rotational speed of the screw was kept 20 rev.·min^{-1}. At first the filament was pulled through the water tank tempered to 60 °C. Secondly, the filament was directed to the draw-off device and wound onto a coil, passing through the air dryer and then to calibration unit in order to ensure a constant diameter of the filament of 1.75 mm.

3.3 Thermal characterisation of prepared materials

3.3.1 Differential scanning calorimetry (DSC)

DSC measurements were performed on DSC 2500 (TA Instruments). The samples of PHB-soap/PLA-SF, PHB/PCL-SF and PHB/PCL-SF-TCP granules and filaments were at first cooled to −30 °C and then subjected to two heating cycles to 200 °C with the heating rate of 10 °C·min^{-1}. All measurements were carried out under the nitrogen atmosphere. Aluminum pans with samples were hermetically sealed before the measurement and the polymer sample masses were approximately 10 mg. The crystallinity was calculated from DSC measurement according to the equation:

$$X_c = \frac{\Delta H_m}{\Delta H_m^0} \cdot 100\ (\%)$$

where ΔH_m, and ΔH^0_m (J/g) are the enthalpy of fusion from the second heating cycle and the enthalpy of fusion of 100% crystalline polymer (146 J/g for PHB and 139 J/g for PCL), respectively.

3.4 Optimisation of processing conditions and printability testing

Original Prusa i3 MK3S and MK3 FDM 3D printers from Prusa Research were used for printing of all specimens. The MK3S printer with a nozzle of diameter 0.25 mm was used for printing of specimens for optical contact angle measurement (OCA), surface roughness analysis and in vitro tests on scaffolds. The MK3 printer with a nozzle of diameter 0.4 mm was used for printing of specimens for temperature tower test, warping test, tensile test, three-point flexural test and compression test. Maximum printing space of both printers is 250 × 210 × 200 mm ($x \times y \times z$), the resolution of x and y axes is 10 μm and the resolution of z axis is 5 μm. The basic printing parameters of the MK3S and MK3 printers are given in *Table 3*.

An important 3D printing parameter is flow, which represents volume passed through the extruder over time. Proper setting of flow is necessary to ensure optimal density and compactness of 3D printed specimens and therefore meaningful mechanical properties. A crucial factor influencing 3D printing process related to flow and to which an attention therefore must be paid is the filament diameter. If the diameter is greater than needed 1.75 mm, the printer must feed an excessive material which leads to the deterioration of specimen's mechanical properties and surface or even to nozzle clogging. In contrast, if the filament is thinner than 1.75 mm, it will cause the specimen to be underfilled with empty spaces between individual perimeters. Correspondingly, an underfilled sample will exhibit unsatisfactory mechanical properties during testing. Therefore, a flow parameter, which both Prusa i3 MK3 and MK3S enable to alternate, was customised during printing of test specimens to avoid their underfilling immediately when visually spotted. Flow of the value 100 % was used for all samples. Exceptionally, flow was changed to 95 % when needed, as the prepared 3D printing filaments tend to be a little bit thicker than desired 1.75 mm.

Table 3: *Basic printing parameters of Prusa i3 MK3S and MK3 FDM 3D printers used for printing of all specimens*

Parameter	MK3S	MK3
Filament diameter	1.75 mm	1.75 mm
Nozzle diameter	0.25 mm	0.4 mm
Layer height	0.15 mm	0.2 mm
Width of printed layer	0.3 mm	0.45 mm
Perimeter printing speed	45 $mm \cdot s^{-1}$	45 $mm \cdot s^{-1}$
Fill print speed	200 $mm \cdot s^{-1}$	200 $mm \cdot s^{-1}$
Bed temperature	20 °C	20 °C
Cooling fan power	100 %	100 %

3.4.1 Temperature tower test (TTT)

3D printing filaments prepared in Chapter 3.2 were subjected to the tests designated to evaluate the printability and to determine optimal processing conditions. First of all, the temperature of the nozzle was optimised by the temperature tower test (TTT). In the TTT test, two towers, composed of several identical floors (usually five) containing different geometrical elements common in 3D printing, were printed. Each floor was printed with a temperature 5 °C higher than the previous floor. [57] This test enabled visual evaluation of the quality of the printed object depending on the printing temperature. As a result, a temperature interval comprising of three consecutive floor temperatures was chosen for each material to use in warping test (e.g. 175–185 °C).

3.4.2 Warping test

Secondly, warping was optimised based on the optimal printing temperatures retrieved from TTT. Warping is a negative phenomenon occurring during 3D printing when with increasing layers the specimen tends to bend upwards because the bottom layers are cooler than the upper layers which are still hot. In extreme cases, warping can cause printed object to detach from the bed, thus not completing the print. In the warping test, the specimen consists of a rectangle platform and with each successive layer one of its shorter sides was moved a little bit forward and above the previous layer making a V-shape. During printing, warping causes the front V-shaped side to lift and detach from the bed at purpose. The maximum printed height before the detachment is recorded and used for the calculation of the warping coefficient:

$$warping\ coefficient = \frac{theoretical\ height\ of\ warping\ test\ specimen\ (10\ mm)}{height\ of\ warping\ test\ specimen\ achieved\ during\ printing\ (mm)}$$

The results are shown as mean ± standard deviation (SD) from five testing specimens. The temperature used for printing showing the least warping coefficient is then chosen as the optimal for the printed material and used for all following printings in the future.

3.5 Compression moulding of testing specimens

3.5.1 Specimens for optical contact angle measurement (OCA) and for in vitro tests

The granules of all five used composite materials were compression moulded using a hydraulic laboratory press Qnubu Rosin Press (Qnubu). For compression moulding of each material 5 g of granulate was weighed and poured on the press plate where it was evenly distributed. Spacer grid with thickness 1 mm was used to determine final thickness of the plate. Bottom and top platform were heated equally to a temperature 190 °C and press plates were put between them. Moulding lasted 100 seconds under a pressure of 20 MPa. Press plates were removed and let to cool at a laboratory temperature for one minute. Finally, press plates were cooled rapidly under the running water until it was possible to remove the moulded plate.

3.6 3D printing of testing specimens

3.6.1 Specimens for tensile test

Standardised double-paddle testing specimens for tensile testing (dogbones 5A with cross section 4 × 2 mm, according to the CSN EN ISO 527-2) were printed from filaments of all five used materials. The G-code for 3D printing the dogbones was made by regular alternating of two layers. The first layer was formed by simple import of fabricated model to original PrusaSlicer software (Prusa Research) with adjusting the perimeters to form the entire neck of the dogbone and the second layer was formed manually by inserting infill parallel to the longest dimension of the dogbone. The development of this G-code is described in a separate article. [58] In the case of dogbones with PCL content, the bed was heated to 60 °C, in order to remove them more easily.

3.6.2 Specimens for three-point flexural test

Rectangular testing specimens for three-point flexural test with dimensions of 80 × 10 × 4 mm were printed from filaments of all five used materials. The G-code for 3D printing was created in original PrusaSlicer software (Prusa Research) so that the entire volume of the specimen was composed exclusively from perimeters. In the case of specimens with PCL content, the bed was heated to 60 °C, in order to remove them more easily.

3.6.3 Specimens for compression test

Rectangular testing specimens for compression with dimensions of 10 × 4 × 10 mm were printed from filaments of all five used materials. The G-code for 3D printing was created in original PrusaSlicer software (Prusa Research).

3.6.4 Specimens for optical contact angle measurement (OCA) and surface roughness analysis

Cubic testing specimens for optical contact angle measurement and for surface roughness analysis by confocal microscopy with dimensions of 10 × 10 × 10 mm were printed from filaments of PHB/PLA-SF and PHB/PLA-SF-TCP. The G-code for 3D printing was created in original PrusaSlicer software (Prusa Research). The top of the cube was designed in a way that the last top two layers created a grid (*Figure 18*). Parameter A was consistent throughout all the printings as it was determined by the diameter of the used nozzle which was still 0.25 mm. Parameter B was altered in a way so that grids with diameter 0, 50, 150 and 250 μm were formed.

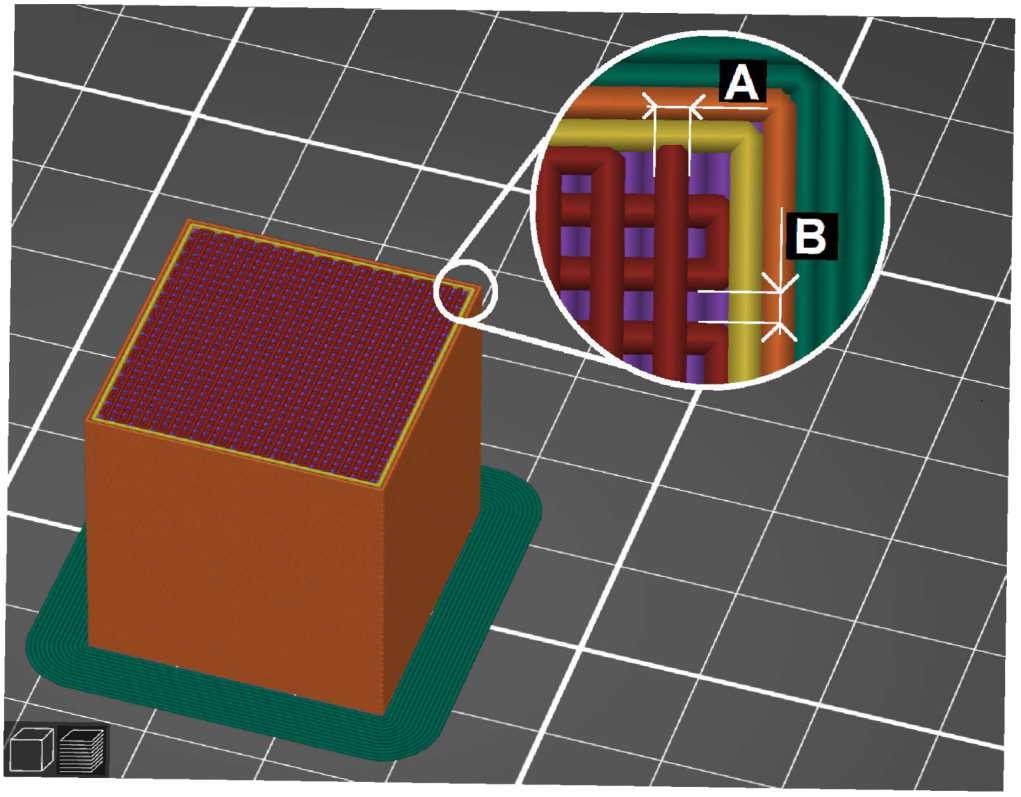

Figure 18: *3D printed testing specimen for OCA and roughness analysis depicted with corresponding dimensions*

3.6.5 Scaffolds for in vitro tests

Cylindrical testing specimens for in vitro tests with 6 mm in diameter and 1.5 mm in height were printed from filaments of materials PHB/PLA-SF_2020 and PHB/PLA-SF-TCP_2020. The G-code for 3D printing was created in original PrusaSlicer software (Prusa Research). The top of the scaffolds was printed in the corresponding way as cubic specimens for OCA and roughness analysis – altering parameter B (*Figure 18*) thus forming grids with diameter 0, 50, 150 and 250 μm. A total of 21 samples of each grid diameter was printed.

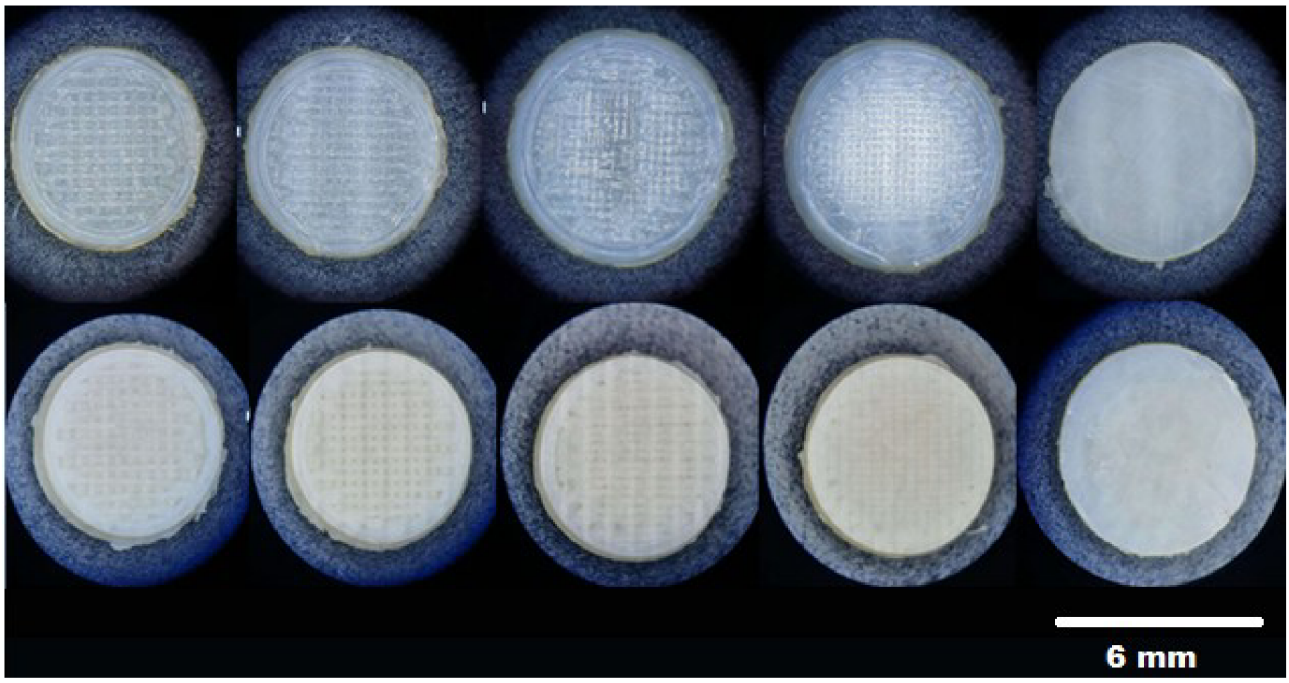

Figure 19: *An image of scaffolds used for in vitro tests, captured under an optical microscope, in order from left to right: 250, 150, 50, 0 μm grid diameters and moulded plate; PHB/PLA-SF_2020 up, PHB/PLA-SF-TCP_2020 down*

3.7 Mechanical testing

In the mechanical testing part, three tests were conducted – tensile test, three-point flexural test and compression test. All measurements were carried out 7 days after the sample preparation to ensure that the material crystallisation process is finished. The results of each test were determined as the average of at least six measurements and are shown as mean ± SD.

3.7.1 Tensile test

The Zwick-Roel Z010 (ZwickRoell GmbH & Co.) device with load indicator of maximum tensile force 1 kN and pneumatic grips with 2.5 kN maximum gripping force were used for the tensile testing measurements of all prepared materials performed according to the CSN EN ISO 527-2 standard method. The deformation rate for the determination of Young's modulus was set to 5 $mm \cdot min^{-1}$ and for the rest of the measurement to 50 $mm \cdot min^{-1}$. However, the Young's modulus was determined without the extensometer and from the deformation range of 0.25–0.50 %.

3.7.2 Three-point flexural test

The three-point flexural test of all prepared materials was performed according to the CSN EN ISO 178 standard method A. The Zwick-Roel Z010 (ZwickRoell GmbH & Co.) device with load indicator of maximum force 1 kN was used for the measurements. The radius of loading nose and supports was 5 mm, the support span was 64 mm. Preload force was set to 1 N. The flexural modulus was determined from the deformation range of 0.05–0.25 %. The test speed was set to 2 $mm \cdot min^{-1}$ and a limit deformation for the end of the measurement to 5 %.

3.7.3 Compression test

The compression test of all prepared materials was performed according to the CSN EN ISO 604 standard method. The Zwick-Roel Z010 (ZwickRoell GmbH & Co.) device with load indicator of maximum force 10 kN was used for the measurements. Preload was set to force 1 N. The compression modulus was determined from the deformation range of 1.25–1.50 %. The test speed was set to 1 $mm \cdot min^{-1}$ and a limit deformation for the end of the measurement to 10 %.

3.8 Characterisation of specimen surface

3.8.1 Surface energy evaluation

The specimens measured to calculate surface energy were moulded plates prepared as described in Chapter 3.5.1. The purpose of measuring different moulded materials was to determine the hydrophilicity or hydrophobicity and surface energy as they are important properties affecting cell proliferation on seeded scaffold.

For calculation of surface energy, including its dispersive and polar component from contact angles and their standard deviations, the OCA measurement of moulded samples on OCA 10 (Dataphysics) using SCA2000 software was performed. Four liquids were used for the measurement – water, diiodomethane, formamide and diethylene glycol. An image of each individual drop was taken by camera and then the contact angle was calculated from it by interleaving of the sphere. The results were determined as the average of at least ten drops, and are shown as mean ± SD. OWRK method (Owens, Wendt, Rabel and Kaelble) was used. Water results according to Rabel, diiodomethane results according to Owens et. al, formamide results according to Rabel and diethylene glycol results according to Erbyl, were added to the method.

3.8.2 Water contact angle measurement

The specimens measured were cubes prepared as described in Chapter 3.6.4 with grid diameter 0, 50, 150 and 250 μm. The purpose of measuring 3D printed specimens with different grid diameters was to characterise the effect of scaffold surface contact angle with water and its roughness on cells proliferation when seeded with cells and/or growth factors in tissue engineering.

The measurement of contact angle with water was performed by OCA measurement on OCA 15 (Advex Instruments) using SeeSystem software for evaluation of results. Water was the only liquid used for the measurement since the human body is composed mostly of it. An image of each individual drop was taken by camera and then the contact angle was calculated from it by interleaving of the sphere. The results were determined as the average of at least ten drops, and are shown as mean ± SD.

3.8.3 Surface roughness analysis

The surface roughness analysis was performed using confocal microscope OLS 3000 (Olympus). The specimens measured were cubes prepared as described in Chapter 3.6.4 with grid diameters 0, 50, 150 and 250 μm. An image of the surface was analysed with LEXT software to determine surface roughness (R_a). However, two different types of roughness depending on the sample orientation were measured. These include roughness along the printed perimeter (abbreviated roughness along) and roughness over the top first and second layer on the surface (abbreviated roughness over – both in *Figure 20*). For roughness along magnification 20× was used, in contrast to roughness over for which magnification 10× was used. Brightness was set to 400 units and filter for semisphere was used for each measurement, except for roughness along where the measurement was made without a filter. The results were determined as the average of at least six measurements, and are shown as mean ± SD.

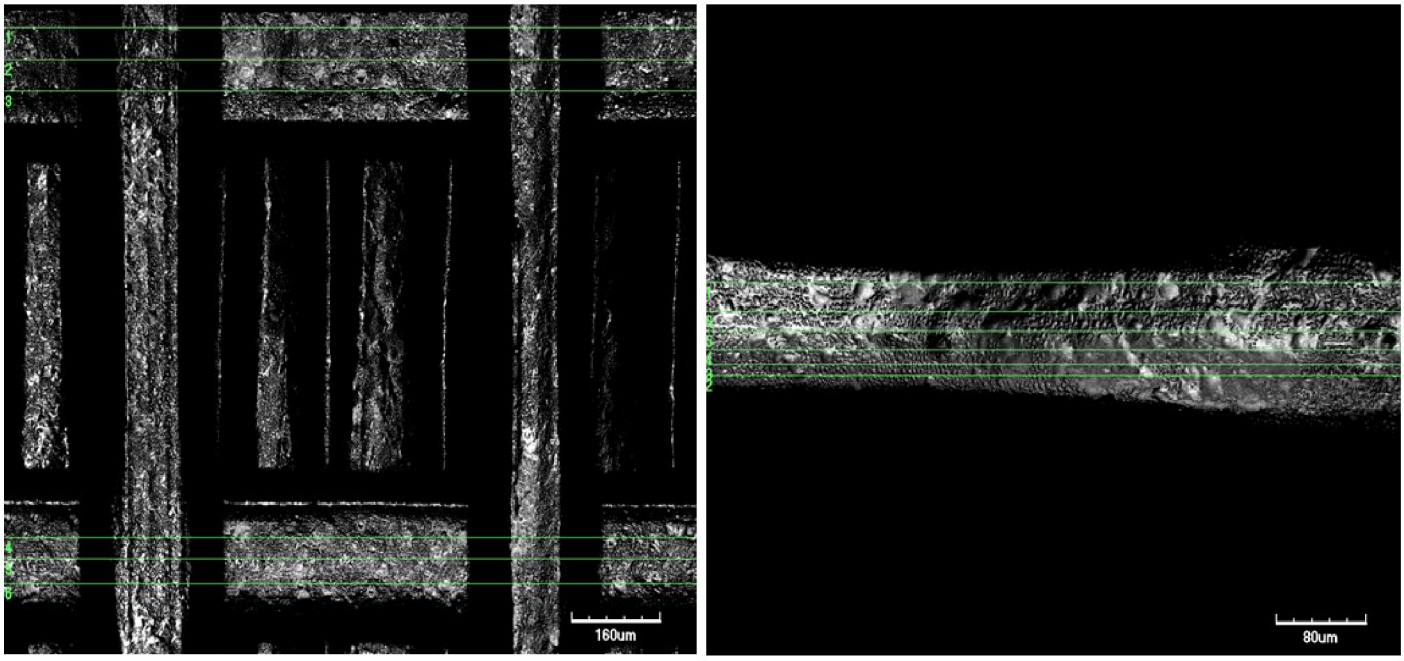

Figure 20: *An image of roughness over (left) and roughness along (right) parameters measured by confocal microscopy*

3.9 In vitro tests on scaffolds

In vitro tests on scaffolds were conducted in collaboration with the Institute of Experimental Medicine, Czech Academy of Sciences. These tests were done to find out whether the three newly prepared materials are non-cytotoxic (part cytotoxicity measurement), so they can be used in tissue engineering and to determine which grid diameter is the most optimal for cell proliferation (part evaluation of cell adhesion on different surfaces). Specimens in both parts were subjected to metabolic activity assay, DNA quantification and cell visualisation. As these tests were conducted at the Institute of Experimental Medicine, the testing processes and conditions are, for the purposes of this thesis, abridged and the complete reports are for seen in the appendices.

3.9.1 Cytotoxicity measurement

Granules of prepared composite materials − PHB-soap/PLA-SF, PHB/PCL-SF and PHB/PCL-SF-TCP – were packed, sterilised with ethylene oxide (Veterinary University Brno) and sent to the Institute of Experimental Medicine. As a control sample cells seeded on tissue culture plastic in the same density were used. Tissue culture plastic is optimised for cell adhesion and growth, so it is normal, when values measured on samples are the same or lower.

3.9.2 Evaluation of cell adhesion on different surfaces

A total of 21 round samples from materials PHB/PLA-SF_2020 and PHB/PLA-SF-TCP_2020 with diameter 6 mm were stamped from moulded samples (plates) prepared by hydraulic pressing as described in Chapter 3.5.1. Another 21 samples used for the test were samples with different grid diameters 250, 150, 50 and 0 μm as described in Chapter 3.6.5. Materials PHB/PLA-SF_2020 and PHB/PLA-SF-TCP_2020 were used, because their non-cytotoxicity was proven in the previous research. All the specimens were sterilised using ethylene oxide (Veterinary University Brno) and sent to the Institute of Experimental Medicine, Czech Academy of Sciences. An overview of all scaffolds measured is given in *Figure 21*. As a control sample were used cells seeded on tissue culture plastic in the same density. In contrast to cytotoxicity measurement, lower cell seeding density was used this time, because of better visualisation of cell adhesion by confocal microscopy.

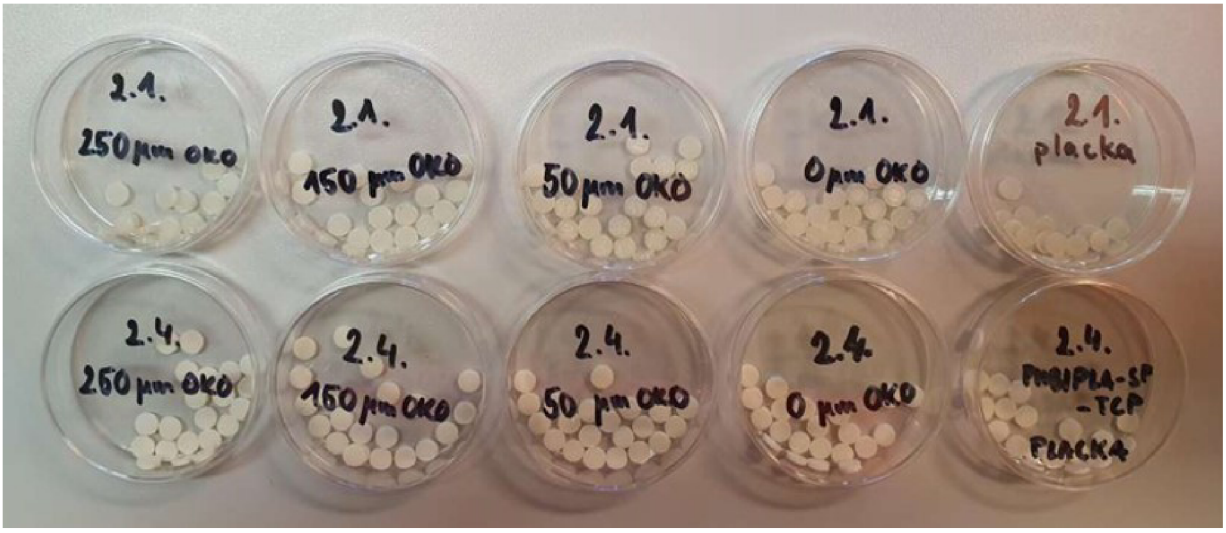

Figure 21: *An image of scaffolds with different surfaces prepared to be shipped to Institute of Experimental Medicine, in order from left to right: 250, 150, 50, 0 μm grid diameters and moulded plate; PHB/PLA-SF_2020 up, PHB/PLA-SF-TCP_2020 down*

3.9.3 Metabolic activity assay

Metabolic activity assay was used to probe cell metabolic activity. The principle of the process is that the MTS substrate is metabolised by mitochondrial enzymes to violet formazan, which absorbs light at 490 nm. This test is not only qualitative but also quantitative, because the more cells there are, the more of the substrate is metabolised, so the more of fluorescent formazan is produced, which results in the higher absorbance measured.

3.9.4 DNA quantification

Quantification of DNA was used to determine cellular proliferation. The principle of the process is that cell lysate retrieved from samples in a reagent solution binds to double strand DNA cells and emits fluorescent signal assessable by absorbance measurement. This test provides the information about the total number of cells including those which died during the test, because these could grow at first, but later could die as the measured material could be cytotoxic.

3.9.5 Visualisation of cells

As the last step, visualisation of cells was carried out. In the case of cytotoxicity measurement optical microscopy was used and in the case of visualisation of cells adhesion on scaffolds confocal microscopy was done using fluorescent staining, which makes cells fluorescing under the wavelength 490 nm.

4 RESULTS AND DISCUSSION

4.1 Properties of prepared materials

4.1.1 Differential scanning calorimetry (DSC)

To evaluate thermal properties of three newly prepared materials – PHB-soap/PLA-SF, PHB/PCL-SF and PHB/PCL-SF-TCP – differential scanning calorimetry (DSC) was conducted. Every material was measured in the form of granulate and prepared 3D printing filament. In the case of granulate "_G" was added at the end of the specimen name and in the case of filaments "_F" was added. Crystallisation temperature (T_c) and crystallinity (X_c) of PHB is shown in *Figure 22*. Crystallisation temperature (T_c) and crystallinity (X_c) of PCL is shown in *Figure 23*. Measured melting temperature (T_m) of both PHB and PHB-soap was in the interval between 168.2–169.7 °C and of PCL in the interval between 52.0–54.2 °C, so for this reason the melting temperatures are not presented in graphes.

Crystallinity of PHB-soap in both granulate and filament form, does not change significantly (only by 0.9 % – *Figure 22*). Also melting and crystallisation temperatures of PHB-soap does not change, thus the process of the preparation of 3D printing filament from granulate by extrusion does not have an impact on PHB-soap/PLA-SF thermal properties.

Focusing on material PHB/PCL-SF, the PHB has greater crystallinity in both granulate and filament form compared with PHB-soap (*Figure 22*), even though the crystallisation temperatures in PHB/PCL-SF_G are comparable with PHB-soap/PLA-SF in both forms. The major difference comes in the PHB crystallisation temperature of PHB/PCL-SF when in filament form as it rises by almost 10 °C. This could have resulted in greater crystallinity compared with granulate, however, it declines. This may be caused by a great growth of crystallisation temperature of PCL in the blend by 26.2 °C (*Figure 23*) which could have caused an increase of PCL crystallinity at the expense of PHB crystallinity.

Moving to PHB/PCL-SF-TCP, the PHB in this case has the greatest crystallinity of all blends (*Figure 22*) and its crystallisation temperatures in both granulate and filament forms are comparable with PHB/PCL-SF_F. The major difference this time is that the crystallinity of PHB declines by almost 20 % with the process of preparation of 3D printing filament from granulate, compared to roughly 9 % with the same process for PHB/PCL-SF. At the same time the crystallisation temperature even slightly decreases by approx. 2 °C by this process (compared to 10 °C rise in case of PHB/PCL-SF) and still the PCL crystallisation temperature of PHB/PCL-SF-TCP blend increases by 27.5 °C which could have resulted in a great increase of PCL crystallinity by 37.8 %, yet again, probably at the expense of PHB crystallinity.

In conclusion, all of the measured thermal properties (T_m, T_c and X_c) of PHB-soap/PLA-SF are not influenced by the process of preparation of 3D printing filament as they all barely change. Comparing properties of PHB-soap and commercial PHB, it is clear that only in the case of PHB/PCL-SF_G blend T_c is comparable to that in both PHB-soap/PLA-SF granulate and filament form. In other blends T_c is greater by approximately 10 °C than of PHB-soap. Also in all other blends with commercial PHB crystallinity (X_c) always takes greater values than of PHB-soap.

In PHB/PCL blends, the extrusion process of 3D printing filaments of PHB/PCL-SF decreases PHB crystallinity compared to granulate form, while at the same time PCL crystallinity increases. The process of filament extrusion (stretching) probably affects nucleation and therefore causes this trend. This also applies for PHB/PCL-SF-TCP, where the same trend as in the case of PHB/PCL-SF is observable, but TCP rather inhibits this effect, because PCL in PHB/PCL-SF-TCP has lower crystallinity and PHB higher than in PHB/PCL-SF.

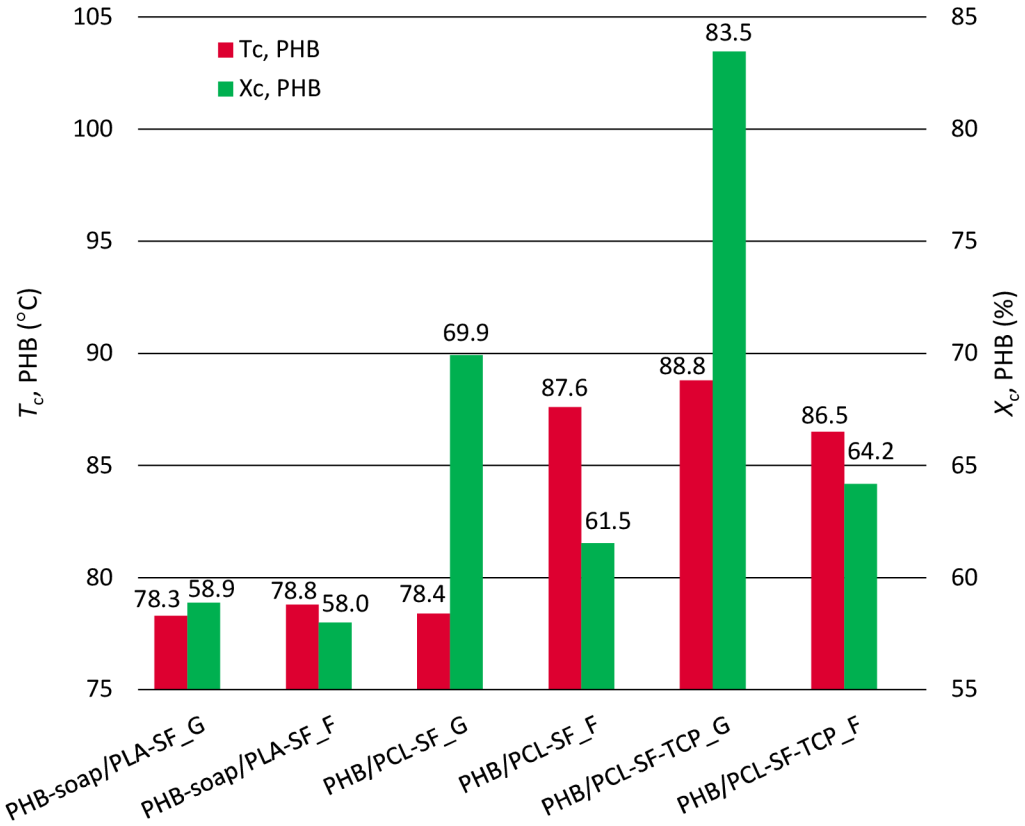

Figure 22: *Graph of crystallisation temperature (T_c) and crystallinity (X_c) of PHB*

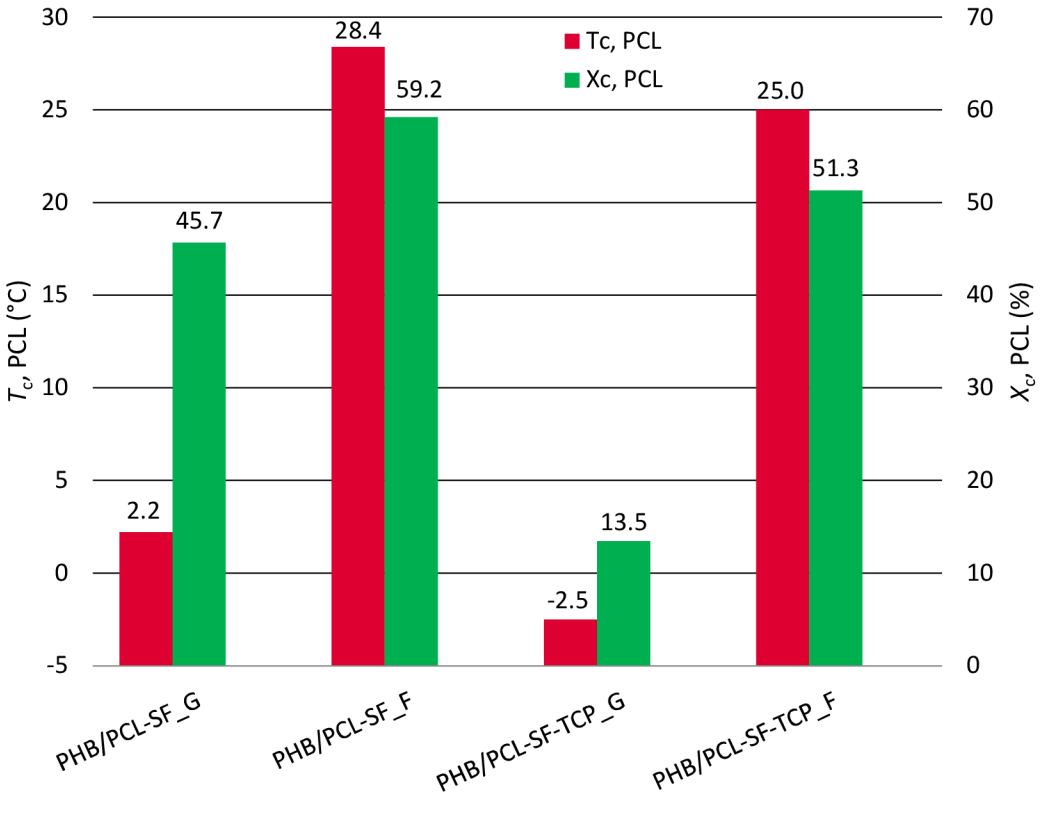

Figure 23: *Graph crystallisation temperature (T_c) and crystallinity (X_c) of PCL*

4.2 Optimisation of processing conditions and printability testing of prepared 3D printing filaments

To determine the processing conditions and printing temperatures for 3D printing of materials PHB-soap/PLA-SF, PHB/PCL-SF and PHB/PCL-SF-TCP temperature tower test (TTT) and warping test were conducted.

4.2.1 Temperature tower test (TTT)

In the temperature tower test, three temperature towers with six floors each were printed. All the results of TTT are presented in *Table 4* and *Table 5*. An example of 3D printed temperatures towers is shown in *Figure 24*. Temperature range of the first tower was 220-195 °C, of the second tower 195-170 °C and of the third 175-150 °C starting with the lowest temperature from the range at the bottom, gradually increasing to the highest temperature at the top. At first, the range of applicable temperatures from each tower was determined (*Table 4*) and finally, considering also the quality of printed geometric elements on the tower, the best temperature (or range of the best temperatures) for 3D printing was chosen (*Table 5*).

Table 4: *The results and evaluation of temperature tower test (TTT)*

Material	Temperature range (°C)	Last printed floor (°C)	Range of applicable temperatures (°C)
PHB-soap/PLA-SF	220–195	195	210–195
	195–170	170	195–170
	175–150	160	175–165
PHB/PCL-SF	220–195	195	–
	195–170	170	–
	175–150	165	–
PHB/PCL-SF-TCP	220–195	195	–
	195–170	170	–
	175–150	165	–

Table 5: *Floor/floors with the best printed geometric element within a single tower*

Material	Temperature range (°C)	Stringing	Colonnade	Diagonal	Holes in structure	Best temperature (°C)
PHB-soap/PLA-SF	220–195	–	–	–	–	–
	195–170	185–170	185–170	170	185–170	175–170
	175–150	175–165	175–170	170	175–165	175–170
PHB/PCL-SF	220–195	–	–	–	–	–
	195–170	–	–	–	–	–
	175–150	170	170	170	170	170
PHB/PCL-SF-TCP	220–195	–	–	–	–	–
	195–170	–	–	–	195–170	170
	175–150	–	–	165	175–165	165

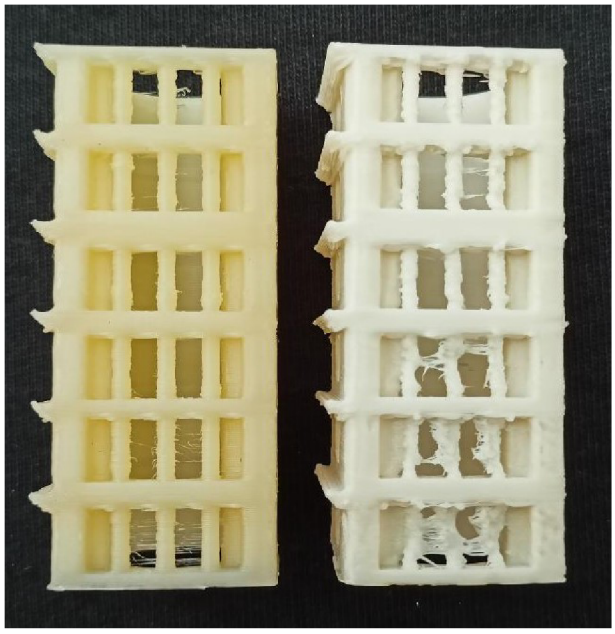

Figure 24: *An image of 3D printed temperature towers of PHB-soap/PLA-SF (temperature range 195–170 °C) with optimal quality of printed elements on the left and PHB/PCL-SF-TCP (temperature range 220–195 °C) with nonoptimal quality of printed elements on the right*

The best temperature (or temperatures) for 3D printing of PHB-soap/PLA-SF by temperature tower test (TTT) was determined on 175-170 °C, of PHB/PCL-SF on 170 °C, and of PHB/PCL-SF-TCP on 170-165 °C. These temperatures were then used for warping test.

4.2.2 Warping test

For the warping test the temperature (or temperatures) deemed as the best from TTT and one or two other temperatures 5 °C above and below it (or them) were used to the maximum number of three temperatures. The results of the warping test are given in *Table 6*. In the case of a warping test, the smaller the warping coefficient is, the better (in *Table 6* the smallest coefficients are highlighted in green). Considering all the results from TTT and warping test, the final processing conditions for three prepared composite materials, namely temperature, were 195/175 °C for PHB-soap/PLA-SF, 195/175 °C for PHB/PCL-SF and 195/165 °C for PHB/PCL-SF-TCP. First temperature of the pair was used to print the brim and first layer of the specimen and second temperature was used to print all other remaining layers.

The flow parameter was not optimised as part of this thesis though, and based on the results of printability tests of materials PHB/PLA-SF and PHB/PLA-SF-TCP from the previous research, the flow was set on 100 % for printing of all materials.

Unfortunately, for PHB-soap/PLA-SF a difficulty, when printing specimens for compression test, occurred. The temperature of 175 °C used for printing of these specimens was not high enough to print the specimens properly and some of them even at all. For this reason, processing temperature was altered until compliant extrusion of filament was achieved. Therefore a new warping test took place, evaluating the temperature of 190 °C as the new best for the printing of this material (thus only the second warping test of PHB-soap blend is presented in *Table 6*). This problem was caused by the fact that the specimens with bigger dimensions (e.g. dogbones for tensile test and specimens for flexural test) compared with specimens with smaller dimensions (compression test) suffice with lower processing temperature in order to be completed successfully. Usually, the printing temperature is suitable for printing of big and small specimens likewise, but in the case of PHB-soap blend it was necessary to raise it. Therefore, the final processing conditions for PHB-soap/PLA-SF were 195/190 °C, flow 100 %, fan disabled and speed of printing 80 % (to give printed layer enough time to cool down before printing the following layer).

Table 6: *The results of warping test (the lowest warping coefficients highlighted in green)*

Material	Temperature (°C)	Average warping coefficient ± SD (-)
PHB-soap/PLA-SF	190	2.59 ± 0.08
	185	3.06 ± 0.11
PHB/PCL-SF	175	1.26 ± 0.02
	170	1.30 ± 0.02
	165	1.55 ± 0.03
PHB/PCL-SF-TCP	175	1.81 ± 0.04
	170	1.65 ± 0.03
	165	1.53 ± 0.03

4.3 Mechanical properties

To evaluate mechanical properties of three newly prepared materials – PHB-soap/PLA-SF, PHB/PCL-SF and PHB/PCL-SF-TCP – tensile testing, three-point flexural test and compression test were conducted. Materials prepared as a part of previous research – PHB/PLA-SF and PHB/PLA-SF-TCP – were also subjected to the tests to evaluate the influence of interchange of PLA to PCL in their respective PHB blends on mechanical properties.

4.3.1 Tensile test

All the results of the tensile test are depicted in graph in *Figure 26* and the rest in *Table 7*. Stress-strain curves are shown in *Figure 25*.

Focusing on PHB/PLA blends, PHB/PLA-SF shows greater tensile strength and elongation at break, but lower Young's modulus than PHB/PLA-SF-TCP. Blend PHB/PLA-SF has even the greatest tensile strength (47.3 MPa) of all specimens measured. These results correspond with PHB/PCL blends, where PHB/PCL-SF shows greater tensile strength and significantly greater elongation at break (over 100 % vs. 5.6 %), while at the same time lower Young's modulus than PHB/PCL-SF-TCP. However, tensile strength and Young's modulus of both PHB/PCL blends are considerably lower than their PHB/PLA counterparts. On the other hand, elongation at break increases, most notably in the case of PHB/PCL-SF. Last but not least, PHB-soap/PLA-SF blend shows very similar tensile strength to PHB/PLA-SF-TCP while Young's modulus and elongation at break are similar to PHB/PLA-SF.

Concluding, in the case of both PHB/PLA and PHB/PCL blends, the addition of TCP to the blend lowers the tensile strength (by 11.2 % in the case of PHB/PLA blends and by 10.5 % in the case of PHB/PCL blends) and ductility of the blend as it performs the function of the concentrator of stress while the Young's modulus increases as it is usual with fillers (by 11.1 % in the case of PHB/PLA blends and by 28.6 % in the case of PHB/PCL blends). PHB/PCL blends compared to their PHB/PLA counterparts do not reach such qualities, maybe because the PCL is more ductile at room temperature than PLA due to its lower glass transition temperature (T_g) of −60 °C compared to 60 °C of PLA, which causes also the specimens to be more ductile. PHB-soap/PLA-SF blend has similar tensile properties as PHB/PLA blends with commercial PHB, so the different process of PHB extraction did not interve the tensile mechanical properties.

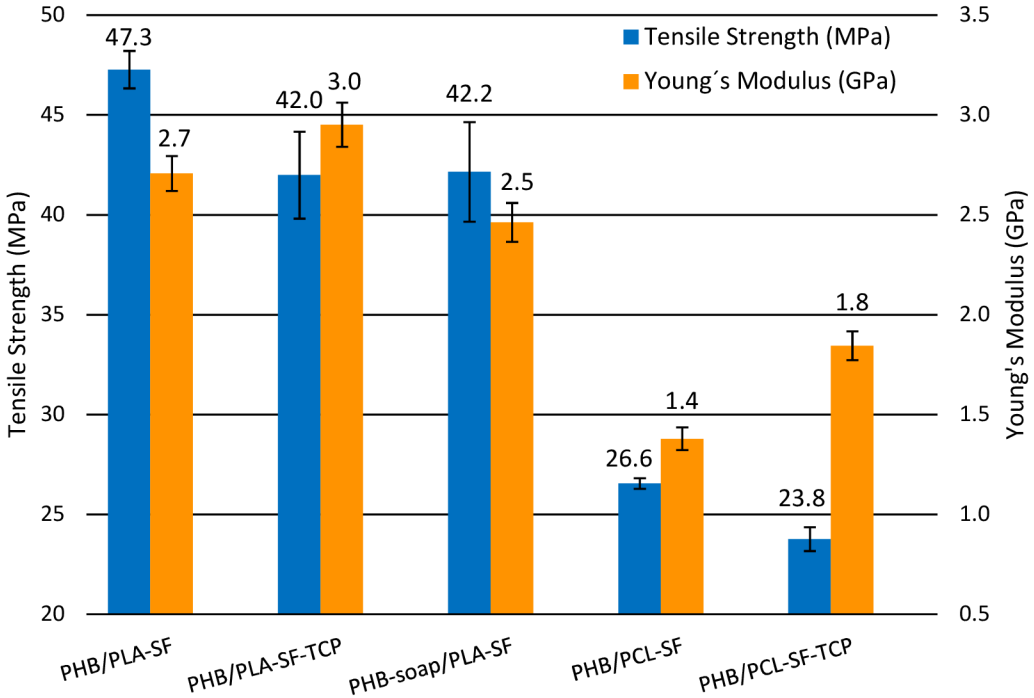

Figure 26: *The results of tensile test of 3D printed dogbones*

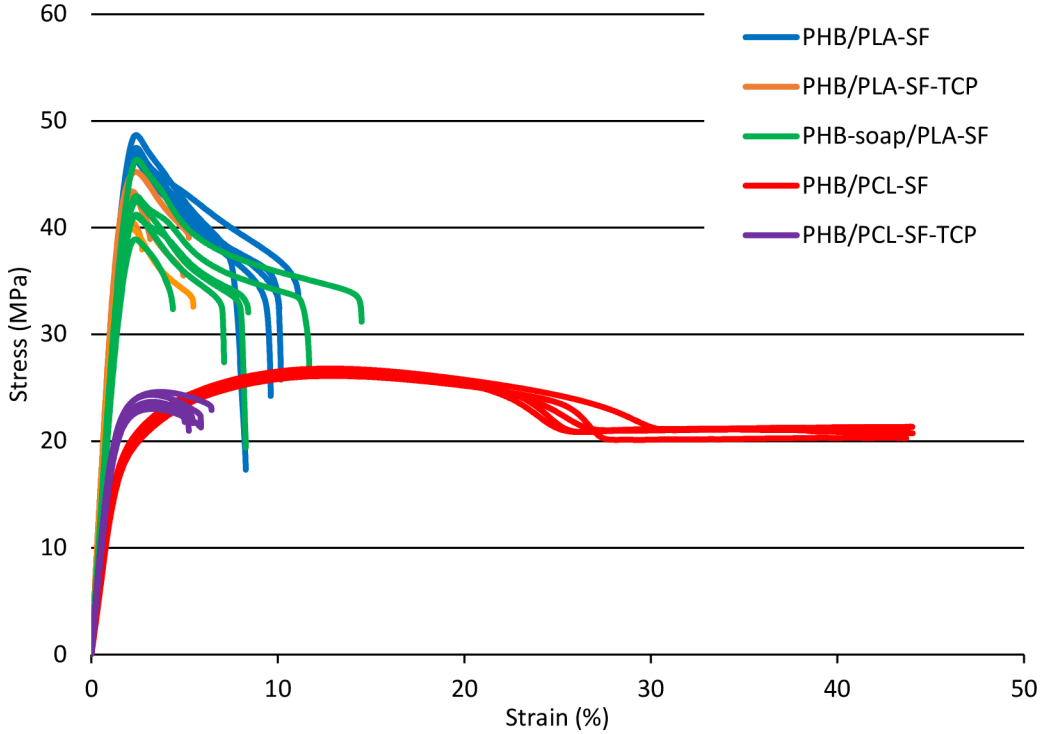

Figure 25: *Stress-strain curves of measured specimens*

Table 7: *Elongation at break results for tensile test*

Material	Elongation at break ε_m (%)
PHB/PLA-SF	9.9 ± 1.0
PHB/PLA-SF-TCP	4.0 ± 1.4
PHB-soap/PLA-SF	9.1 ± 3.6
PHB/PCL-SF	> 100
PHB/PCL-SF-TCP	5.6 ± 0.5

4.3.2 Three-point flexural test

All the results of the flexural test are depicted in graph in *Figure 28* and stress-deformation curves are shown in *Figure 27*.

Focusing on PHB/PLA blends, PHB/PLA-SF-TCP shows greater flexural strength as well as flexural modulus than PHB/PLA-SF (40.4 MPa vs. 36.8 MPa and 2.0 GPa vs. 1.5 GPa). Even though this time, compared to the tensile test, both of the measured properties rose, the results again correspond with PHB/PCL blends as the flexural strength and modulus of blend with TCP increase even almost by the same values as with the addition of TCP to PHB/PLA-SF. In the case of PHB/PLA blends the flexural strength rises by 3.6 MPa, which is by 9.8 % and flexural modulus by 0.5 GPa, which is by 33.3 %, with the addition of TCP to the blend. In the case of PHB/PCL blends, flexural strength rises by 2.6 MPa, which is by 11.1 % and flexural modulus by 0.4 GPa, which is by 36.4 %, with the addition of TCP to the blend. On the other hand, flexural strength and modulus of PHB/PCL blends are again considerably lower than their PHB/PLA counterparts. Correspondingly to the tensile test, PHB-soap/PLA-SF show similar flexural strength and flexural modulus as materials PHB/PLA-SF and PHB/PLA-SF-TCP.

Concluding, in the case of both PHB/PLA and PHB/PCL blends, the addition of TCP to the blend increases the flexural strength and modulus of the blend as it reinforces the specimen against bending stress. PHB/PCL blends compared to their PHB/PLA counterparts again do not reach such mechanical properties and qualities, although the differences between the blends are of the smaller extent contrary to the tensile test. PHB-soap/PLA-SF blend has similar flexural properties as PHB/PLA blends with commercial PHB, so the different process of PHB extraction did not interve nor the flexural mechanical properties.

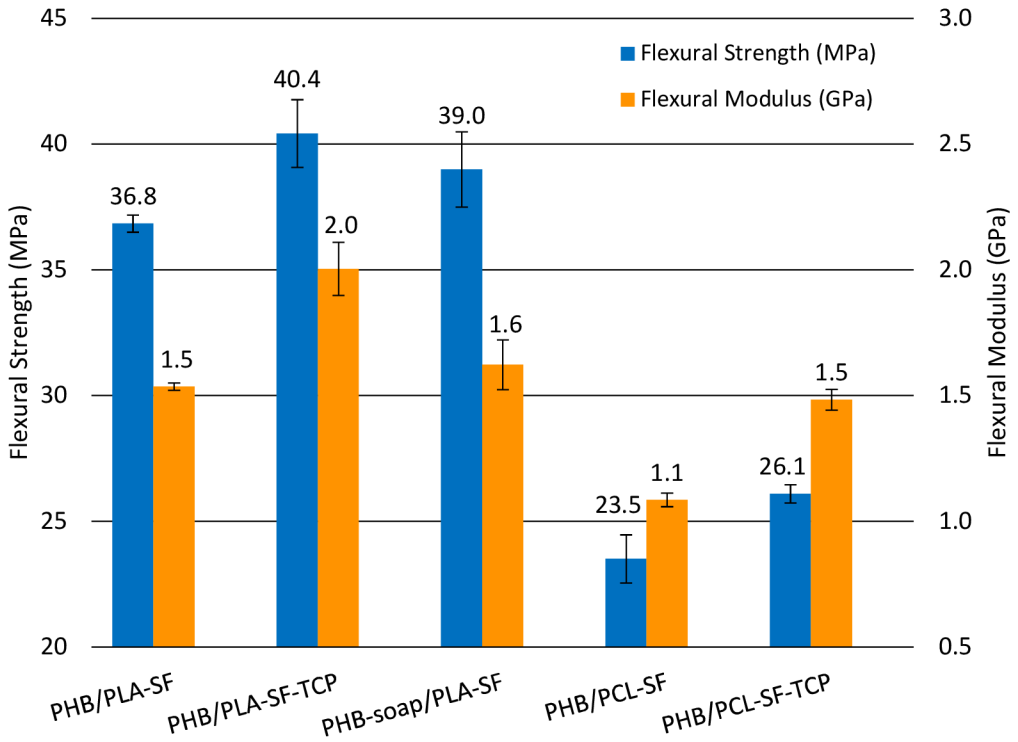

Figure 28: *The results of three-point flexural test of 3D printed specimens*

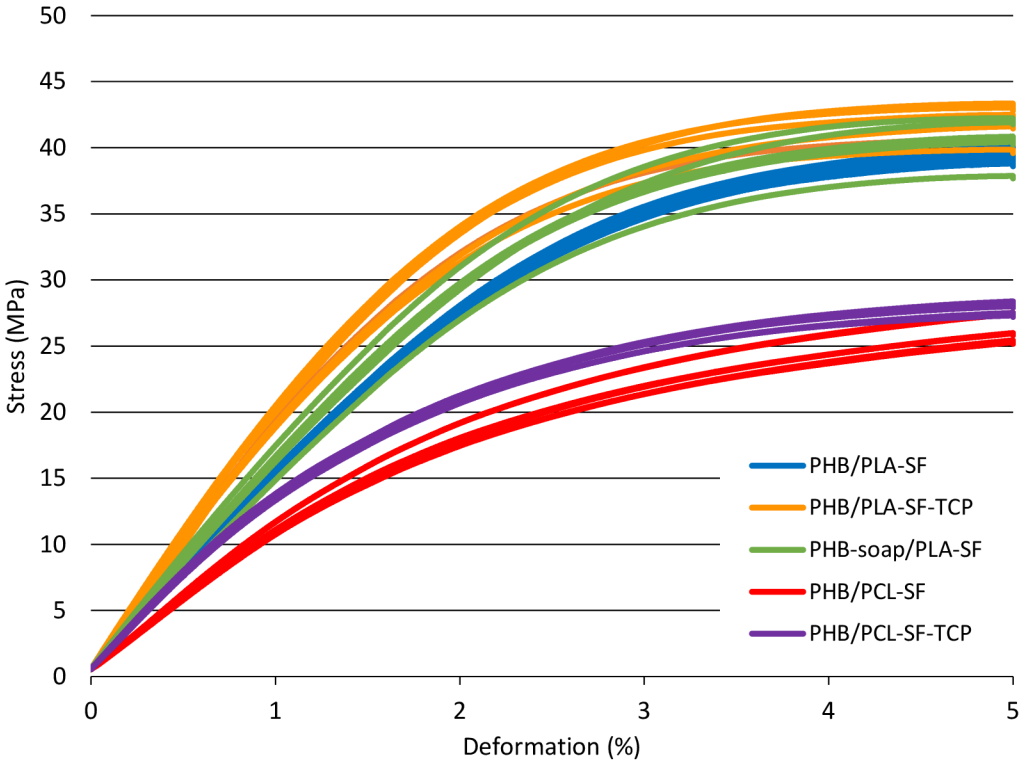

Figure 27: *Stress-deformation curves of measured specimens*

4.3.3 Compression test

All the results of the compression test are depicted in graph in *Figure 29* and stress-deformation curves are shown in *Figure 30*.

Looking at PHB/PLA blends, PHB/PLA-SF-TCP blend, as well as in the case of three-point flexural test, shows greater compressive strength and modulus than PHB/PLA-SF (48.1 MPa vs. 44.7 MPa and 1.2 GPa vs. 0.8 GPa). These results yet again correspond with PHB/PCL blends as the compressive strength and modulus rise with the addition of TCP to the blend. In the case of PHB/PLA blends the compressive strength rises by 3.4 MPa, which is by 7.6 % and compression modulus by 0.4 GPa, which is by 50 %, with the addition of TCP to the blend. In the case of PHB/PCL blends compressive strength rises by 2.8 MPa, which is by 18.5 % and compression modulus by 0.1 GPa, which is by 33.3 %, with the addition of TCP to the blend. Though again mechanical properties of PHB/PCL blends are significantly lower than of PHB/PLA blends (*Figure 29*). PHB-soap/PLA-SF, also in the compression test, shows similar mechanical properties as materials PHB/PLA-SF and PHB/PLA-SF-TCP.

Concluding, the addition of TCP to the blend, regardless of whether it is PHB/PLA or PHB/PCL, increases the compressive strength and compression modulus of the blend as it reinforces the specimen against pressure. PHB/PCL blends compared to their PHB/PLA counterparts do not reach such mechanical properties and qualities, and PHB-soap/PLA-SF blend has very similar mechanical properties as PHB/PLA blends with commercial PHB.

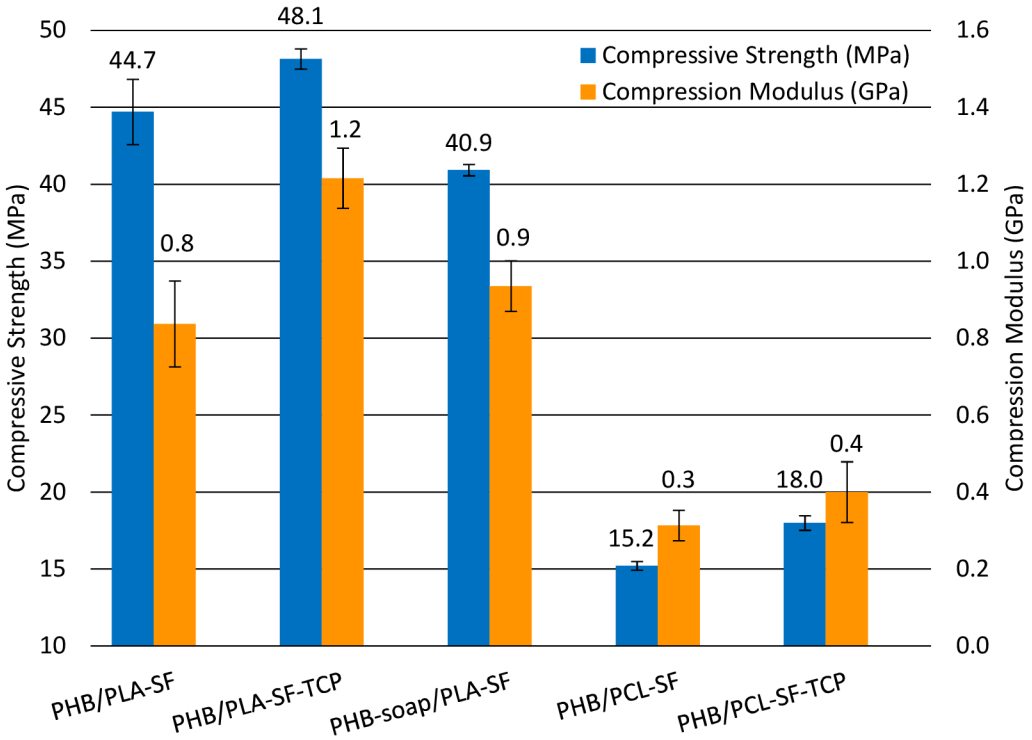

Figure 30: *The results of compression test of 3D printed specimens*

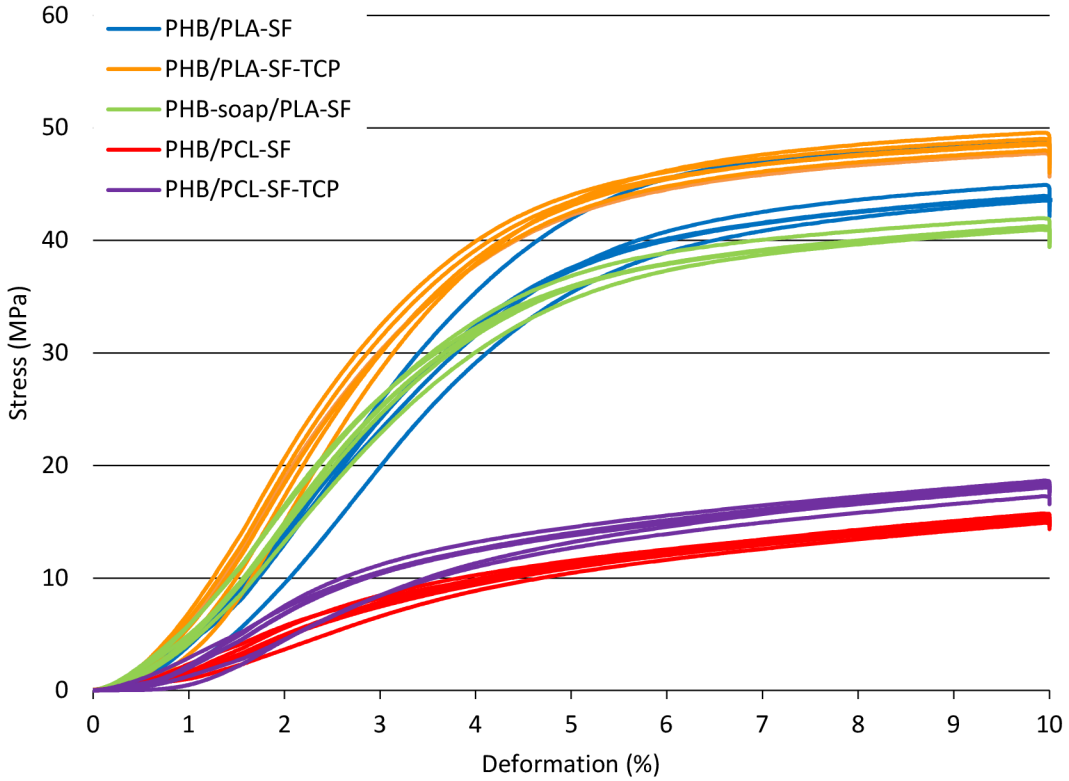

Figure 29: *Stress-deformation compression curves of measured specimens*

Concluding the results of all three mechanical tests, in the case of PHB/PLA blends the highest strength was achieved by the specimens during compression test (48.1 MPa of PHB/PLA-SF-TCP). Although, their strengths also during tensile (around 45 MPa) and flexural test (around 40 MPa) were still very similar to compression test. The highest modulus was shown by the specimens during tensile test (3.0 GPa of PHB/PLA-SF-TCP), but flexural moduli were only around 2 GPa and compression moduli even lower around 1 GPa. A perfectly homogeneous specimen with the same dimensions in all three axes should theoretically have all moduli equal. This means that PHB/PLA blends are the most resilient against tensile stress.

In the case of PHB/PCL blends, the highest strength was achieved by the specimens during tensile test (26.6 MPa of PHB/PCL-SF). This time only flexural strength was comparable (around 25 MPa), because compressive strength was only around 15 MPa. The highest modulus was shown by the specimens during tensile test (1.8 GPa of PHB/PCL-SF-TCP), while flexural moduli were around 1.5 GPa and compression moduli even lower than 0.5 GPa. This means that also PHB/PCL blends are the most resilient against tensile stress.

For comparison, the moduli of human trabecular bone, which is porous and relatively poorly calcified, can range between 0.01–3 GPa and strengths between 0.1–30 MPa. This of course heavily depends on the bone type, its location in the body and on the orientation of applied stress. [59]

PHB-soap/PLA-SF always had very similar mechanical properties as PHB/PLA-SF or PHB/PLA-SF-TCP in all three tests.

The addition of TCP into the blends increases Young's modulus, flexural strength, flexural modulus, compressive strength and compression modulus, but lowers tensile strength and ductility. The most notable rise in terms of strength is of compressive strength of PHB/PCL blend by 18.5 %, while the lowest rise is of compressive strength of PHB/PLA blend by 7.6 %. In all the other cases the strengths rise by approximately 10 %. In terms of modulus, the most notable rise is of compression modulus of PHB/PLA blend by 50 %, while the lowest rise is of Young's modulus of PHB/PLA by 11.1 %. In all other cases the moduli rise approximately by 30 %. This means that TCP particles in 3D printed specimens of PHB/PLA blend as well as of PHB/PCL blend very significantly and positively influence their mechanical properties, eventhough their ductility decreases, but this is of lesser importance for scaffolds intended for bone tissue engineering.

4.4 Surface properties and their influence on cell adhesion

4.4.1 Surface characterization of moulded specimen

4.4.1.1 Optical contact angle measurement (OCA) and surface energy calculation

The optical contact angle measurement (OCA) was conducted on moulded plates of all five composite materials used in this thesis. The liquids used were water, diiodomethane, formamide and diethylene glycol. Water and diethylene glycol served as polar liquids, whereas diiodomethane and formamide served as nonpolar liquids. All the results are presented in *Table 8*.

In all of the cases, water shows the greatest contact angle from all liquids used (84.6° for PHB-soap blend). This means that all prepared materials exhibit nonpolar hydrophobic character as they repel polar liquids. The greater the contact angle with a certain liquid is, it means that the bigger effort of the liquid is to minimise its contact with the surface. The second polar liquid used (diethylene glycol) has the second greatest contact angle only in the case of PHB-soap/PLA blend. This is probably due to the fact, that eventhough diethylene glycol is a polar liquid, it is not as considerably polar as water and moreover all other remaining liquids show very similar contact angle as diethylene glycol (except PHB/PCL-SF) with the difference of only approx. 2°. In three of five cases, the lowest contact angle shows the diiodomethane (most notably for PHB/PCL-SF of just 22.9°). This further supports the claim of all five materials being hydrophobic as diiodomethane is the least polar of all four liquids used. An example of good wetting and poor wetting is given in *Figure 32* and *Figure 31*.

In terms of surface energy, all materials, except for PHB/PLA-SF-TCP, show similar surface energy around 40 mN/m (similar to PMMA or PEO [60]) with dispersive component being approximately 30 mN/m and polar component 10 mN/m. The only exception is PHB-soap/PLA-SF, which has dispersive component of 5 mN/m greater and polar component lower by the same amount. This means that PHB-soap blend is even less polar and more hydrophobic than other materials.

For comparison, the surface energy of a P3HB homopolymer is 46.89 mN/m with dispersive component 38.08 mN/m and polar component 8.81 mN/m. [61] Surface energy of PLA is 35.50 mN/m with dispersive component 26.44 mN/m and polar component 9.06 mN/m [62] and of PCL is 30.80 mN/m with dispersive component 26.10 mN/m and polar component 4.70 mN/m. [63] This means that P3HB, PLA and PCL are hydrophobic also on their own.

When a certain material has no polar groups, it has a large dispersive component and a small polar component. Substances, which don't have any polar groups, don't have any polar component, therefore their surface energy is purely dispersive. This corresponds with the results of prepared materials as their dispersive component makes up the majority of surface energy, so they are nonpolar and hydrophobic.

Material PHB/PLA-SF-TCP has surface energy 45 mN/m and especially the greatest polar component (18 mN/m) at almost double that of PHB/PLA-SF. This rise of surface energy may be caused by presence of TCP particles and their synergic effect with PLA, because polar component of PHB/PCL-SF-TCP compared to PHB/PCL-SF also rises, but not nearly as much as PHB/PLA-SF-TCP.

Table 8: *Optical contact angle measurement (OCA) and surface energy of moulded specimens*

Material	Liquid	Contact angle (°) ± SD	Surface energy (mN/m)	Dispersive component	Polar component
PHB/PLA-SF	Water	74.2 ± 1.0	39.98	30.88	9.1
	Diiodomethane	38.1 ± 1.9			
	Formamide	48.0 ± 1.9			
	Diethylene glycol	42.5 ± 2.7			
PHB/PLA-SF-TCP	Water	61.4 ± 3.4	45.26	27.29	17.97
	Diiodomethane	40.2 ± 2.3			
	Formamide	36.8 ± 2.8			
	Diethylene glycol	38.7 ± 1.5			
PHB-soap/PLA-SF	Water	84.6 ± 2.6	39.97	35.06	4.91
	Diiodomethane	39.2 ± 1.7			
	Formamide	38.7 ± 2.5			
	Diethylene glycol	42.3 ± 2.0			
PHB/PCL-SF	Water	72.7 ± 3.5	40.33	30.52	9.8
	Diiodomethane	22.9 ± 1.4			
	Formamide	55.5 ± 1.8			
	Diethylene glycol	42.2 ± 1.6			
PHB/PCL-SF-TCP	Water	72.1 ± 4.2	40.59	30.24	10.36
	Diiodomethane	35.1 ± 2.2			
	Formamide	47.7 ± 2.7			
	Diethylene glycol	43.3 ± 0.9			

In conclusion, all five measured materials exhibit nonpolar hydrophobic behaviour with surface energy around 40 mN/m, where 30 mN/m are made by dispersive component and the rest by polar component. PHB/PLA-SF compared to PHB-soap/PLA-SF has the same surface energy (difference is only 0.01 mN/m), however, its polar component is half, which makes it the least polar material of all five. The surface energy rises with the addition of TCP to blend, with the most significant difference in PHB/PLA-SF-TCP rising by 5 mN/m.

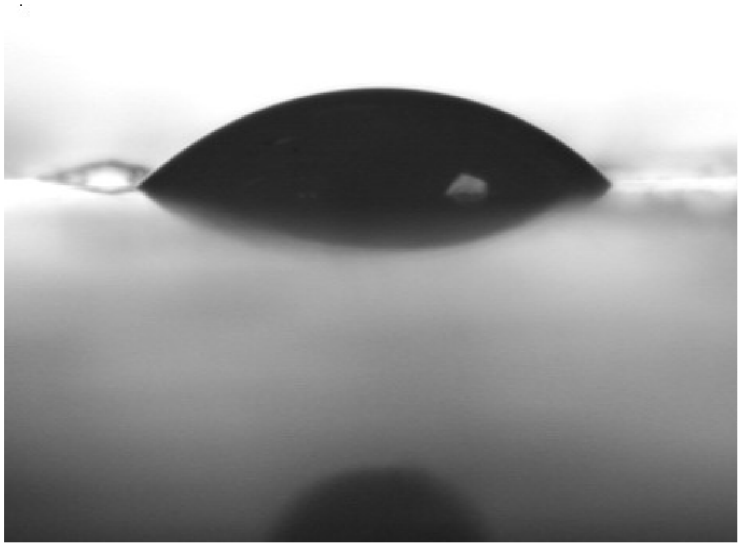

Figure 32: *An image of PHB/PCL-SF-TCP surface with a diethylene glycol drop*

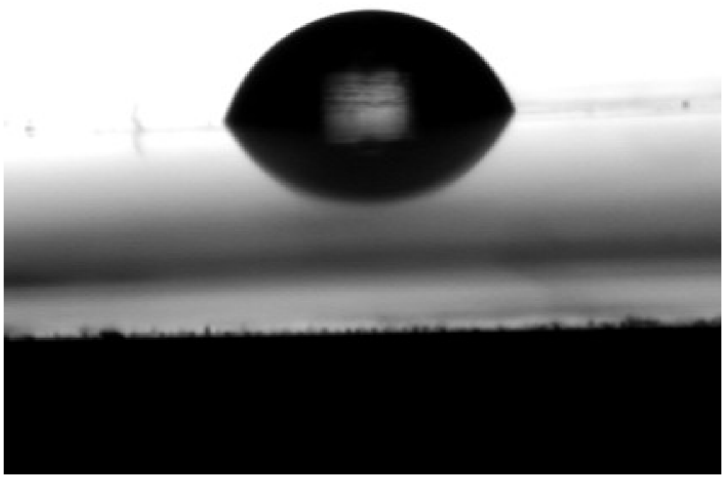

Figure 31: *An image of PHB-soap/PLA-SF surface with a water drop*

4.4.2 Surface characterization of 3D printed specimens

4.4.2.1 Optical contact angle measurement (OCA)

The optical contact angle measurement (OCA) with water was conducted on 3D printed specimens and moulded plates from two different materials – PHB/PLA-SF and PHB/PLA-SF-TCP. 3D printed specimens were cubes printed with grid diameters of 0, 50, 150 and 250 µm. All the results of this OCA measurement are presented in graph in *Figure 33*.

It is obvious that contact angle with water increases with greater grid diameters and is at the lowest level for a moulded plate. This effect is probably caused by the hydrophobicity of materials PHB/PLA-SF and PHB/PLA-SF-TCP on their own. This statement is based on the findings in Chapter 4.4.1. When the surface starts to get rough, the effect of hydrophobicity and water repulsion are even more amplified. This phenomenon can be compared to the "lotus effect" when lotus leaves are covered with many small bumps making them non-wetting due to high contact angle (more than 140°). When the drop is exposed to contact with the rough surface of the hydrophobic nonpolar specimen the surface tension force starts to dominate even more, trying to minimise the contact area of the droplet with the surface, so that the contact angle increases even more.

In the results of work by Kennedy et al. it is stated that ideal contact angle with water for osteoblasts is around 55-60°, whereby more hydrophobic materials (contact angle 80-90°) are preferable than very hydrophilic ones (contact angle 30-40°). [64]

In the work by Du et al., porous PCL/HAp composites were obtained by microsphere-based selective laser sintering. The scaffolds exhibited a con

The difference between contact angles of PHB/PLA-SF and PHB/PLA-SF-TCP falls within the standard deviation range, thus no significant influence of the addition of TCP to blend on contact angle with water can be discussed.

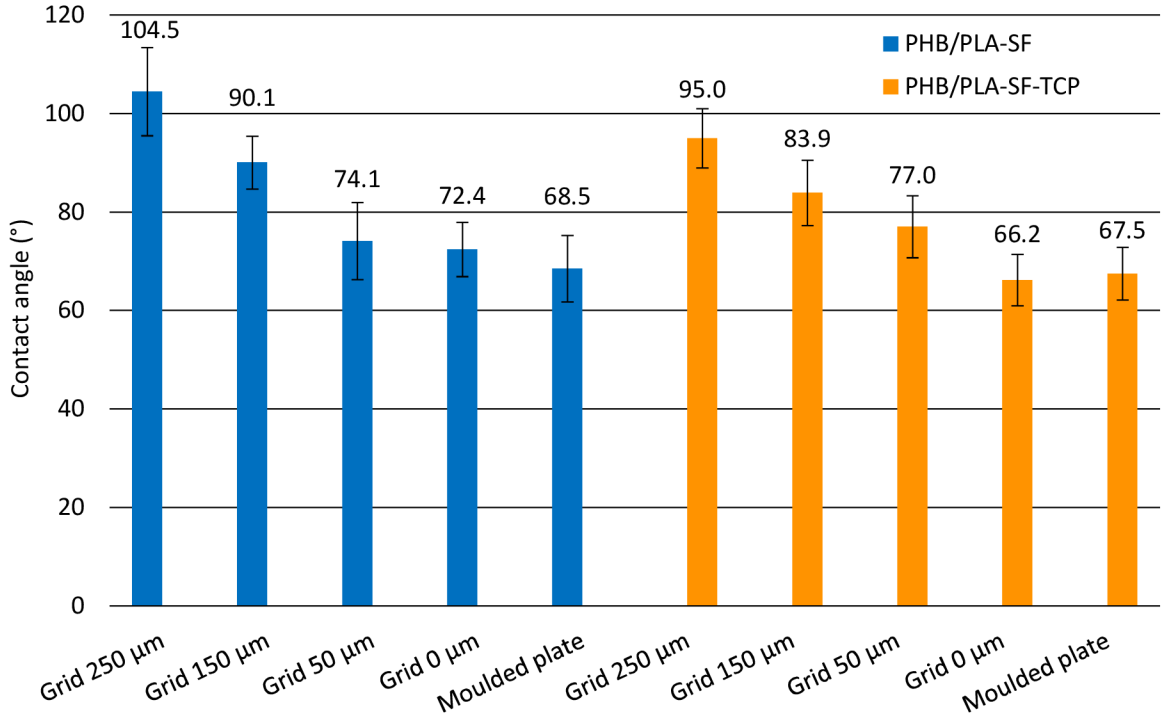

Figure 33: *Graph of the water contact angle dependence on the surface and material*

4.4.2.2 Surface roughness analysis

Surface roughness analysis was conducted on 3D printed specimens and moulded plates from two different materials – PHB/PLA-SF and PHB/PLA-SF-TCP. 3D printed specimens were cubes printed with grid diameters of 0, 50, 150 and 250 µm. In graphs in *Figure 34* and *Figure 36* all the results are presented. *Figure 34* focuses on roughness over and *Figure 36* on roughness along as described in Chapter 3.8.3.

In the case of material PHB/PLA-SF it is evident that roughnesses over of grid diameter 250 and 150 µm fall within the standard deviation range, therefore they can be deemed as equal with roughness 120 µm. Starting with grid diameter 50 µm, roughness over decreases very rapidly with the most significant difference in roughness between diameters 50 and 0 µm (from 93.8 µm to 20.7 µm). The lowest roughness shows the moulded plate, because its surface is after moulding completely smooth.

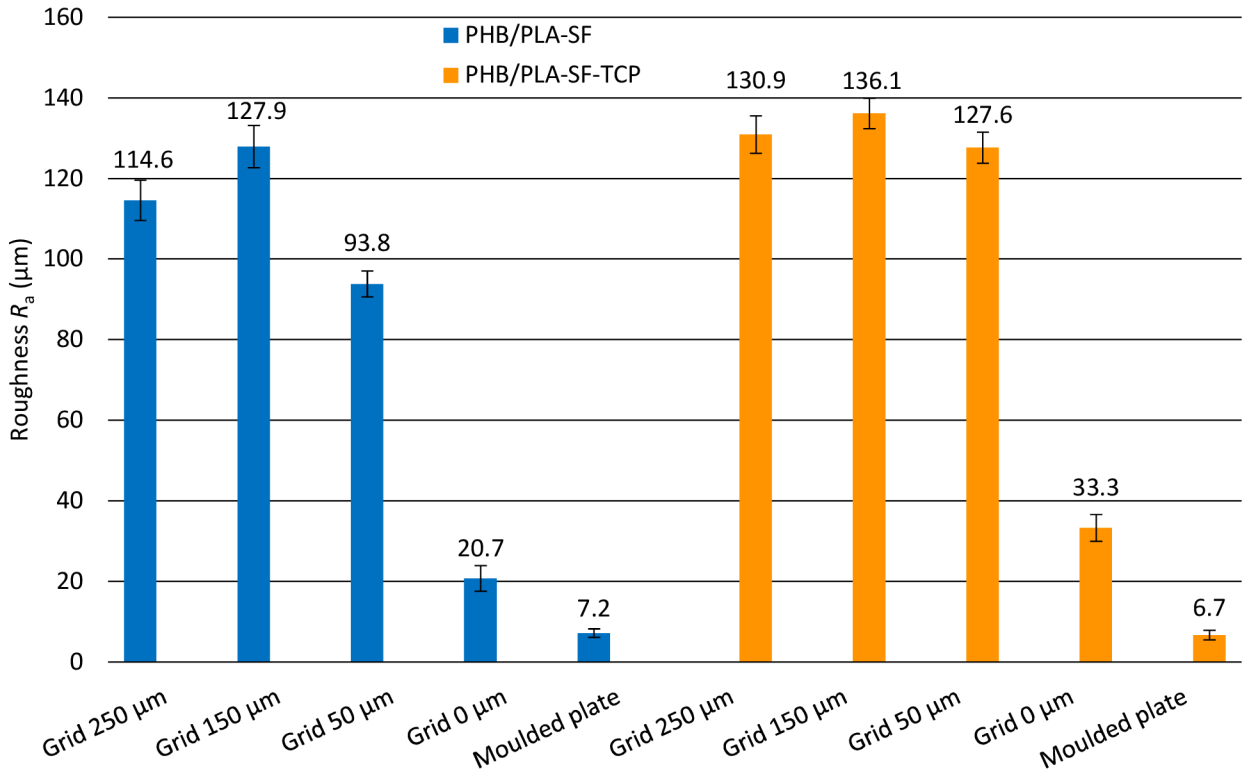

Figure 34: *Graph of the roughness over dependence on the surface and material*

In conclusion, the major influence on surface roughness is the presence of the grid (of at least some small diameter, optimally around 50 µm) more than the magnitude of the diameter itself. Moreover this statement is supported by the results of material PHB/PLA-SF-TCP measurement where the same trend can be observed with the only difference that surfaces with grid diameters 250, 150 and also 50 µm can be deemed as equal. Also the roughness over of PHB/PLA-SF-TCP is greater than PHB/PLA-SF which can be caused by presence of TCP particles in perimeters on the top of the measured surface (*Figure 35*). Due to this fact, the roughness over of both moulded plates is almost identical, independent of material, because the TCP particles were pressed during moulding into the surface of plate.

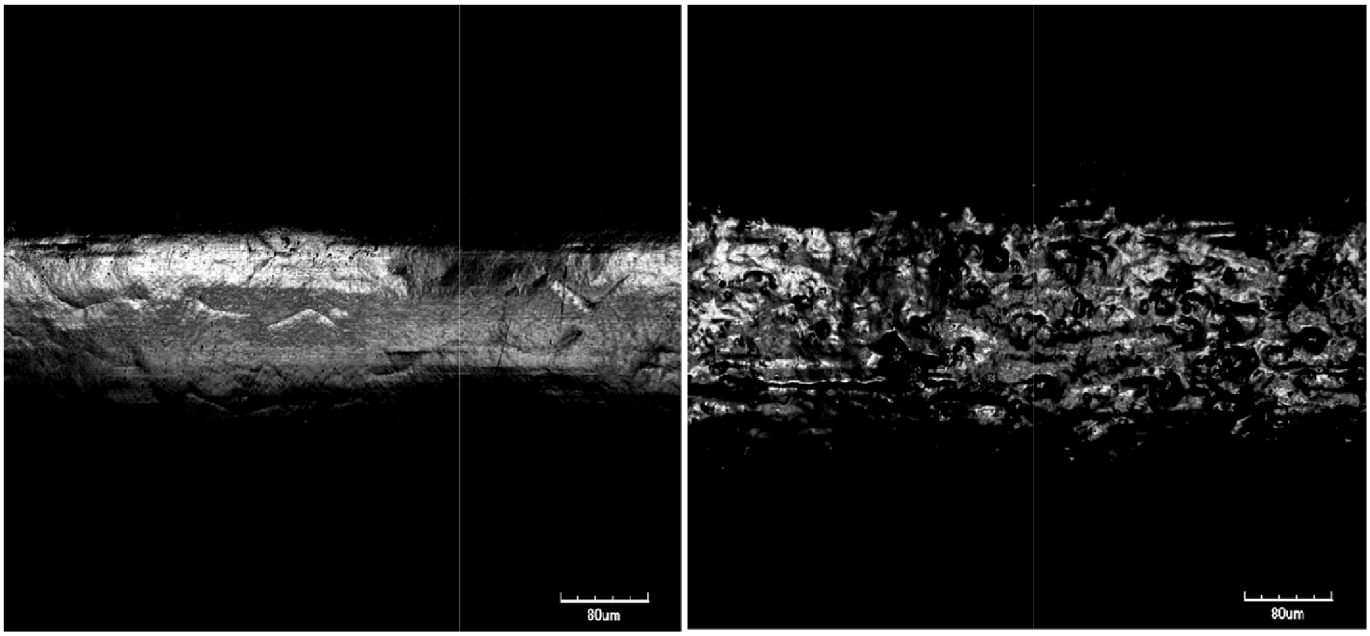

Figure 35: *An image of perimeters of grid diameter 250 μm measured for roughness along; PHB/PLA-SF left, PHB/PLA-SF-TCP right*

Roughness along in terms of material PHB/PLA-SF is stable (approx. 2 μm) and does not change with the grid diameter (*Figure 36*). Roughness along of PHB/PLA-SF-TCP is higher (approx. 4.5 μm), but it fluctuates as it heavily depends on uneven distribution of the TCP particles (if and how many) within the measured perimeter, because TCP particles can be exposed on the surface of perimeter (enhancing roughness along) or hidden in the volume of perimeter (having no influence on roughness and moving it closer to roughness along of PHB/PLA-SF).

In conclusion, surface roughness (R_a) generally increases with greater grid diameters. Material PHB/PLA-SF-TCP has greater roughness over and along, due to the presence of TCP particles on the surface of its perimeters.

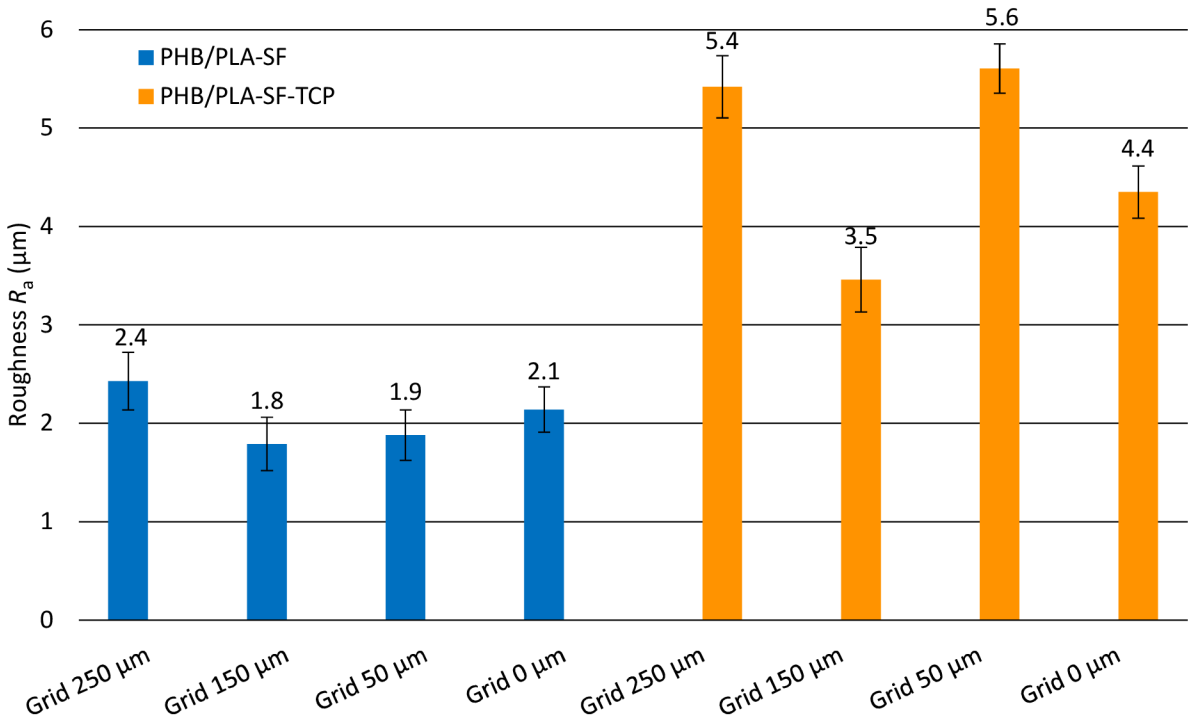

Figure 36: *Graph of the roughness along dependence on the surface and material*

4.5 In vitro tests on scaffolds

4.5.1 Cytotoxicity measurement

All the results and graphs corresponding to cytotoxicity measurements are for seen in the appendices. The highest absorbance after 24 hours was measured in control group. The lowest value after 24 hours was shown by PHB-soap/PLA-SF. Blends of PHB/PCL had after the first day almost similar absorbance. On the other hand, metabolic activity increased in the case of PHB/PCL-SF even so profoundly that it was statistically comparable with the control group after 72 hours. Metabolic activity of PHB/PCL-SF-TCP after 3 days was not even at the level of control group after 24 hours, and of PHB-soap/PLA-SF was negligible and on top of that lower than after first day.

In conclusion, the worst results were reported by PHB-soap/PLA-SF and this material was obviously cytotoxic, because the number of cells measured in metabolic activity assay even decreased between the first and the third day. Eventhough, the results of PHB/PCL-SF-TCP were much better and in the DNA quantification the overall number of cells increased between the first and third day, most of them did not survive and became apoptic. According to ISO method, which states that at least 70 % of cells have to survive compared with the control group, this material was deemed cytotoxic too. The results were clearly the best in the case of PHB/PCL-SF. Metabolic activity assay showed significant rise after the 72 hours, which was even comparable with the control group and DNA quantification showed that the total number of cells that proliferated was also comparable with the control group and of all materials the least of them became apoptic. Due to this fact, PHB/PCL-SF was the only material found to be non-cytotoxic and biocompatible in the end.

Cytotoxicity measurement was later repeated with granules of materials PHB-soap/PLA-SF, PHB/PCL-SF and PHB/PCL-SF-TCP from the same batch as in the first measurement, and with the granules of same three materials, but compounded again in the smaller amount (200 g in total). The results confirmed the cytotoxicity of PHB-soap/PLA-SF, but both old and new granules of PHB/PCL-SF and PHB/PCL-SF-TCP were not cytotoxic this time.

4.5.2 Evaluation of cell adhesion on different surfaces

All the results and graphs corresping to evaluation of cell adhesion are for seen in the appendices. The results of MTS analysis, unfortunately, showed that the activity of cells on all tested specimens was very low after 24 hours and even decreased after 72 hours. Between all the values, there was no statistical difference, so we can claim all the specimens are all the same. The results suggest the cytotoxicity of all specimens.

Cell adhesion was low on all specimens, but the lowest of all was measured on sample PHB/PLA-SF-TCP_2020 moulded plate after 24 hours. Interestingly, the results of the control group were also very low and comparable with the measured specimens. The cells grew in small amounts and slowly on the scaffolds and there was no significant difference between them. The reason for this behaviour can be insufficient lysis of cells cultured on tissue culture plastic or due to low seeding density that was used in order to visualise the cell adhesion by confocal microscopy well.

In the last part of cell adhesion study the visualisation of cells on measured surfaces was conducted by confocal microscopy (*Figure 37*). The shape of the cells gave us information about the suitability of the surface for cell growth. When the cells are more round or mostly circular, it means that they are not prospering as they are trying to minimise the contact area with the surface and not to touch it at all. On the other hand, when the cells are elongated or increasingly oval, it means that they are thriving and trying to occupy as much space as possible. According to the microscopy, the cells were viable also on day 3. In the case of material PHB/PLA-SF_2020 on all surfaces and PHB/PLA-SF-TCP_2020 on some of them, the cells were nicely adhered and even rather oval, but in some samples they were round and apoptotic.

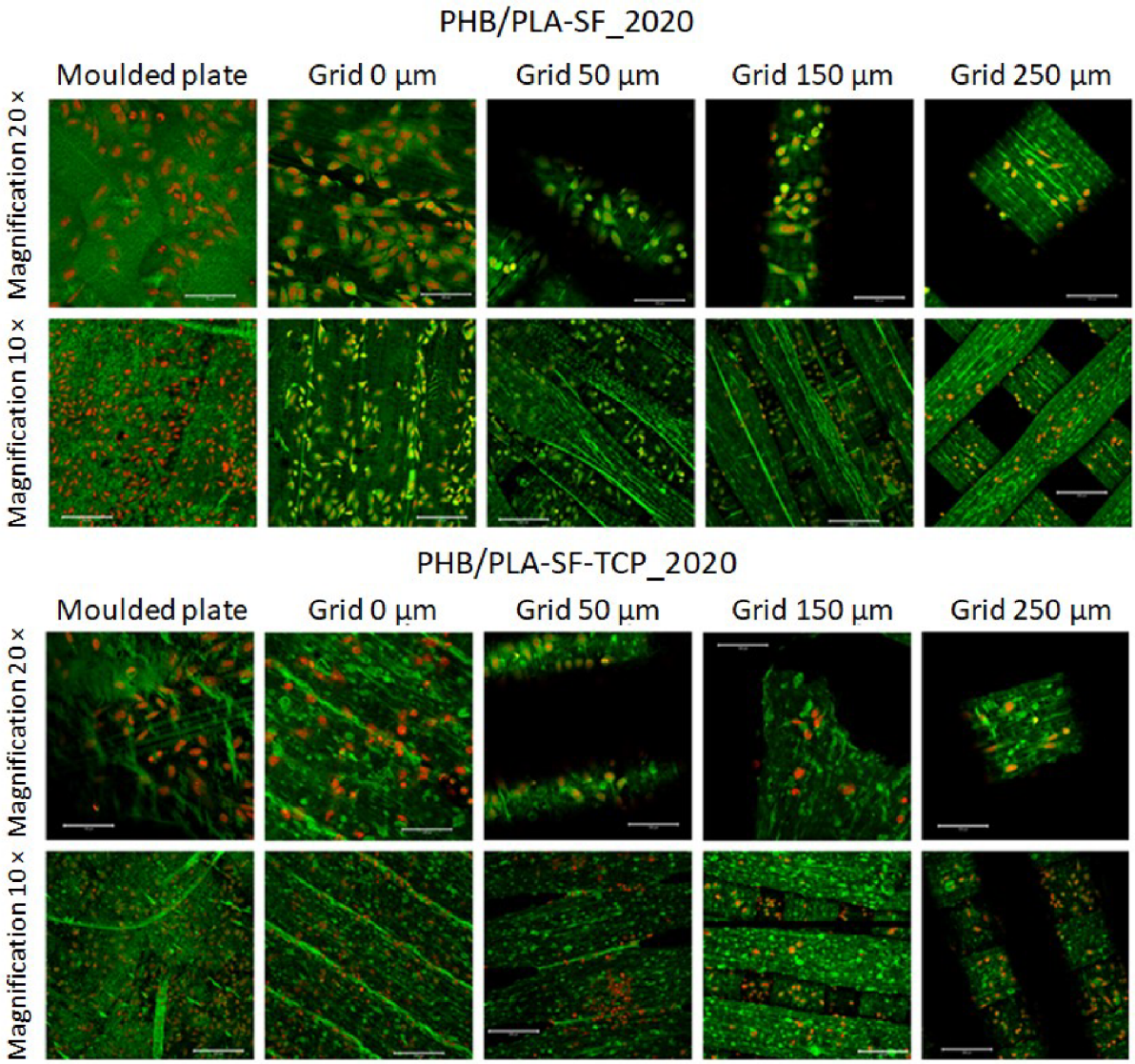

Figure 37: *An image of cells cultured on different surfaces captured by confocal microscopy after 24 hours*

5 CONCLUSION

The aim of this thesis was to conduct research on 3D printable polymers and their blends for bone tissue engineering. To prepare polymer blends in the form of granulate and process them into the form of 3D printing filament with precise diameter 1.75 mm. Then to characterise thermal and mechanical properties of these materials and to evaluate their surface energy. And finally, to use prepared filaments for 3D printing by fused deposition modelling (FDM) to print scaffolds with different surfaces and to evaluate optimal surface for adhesion and proliferation of cells with respect to surface properties and roughness.

Three polymeric blends were prepared in total. These were PHB-soap/PLA-SF (blend of poly(3-hydroxybutyrate prepared by chloroform-free extraction process, poly(lactic acid) and plasticizer Syncroflex), PHB/PCL-SF (blend of commercial poly(3-hydroxybutyrate), polycaprolactone and plasticizer Syncroflex) and PHB/PCL-SF-TCP (the same blend as PHB/PCL-SF with the addition of tricalcium phosphate (TCP) particles as a filler) in the form of granulate and then processed into the form of 3D printing filaments.

Crystallinity, crystallisation temperature and melting temperature did not change significantly in the case of PHB-soap/PLA-SF, thus the process of the preparation of 3D printing filament was declared to have no effect on thermal properties of this blend. Commercial PHB had higher crystallinity in both granulate and filament form than PHB-soap. Crystallisation temperatures of PHB/PCL blends were higher than of PHB-soap by roughly 10 °C. On the other hand, in PHB/PCL blends the extrusion process of 3D printing filaments decreased PHB crystallinity compared to granulate form, while at the same time PCL crystallinity increased. Although in the case of PHB/PCL-SF-TCP, this effect was probably inhibited by TCP particles, because the same trend was observed, but less significant.

Considering all the results from temperature tower test (TTT) and warping test, the final processing conditions for three prepared composite materials, namely temperature, were 195/190 °C for PHB-soap/PLA-SF, 195/175 °C for PHB/PCL-SF and 195/165 °C for PHB/PCL-SF-TCP. First temperature of the pair was used to print the brim and first layer of the specimen and second temperature was used to print all other remaining layers. In the case of PHB-soap/PLA-SF flow was set on 80 %, fan was disabled and speed of printing was 80 %, otherwise flow was set on 100 %, fan was on and speed at 100 %.

PHB-soap/PLA-SF blend showed very similar mechanical properties as PHB/PLA blends with commercial PHB in all three mechanical tests (strengths around 40 MPa and moduli around 2 GPa). Compared to human trabecular bone the measured specimens showed very similar or even better mechanical properties. PHB/PCL blends compared to their PHB/PLA counterparts (PHB/PLA-SF and PHB/PLA-SF-TCP) did not reach such mechanical properties and qualities in any test performed. The addition of TCP to the blend, regardless of whether it is PHB/PLA or PHB/PCL, very significantly improved all the mechanical properties (most notably against deformation by pressure) with the exception of ductility and tensile strength. The compressive strength of PHB/PCL-SF-TCP increased by 18.5 % and compression modulus by 33.3 % in comparison with PHB/PCL-SF.

Within the surface energy measurement, all five materials exhibited nonpolar hydrophobic behaviour with surface energy around 40 mN/m (similar to PMMA or PEO), where 30 mN/m was made by dispersive component and the rest by polar component. The surface energy rose with the addition of TCP to the blend, with the most significant difference in PHB/PLA-SF-TCP rising by 5 mN/m.

In optical contact angle (OCA) measurement with water, contact angle was increasing with greater grid diameters and was at the lowest level for a moulded plate (68.5°) and highest for grid diameter 250 μm (104.5°). When the surface started to get rougher, the effect of hydrophobicity and water repulsion was even amplified. The difference between water contact angles of PHB/PLA-SF and PHB/PLA-SF-TCP was not observed.

In terms of surface roughness analysis, it was found that material PHB/PLA-SF-TCP had greater roughness over and along, due to the presence of TCP particles on the surface of its perimeters. The major influence on surface roughness was the presence of the grid (of at least some small diameter) more than the magnitude of the grid diameter itself.

Within the cytotoxicity measurement, the worst results were reported by PHB-soap/PLA-SF and this material was obviously cytotoxic. PHB/PCL-SF and PHB/PCL-SF-TCP were found to be non-cytotoxic and biocompatible.

As a part of the evaluation of cell adhesion on different surfaces the results, unfortunately, showed that the activity of cells on all tested specimens was very low after 24 hours and even decreased after 72 hours. Cell adhesion was low on all specimens, the cells grew in small amounts and slow on the scaffolds and there was no significant difference between them. According to the confocal microscopy, the cells were viable also on day 3. Due to this fact, no surface type was chosen as the most optimal for cell growth and proliferation.

Concluding, both PHB/PCL blends could be used for future research as they were proven not to be cytotoxic. Their crystallinity was even found to be higher than that of PHB-soap/PLA-SF. On the other hand, their mechanical properties were considerably worse than PHB/PLA blends in any of the mechanical tests, but still comparable with human trabecular bone. They were found to be hydrophobic with surface energy around 40 mN/m, which is suitable for cell growth. As the most optimal surface could probably be chosen grid diameter 50 μm, because its contact angle with water (around 75°) and roughness along the perimeter (around 3 μm) is preferable for cell growth. However, the evaluation of cell adhesion on various surfaces did not show considerable differences between them, so as a part of future research also other surfaces could be studied.

6 BIBLIOGRAPHY

[1] *What Is Medical 3D Printing—and How Is it Regulated?* [online]. [vid. 2022-02-06]. Available at: https://pew.org/3l8s9mm

[2] BOCCACCIO, Antonio, Antonio E. UVA, Michele FIORENTINO, Giuseppe MONNO, Andrea BALLINI a Apollonia DESIATE. Optimal Load for Bone Tissue Scaffolds with an Assigned Geometry. *International Journal of Medical Sciences* [online]. 2018, **15**(1), 16–22. ISSN 1449-1907. Available at: doi:10.7150/ijms.20522

[3] SHUNMUGASUNDARAM, Manoharan, Maughal BAIG a Ajay MADALA. A review of bio-degradable materials for fused deposition modeling machine. *Materials Today: Proceedings* [online]. 2020, **27**. Available at: doi:10.1016/j.matpr.2020.03.267

[4] NGO, Tuan D., Alireza KASHANI, Gabriele IMBALZANO, Kate T. Q. NGUYEN a David HUI. Additive manufacturing (3D printing): A review of materials, methods, applications and challenges. *Composites Part B: Engineering* [online]. 2018, **143**, 172–196. ISSN 1359-8368. Available at: doi:10.1016/j.compositesb.2018.02.012

[5] PARK, Byeong Ju, H. J. CHOI, Sang Ji MOON, Seong Jun KIM, Rajiv BAJRACHARYA, J. MIN a Hyo-Kyung HAN. Pharmaceutical applications of 3D printing technology: current understanding and future perspectives. *Journal of Pharmaceutical Investigation* [online]. 2018. Available at: doi:10.1007/s40005-018-00414-y

[6] AN, Jia, Joanne Ee Mei TEOH, Ratima SUNTORNNOND a Chee Kai CHUA. Design and 3D Printing of Scaffolds and Tissues. *Engineering* [online]. 2015, **1**(2), 261–268. ISSN 2095-8099. Available at: doi:10.15302/J-ENG-2015061

[7] LAU, Gih-Keong a Milan SHRESTHA. Ink-Jet Printing of Micro-Electro-Mechanical Systems (MEMS). *Micromachines* [online]. 2017, **8**(6), 194. ISSN 2072-666X. Available at: doi:10.3390/mi8060194

[8] KLUSKA, Ewelina, Piotr GRUDA a Natalia MAJCA-NOWAK. The Accuracy and the Printing Resolution Comparison of Different 3D Printing Technologies. *Transactions on Aerospace Research* [online]. 2018, **2018**(3), 69–86. Available at: doi:10.2478/tar-2018-0023

[9] MOHAMMED, Mazher Iqbal, Parminder Singh BADWAL a Ian GIBSON. Design and fabrication considerations for three dimensional scaffold structures. *KnE Engineering* [online]. 2017, 120–126. ISSN 2518-6841. Available at: doi:10.18502/keg.v2i2.604

[10] BAHRAMINASAB, Marjan. Challenges on optimization of 3D-printed bone scaffolds. *BioMedical Engineering OnLine* [online]. 2020, **19**(1), 69. ISSN 1475-925X. Available at: doi:10.1186/s12938-020-00810-2

[11] VOJTOVÁ, Lucy a Jana BRTNÍKOVÁ. Metody přípravy skafoldů. In: Brno. 17th March, 2020.

[12] *SLA 3D Printing - Jules Topart - Fab Academy* [online]. [vid. 2022-03-22]. Available at: https://fabacademy.org/2021/labs/lamachinerie/students/jules-topart/assignments/6b_sla/

[13] *The Williams Dictionary of Biomaterials* [online]. B.m.: Liverpool University Press, 1999 [vid. 2022-03-25]. ISBN 978-0-85323-734-1. Available at: doi:10.5949/UPO9781846314438

[14] *Handbook of Biopolymers and Biodegradable Plastics - 1st Edition* [online]. [vid. 2022-02-07]. Available at: https://www.elsevier.com/books/handbook-of-biopolymers-and-biodegradable-plastics/ebnesajjad/978-1-4557-2834-3

[15] OJUMU, T. V., J. YU a B. O. SOLOMON. Production of Polyhydroxyalkanoates, a bacterial biodegradable polymer. *African Journal of Biotechnology* [online]. 2004, **3**(1), 18–24. ISSN 1684-5315. Available at: doi:10.5897/AJB2004.000-2004

[16] HIGUCHI-TAKEUCHI, Mieko, Kumiko MORISAKI, Kiminori TOYOOKA a Keiji NUMATA. Synthesis of High-Molecular-Weight Polyhydroxyalkanoates by Marine Photosynthetic Purple Bacteria. *PLOS ONE* [online]. 2016, **11**(8), e0160981. ISSN 1932-6203. Available at: doi:10.1371/journal.pone.0160981

[17] POSPISILOVA, Aneta, Ivana NOVACKOVA a Radek PRIKRYL. Isolation of poly(3-hydroxybutyrate) from bacterial biomass using soap made of waste cooking oil. *Bioresource Technology* [online]. 2021, **326**, 124683. ISSN 0960-8524. Available at: doi:10.1016/j.biortech.2021.124683

[18] BYROM, D. Miscellaneous biomaterials. In: David BYROM, ed. *Biomaterials: Novel Materials from Biological Sources* [online]. London: Palgrave Macmillan UK, 1991 [vid. 2022-03-10], s. 333–359. ISBN 978-1-349-11167-1. Available at: doi:10.1007/978-1-349-11167-1_8

[19] SANTOS, Antonio, Luiz DALLA VALENTINA, Andrey SCHULZ a Marcia DUARTE. From Obtaining to Degradation of PHB:Material Properties. Part I. *Ingeniería y Ciencia* [online]. 2017, **13**, 269–298. Available at: doi:10.17230/ingciencia.13.26.10

[20] LENZ, Robert W. a Robert H. MARCHESSAULT. Bacterial Polyesters: Biosynthesis, Biodegradable Plastics and Biotechnology. *Biomacromolecules* [online]. 2005, **6**(1), 1–8. ISSN 1525-7797. Available at: doi:10.1021/bm049700c

[21] RUDNIK, Ewa. Compostable Polymer Materials: Definitions, Structures, and Methods of Preparation. Definitions, Structures, and Methods of Preparation. In: *Handbook of Biopolymers and Biodegradable Plastics: Properties, Processing and Applications* [online]. 2008, s. 10–36. ISBN 978-0-08-045371-2. Available at: doi:10.1016/B978-008045371-2.50004-4

[22] RAI, R., T. KESHAVARZ, J. A. ROETHER, A. R. BOCCACCINI a I. ROY. Medium chain length polyhydroxyalkanoates, promising new biomedical materials for the future. *Materials Science and Engineering R: Reports* [online]. 2011, **72**(3), 29–47. ISSN 0927-796X. Available at: doi:10.1016/j.mser.2010.11.002

[23] LIM, Janice, Mingliang YOU, Jian LI a Zibiao LI. Emerging bone tissue engineering via Polyhydroxyalkanoate (PHA)-based scaffolds. *Materials Science & Engineering. C, Materials for Biological Applications* [online]. 2017, **79**, 917–929. ISSN 1873-0191. Available at: doi:10.1016/j.msec.2017.05.132

[24] BUTT, Fatima Imran, Nawshad MUHAMMAD, Almas HAMID, Muhammad MONIRUZZAMAN a Faiza SHARIF. Recent progress in the utilization of biosynthesized polyhydroxyalkanoates for biomedical applications - Review. *International Journal of Biological Macromolecules* [online]. 2018, **120**(Pt A), 1294–1305. ISSN 1879-0003. Available at: doi:10.1016/j.ijbiomac.2018.09.002

[25] JIANG, Long a Jinwen ZHANG. Biodegradable Polymers and Polymer Blends. In: [online]. 2013, s. 109–128. ISBN 978-1-4557-2834-3. Available at: doi:10.1016/B978-1-4557-2834-3.00006-9

[26] PEREIRA, Tatiana F., Marcelo F. OLIVEIRA, Izaque A. MAIA, Jorge V. L. SILVA, Marysilvia F. COSTA a Rossana M. S. M. THIRÉ. 3D Printing of Poly(3-hydroxybutyrate) Porous Structures Using Selective Laser Sintering. *Macromolecular Symposia* [online]. 2012, **319**(1), 64–73. ISSN 1521-3900. Available at: doi:10.1002/masy.201100237

[27] KOVALCIK, Adriana, Leire SANGRONIZ, Michal KALINA, Katerina SKOPALOVA, Petr HUMPOLÍČEK, Maria OMASTOVA, Norbert MUNDIGLER a Alejandro J. MÜLLER. Properties of scaffolds prepared by fused deposition modeling of poly(hydroxyalkanoates). *International Journal of Biological Macromolecules* [online]. 2020, **161**, 364–376. ISSN 0141-8130. Available at: doi:10.1016/j.ijbiomac.2020.06.022

[28] GOMES, Manuela, Helena AZEVEDO, Patrícia MALAFAYA, Simone SILVA, Joaquim OLIVEIRA, Gabriela SILVA, Rui SOUSA, João MANO a Rui REIS. Chapter 6 - Natural Polymers in tissue engineering applications. In: Clemens van BLITTERSWIJK, Peter THOMSEN, Anders LINDAHL, Jeffrey HUBBELL, David F. WILLIAMS, Ranieri CANCEDDA, Joost D. de BRUIJN a Jérôme SOHIER, ed. *Tissue Engineering* [online]. Burlington: Academic Press, 2008 [vid. 2022-03-14], s. 145–192. ISBN 978-0-12-370869-4. Available at: doi:10.1016/B978-0-12-370869-4.00006-9

[29] NARAYANAN, Niju, Pradip K. ROYCHOUDHURY a Aradhana SRIVASTAVA. L (+) lactic acid fermentation and its product polymerization. *Electronic Journal of Biotechnology* [online]. 2004, **7**(2), 0–0. ISSN 0717-3458, 0717-3458. Available at: doi:10.2225/vol7-issue2-fulltext-7

[30] VITETTA, Luis, Samantha COULSON, Michael THOMSEN, Tony NGUYEN a Sean HALL. Probiotics, D–Lactic acidosis, oxidative stress and strain specificity. *Gut Microbes* [online]. 2017, **8**(4), 311–322. ISSN 1949-0976. Available at: doi:10.1080/19490976.2017.1279379

[31] NAM, Tran, Shinji OGIHARA a Satoshi KOBAYASHI. Interfacial, Mechanical and Thermal Properties of Coir Fiber-Reinforced Poly(Lactic Acid) Biodegradable Composites. *Advanced Composite Materials* [online]. 2012, **21**, 103–122. Available at: doi:10.1163/156855112X629540

[32] MADHAVAN NAMPOOTHIRI, K., Nimisha Rajendran NAIR a Rojan Pappy JOHN. An overview of the recent developments in polylactide (PLA) research. *Bioresource Technology* [online]. 2010, **101**(22), 8493–8501. ISSN 1873-2976. Available at: doi:10.1016/j.biortech.2010.05.092

[33] GUPTA, A. P. a Vimal KUMAR. New emerging trends in synthetic biodegradable polymers – Polylactide: A critique. *European Polymer Journal*. 2007, **43**(10), 4053–4074. ISSN 0014-3057.

[34] BEREZINA, Nathalie, Nicolas LANDERCY, Pierre-Antoine MARIAGE a Benoit MOREA. Separation of the Enantiomers of Lactide, Lactic Acid Dimer, for a Sustainable Bioplastic Management. *World Journal of Organic Chemistry* [online]. 2013, **1**(2), 20–23. Available at: doi:10.12691/wjoc-1-2-3

[35] KRAMSCHUSTER, Adam a Lih-Sheng TURNG. 17 - Fabrication of Tissue Engineering Scaffolds. In: Sina EBNESAJJAD, ed. *Handbook of Biopolymers and Biodegradable Plastics* [online]. Boston: William Andrew Publishing, 2013 [vid. 2022-03-14], Plastics Design Library, s. 427–446. ISBN 978-1-4557-2834-3. Available at: doi:10.1016/B978-1-4557-2834-3.00017-3

[36] CHIULAN, Ioana, Adriana Nicoleta FRONE, Călin BRANDABUR a Denis Mihaela PANAITESCU. Recent Advances in 3D Printing of Aliphatic Polyesters. *Bioengineering (Basel, Switzerland)* [online]. 2017, **5**(1), E2. ISSN 2306-5354. Available at: doi:10.3390/bioengineering5010002

[37] Amazon.com: Gizmo Dorks PLA Filament for 3D Printers 1.75mm 200g, 4 Color Pack - Blue, Green, Orange, Red : Industrial & Scientific [online]. [vid. 2022-03-13]. Available at: https://www.amazon.com/Gizmo-Dorks-Filament-Printers-1-75mm/dp/B074W1XFRX

[38] GREGOR, A., E. FILOVÁ, M. NOVÁK, J. KRONEK, H. CHLUP, M. BUZGO, V. BLAHNOVA, V. LUKÁŠOVÁ, M. BARTOŠ, A. NEČAS a J. HOŠEK. Designing of PLA scaffolds for bone tissue replacement fabricated by ordinary commercial 3D printer. *Journal of biological engineering* [online]. 2017. Available at: doi:10.1186/s13036-017-0074-3

[39] SIN, Lee Tin, Abdul R. RAHMAT a Wan A. W. A. RAHMAN. 2 - Overview of Poly(lactic Acid). In: Sina EBNESAJJAD, ed. *Handbook of Biopolymers and Biodegradable Plastics* [online]. Boston: William Andrew Publishing, 2013 [vid. 2022-03-14], Plastics Design Library, s. 11–54. ISBN 978-1-4557-2834-3. Available at: doi:10.1016/B978-1-4557-2834-3.00002-1

[40] CHEN, Guo-Qiang. *Plastics from Bacteria: Natural Functions and Applications* [online]. 2010. ISBN 978-3-642-03286-8. Available at: doi:10.1007/978-3-642-03287-5

[41] XIA, Yan, Panyu ZHOU, Xiaosong CHENG, Yang XIE, Chong LIANG, Chao LI a Shuogui XU. Selective laser sintering fabrication of nano-hydroxyapatite/poly-ε-caprolactone scaffolds for bone tissue engineering applications. *International Journal of Nanomedicine* [online]. 2013, **8**, 4197–4213. ISSN 1178-2013. Available at: doi:10.2147/IJN.S50685

[42] ZEIN, Iwan, Dietmar W. HUTMACHER, Kim Cheng TAN a Swee Hin TEOH. Fused deposition modeling of novel scaffold architectures for tissue engineering applications. *Biomaterials* [online]. 2002, **23**(4), 1169–1185. ISSN 0142-9612. Available at: doi:10.1016/S0142-9612(01)00232-0

[43] CAO, Tong, Kee-Hai HO a Swee-Hin TEOH. Scaffold design and in vitro study of osteochondral coculture in a three-dimensional porous polycaprolactone scaffold fabricated by fused deposition modeling. *Tissue Engineering* [online]. 2003, **9 Suppl 1**, S103-112. ISSN 1076-3279. Available at: doi:10.1089/10763270360697012

[44] ZHAO, J., L. Y. GUO, X. B. YANG a J. WENG. Preparation of bioactive porous HA/PCL composite scaffolds. *Applied Surface Science* [online]. 2008, **255**(5, Part 2), 2942–2946. ISSN 0169-4332. Available at: doi:10.1016/j.apsusc.2008.08.056

[45] DU, Yingying, Haoming LIU, Qin YANG, Shuai WANG, Jianglin WANG, Jun MA, Insup NOH, Antonios G. MIKOS a Shengmin ZHANG. Selective laser sintering scaffold with hierarchical architecture and gradient composition for osteochondral repair in rabbits. *Biomaterials* [online]. 2017, **137**, 37–48. ISSN 0142-9612. Available at: doi:10.1016/j.biomaterials.2017.05.021

[46] KOSORN, Wasana, Morakot SAKULSUMBAT, Paweena UPPANAN, Pakkanun KAEWKONG, Surapol CHANTAWEROAD, Jaturong JITSAARD, Kriskrai SITTHISERIPRATIP a Wanida JANVIKUL. PCL/PHBV blended three dimensional scaffolds fabricated by fused deposition modeling and responses of chondrocytes to the scaffolds. *Journal of Biomedical Materials Research Part B: Applied Biomaterials* [online]. 2017, **105**(5), 1141–1150. ISSN 1552-4981. Available at: doi:10.1002/jbm.b.33658

[47] CHOCHOLATA, Petra, Vlastimil KULDA a Vaclav BABUSKA. Fabrication of Scaffolds for Bone-Tissue Regeneration. *Materials* [online]. 2019, **12**(4), 568. ISSN 1996-1944. Available at: doi:10.3390/ma12040568

[48] KIM, Jong Young a Dong-Woo CHO. Blended PCL/PLGA scaffold fabrication using multi-head deposition system. *Microelectronic Engineering* [online]. 2009, **86**(4), MNE '08, 1447–1450. ISSN 0167-9317. Available at: doi:10.1016/j.mee.2008.11.026

[49] VOJTOVÁ, Lucy. Biomateriály - úvod. In: Brno. 25th February, 2020.

[50] CHAN, Clement Matthew, Luigi-Jules VANDI, Steven PRATT, Peter HALLEY, Desmond RICHARDSON, Alan WERKER a Bronwyn LAYCOCK. Insights into the biodegradation of PHA / wood composites: Micro- and macroscopic changes. *Sustainable Materials and Technologies* [online]. 2019, **21**, e00099. ISSN 2214-9937. Available at: doi:10.1016/j.susmat.2019.e00099

[51] ZENG, Jian-Hua, Shi-Wei LIU, Long XIONG, Peng QIU, Ling-Hua DING, Shi-Lang XIONG, Jing-Tang LI, Xin-Gen LIAO a Zhi-Ming TANG. Scaffolds for the repair of bone defects in clinical studies: a systematic review. *Journal of Orthopaedic Surgery and Research* [online]. 2018, **13**, 33. ISSN 1749-799X. Available at: doi:10.1186/s13018-018-0724-2

[52] QU, Huawei, Hongya FU, Zhenyu HAN a Yang SUN. Biomaterials for bone tissue engineering scaffolds: a review. *RSC Advances* [online]. 2019, **9**(45), 26252–26262. ISSN 2046-2069. Available at: doi:10.1039/C9RA05214C

[53] WANG, Minqi, Yiqi YANG, Guanghao CHI, Kai YUAN, Feng ZHOU, Liang DONG, Haibei LIU, Qinghui ZHOU, Weihua GONG, Shengbing YANG a Tingting TANG. A 3D printed Ga containing scaffold with both anti-infection and bone homeostasis-regulating properties for the treatment of infected bone defects. *Journal of Materials Chemistry B* [online]. 2021, **9**(23), 4735–4745. ISSN 2050-7518. Available at: doi:10.1039/D1TB00387A

[54] GHASSEMI, Toktam, Azadeh SHAHROODI, Mohammad H. EBRAHIMZADEH, Alireza MOUSAVIAN, Jebraeel MOVAFFAGH a Ali MORADI. Current Concepts in Scaffolding for Bone Tissue Engineering. *Archives of Bone and Joint Surgery*. 2018, **6**(2), 90–99. ISSN 2345-4644.

[55] KANIS, John A., Nicholas NORTON, Nicholas C. HARVEY, Trolle JACOBSON, Helena JOHANSSON, Mattias LORENTZON, Eugene V. MCCLOSKEY, Carl WILLERS a Fredrik BORGSTRÖM. SCOPE 2021: a new scorecard for osteoporosis in Europe. *Archives of Osteoporosis* [online]. 2021, **16**(1), 82. ISSN 1862-3522, 1862-3514. Available at: doi:10.1007/s11657-020-00871-9

[56] MELČOVÁ, Veronika, Kateřina SVORADOVÁ, Přemysl MENČÍK, Soňa KONTÁROVÁ, Michala RAMPICHOVÁ, Věra HEDVIČÁKOVÁ, Věra SOVKOVÁ, Radek PŘIKRYL a Lucy VOJTOVÁ. FDM 3D Printed Composites for Bone Tissue Engineering Based on Plasticized Poly(3-hydroxybutyrate)/poly(d,l-lactide) Blends. *Polymers* [online]. 2020, **12**(12), 2806. ISSN 2073-4360. Available at: doi:10.3390/polym12122806

[57] KONTÁROVÁ, Soňa, Radek PŘIKRYL, Veronika MELČOVÁ, Přemysl MENČÍK, Matyáš HORÁLEK, Silvestr FIGALLA, Roderik PLAVEC, Jozef FERANC, Jiří SADÍLEK a Aneta POSPÍŠILOVÁ. Printability, Mechanical and Thermal Properties of Poly(3-Hydroxybutyrate)-Poly(Lactic Acid)-Plasticizer Blends for Three-Dimensional (3D) Printing. *Materials* [online]. 2020, **13**(21), 4736. ISSN 1996-1944. Available at: doi:10.3390/ma13214736

[58] MENČÍK, Přemysl, Radek PŘIKRYL, Ivana STEHNOVÁ, Veronika MELČOVÁ, Soňa KONTÁROVÁ, Silvestr FIGALLA, Pavol ALEXY a Ján BOČKAJ. Effect of Selected Commercial Plasticizers on Mechanical, Thermal, and Morphological Properties of Poly(3-hydroxybutyrate)/Poly(lactic acid)/Plasticizer Biodegradable Blends for Three-Dimensional (3D) Print. *Materials* [online]. 2018, **11**(10), 1893. ISSN 1996-1944. Available at: doi:10.3390/ma11101893

[59] MORGAN, Elise F., Ginu U. UNNIKRISNAN a Amira I. HUSSEIN. Bone Mechanical Properties in Healthy and Diseased States. *Annual review of biomedical engineering* [online]. 2018, **20**, 119–143. ISSN 1523-9829. Available at: doi:10.1146/annurev-bioeng-062117-121139

[60] ŻENKIEWICZ, Marian. Methods for the calculation of surface free energy of solids. *Journal of Achievements in Materials and Manufacturing Engineering*. 2007, **24**.

[61] ZUBAIRI, Ts. Dr. Saiful, Alexander BISMARCK a Athanasios MANTALARIS. The Effect of Surface Heterogeneity on Wettability of Porous Three Dimensional (3-D) Scaffolds of Poly(3-Hydroxybutyric Acid) (PHB) and Poly(3-Hydroxybutyric-co-3-Hydroxyvaleric Acid) (PHBV). *Jurnal Teknologi* [online]. 2015, **75**, 305–312. Available at: doi:10.11113/jt.v75.3960

[62] MEHRABI MAZIDI, Majid, Arman EDALAT, Reyhane BERAHMAN a Fatemeh HOSSEINI. Highly-Toughened Polylactide- (PLA-) Based Ternary Blends with Significantly Enhanced Glass Transition and Melt Strength: Tailoring the Interfacial Interactions, Phase Morphology, and Performance. *Macromolecules* [online]. 2018, **51**. Available at: doi:10.1021/acs.macromol.8b00557

[63] LINS, Luanda, Valeria BUGATTI, Sébastien LIVI a Giuliana GORRASI. Ionic Liquid as Surfactant Agent of Hydrotalcite: Influence on the Final Properties of Polycaprolactone Matrix. *Polymers* [online]. 2018, **10**, 44. Available at: doi:10.3390/polym10010044

[64] KENNEDY, Scott B., Newell R. WASHBURN, Carl George SIMON a Eric J. AMIS. Combinatorial screen of the effect of surface energy on fibronectin-mediated osteoblast adhesion, spreading and proliferation. *Biomaterials* [online]. 2006, **27**(20), 3817–3824. ISSN 0142-9612. Available at: doi:10.1016/j.biomaterials.2006.02.044

7 LIST OF FIGURES

8 LIST OF TABLES

9 LIST OF ABBREVIATIONS

3HV – 3-hydroxyvalerate
ABS – acrylonitrile-butadiene-styrene
BMP – bone morphogenetic protein
CAD – computer-aided design
CIJ – continuous inkjet
CNWs – cellulose nanowhiskers
DLP – digital light projection
DOD – drop-on-demand
EBM – electron beam melting
ECM – extracellular matrix
EPG – epidermal growth factor
FDM – fused deposition modelling
FGF – fibroblast growth factor
GAG – glycosaminoglycan
HAp – hydroxyapatite
HDPE – high-density polyethylene
HDT – heat deflection/distortion temperature
IGF – insulin-like growth factor
IJ – inkjet
MSCs – mesenchymal stem cells
OCA – optical contact angle
P3HB – poly(3-hydroxybutyrate)
P4HB – poly(4-hydroxybutyrate)
PAM – pressure-assisted microsyringes
PAs – polyanhydrides
PBAT – polybutylene adipate terephthalate
PBS – polybutylene succinate
PC – polycarbonate
PCL – polycaprolactone
PDGF – platelet-derived growth factor
PDLA – poly(D-lactic acid)
PDLLA – poly(D,L-lactic acid)
PE – polyethylene
PEG – polyethylene glycol
PEO – polyethylene oxide
PETG – polyethylene terephthalate glycol
PGA – poly(glycolic acid)
PHAs – polyhydroxyalkanoates
PHB – polyhydroxybutyrate
PHBV – poly(hydroxybutyrate-co-hydroxyvalerate)
PLA – poly(lactic acid)
PLGA – poly(lactic-co-glycolic acid)
PLLA – poly(L-lactic acid)
PMMA – poly(methyl methacrylate)
PP – polypropylene
PVAc – polyvinyl acetate
PVDF – polyvinylidene fluoride
ROP – ring-opening polymerisation
SLA – stereolithography
SLS – selective laser sintering
TCP – tricalcium phosphate
TE – tissue engineering
TGF-β – transforming growth factor beta

10 APPENDICES

Report of cytotoxicity measurement – 12/21

3 types of samples were delivered from VUT, sterilized using ethylenoxide:

PHB/PCL-SF-TCP

PHB/PCL-SF

PHB-soap/PLA-SF

Contr – cells seeded on tissue culture plastic in the same density were used as a control

1. Methods

1.1 Infusion preparation

Samples were incubated in growth medium: DMEM (Sigma Aldrich) supplemented with 10 % of foetal bovine serum and 1 % of antibiotics (Penicilin/Streptomycin) at 37 °C for 48 hod, 250 µl/sample.

1.2 Cell seeding and culture

3T3 mice fibroblasts were seeded in density 2×10^3 cells per well of 96-well plate in growth medium. After 24 hours, 250 µl of extract was added. Cells were cultured in extracts for 24 and 72 hours at 37 °C and 10 % CO_2.

1.3 Visualization of cells using optical microscopy

Cells cultured in extracts were visualized using optical microscopy 24 and 72 hours after seeding (microscope Olympus IX51, camera Olympus DP80).

1.4 Measurement of metabolic activity

MTS assay (CellTiter 96® AQueous One Solution Cell Proliferation Assay; Promega) was used to probe cell metabolic activity. Cells were incubated in MTS solution (20 µL) and 100 µL of the fresh culture medium at 37 °C for 2 hours. The MTS substrate is metabolized by mitochondrial enzymes to violet formazan, which absorbs light at 490 nm. The absorbance of the solution (100 µL) was read in clean microplates using microplate reader (Infinite M200 PRO, Tecan, Switzerland) at 490 nm and reference wavelength 690 nm. The absorbance of the pure medium with MTS substrate was subtracted from the values.

1.5 Analysis of cell proliferation

Quantification of DNA was used to determine cellular proliferation. The cells were analyzed using Quant-iT™ dsDNA Assay Kit (Life Technologies). 100 µl of lysis buffer (0.2 % v/v Triton X-100, 10 mM Tris (pH 7.0), and 1 mM EDTA) was added to cells after MTS assay and lysed by freeze-thawing (3 cycles with rough vortexing). For analysis, 10 µL of cell lysate from samples was added to 200 µL of reagent solution, which binds to double strand DNA of cells and emit florescent signal. The fluorescence intensity was recorded on multimode fluorescence reader (Infinite M200 PRO, Tecan, Switzerland; λ_{ex} = 485 nm, λ_{em} = 523 nm). Results were evaluated using the calibration curve of the standards in the kit.

1.6 Statistics

MTS assay and DNA quantification were performed on 6 independently prepared samples. Because of the variability of the measured results, margin values were not included. Nevertheless, at least 4 samples were used for the statistic evaluation. Quantitative data are presented as mean values ± standard deviation (SD). Results were evaluated statistically using SigmaStat 12.0, Systat. If the data passed the normality test and the test of equality of variances, statistical significance between a pair of groups was determined by ANOVA test and Student-Newman-Keuls test for post-hoc analysis. If the data were without normal distribution, statistical significance between a pair of groups was determined using Kruskal-Wallis One Way Analysis of Variance on Ranks and Dunn's multiple comparisons test for post hoc analysis. All results were considered statistically significant if p was <0.05.

2. Results

2.1 Cell visualization using optical microscopy

The cells of control group cultured in normal medium were in good condition and their amount was increasing till day 3 (Fig. 1). Similar result was shown for group PHB/PCL-SF. Although some of the cells in this group were more rounded 24 hours after seeding, their number increased and they spread on the surface of the well on day 3. Similarly, morphology of the most of the cells in group PHB/PCL-SF-TCP was fine, but the proliferation rate was slow. On the other hand, cells in group PHB-soap/PLA-SF showed rounded apoptotic morphology and their number stagnated.

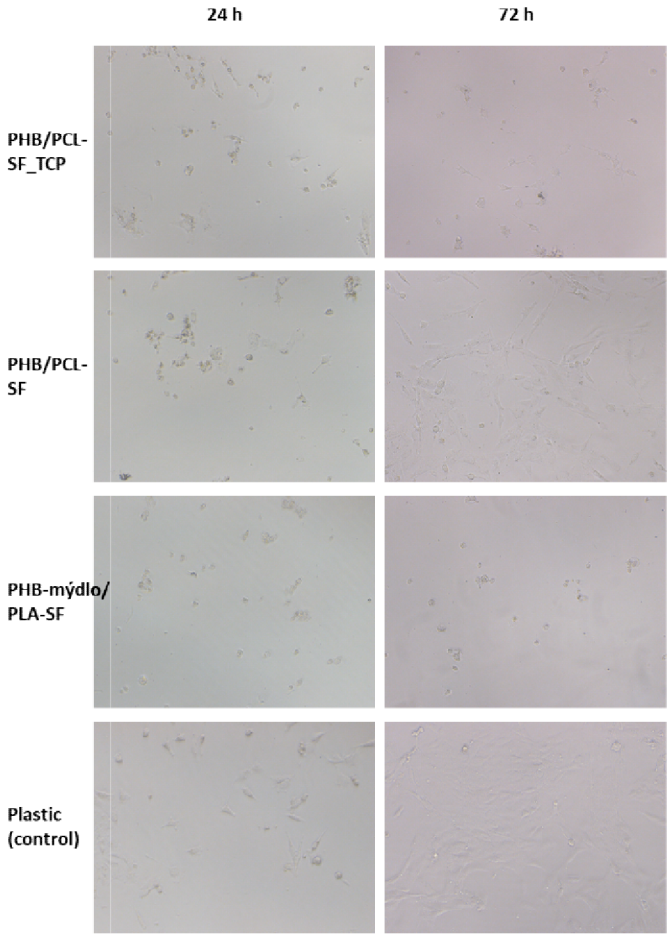

Fig. 1: *Optical microscopy of cells cultured in extracts. Magnification 100 ×.*

2.2 Measurement of metabolic activity

The cell metabolic activity was measured using MTS test 24 and 72 hours after adding of the extracts (Fig. 2). The highest absorbance was measured in control group 24 hours after seeding. The lowest value was measured for group PHB-soap/PLA-SF. Metabolic activity increased in group PHB/PCL-SF and was statistically comparable with the control on day 3. Metabolic activity of cells in group PHB/PCL-SF-TCP was low and negligible in group PHB-soap/PLA-SF on day 3.

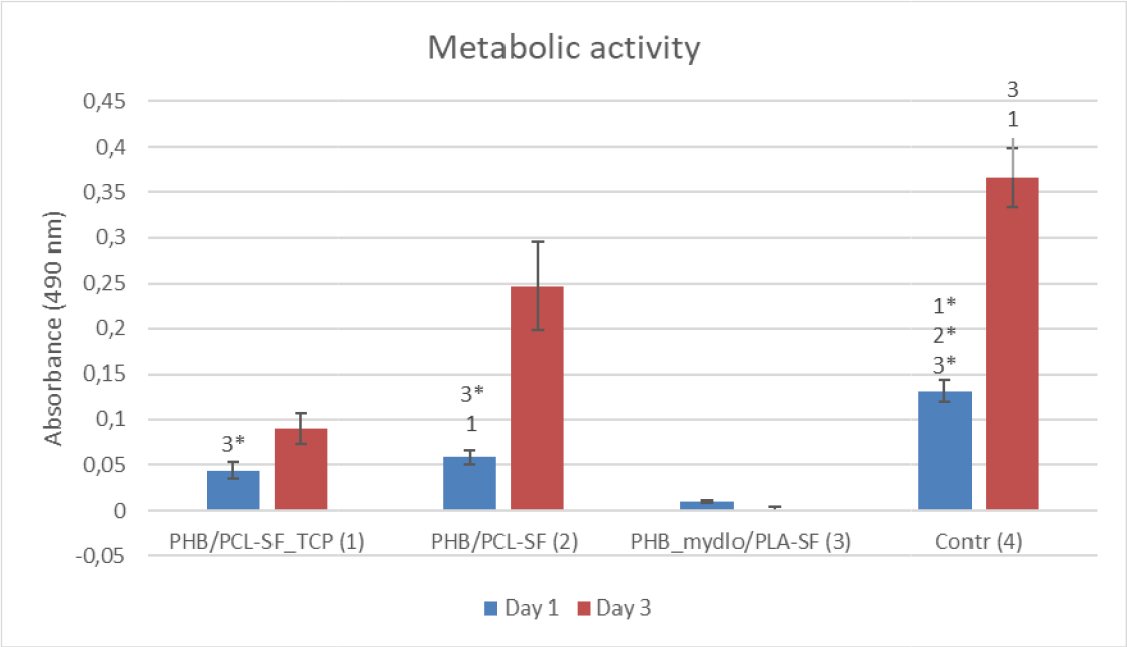

Fig. 2: *Metabolic activity of 3T3 fibroblasts cultured in extracts measured using MTS test 24 and 72 hours after seeding. 3T3 fibroblasts cultured in growth medium were used as a control (Contr). The numbers above the columns sign statistical significance ($p<0,05$, *$p<0,001$).*

2.3 Measurement of cell proliferation using DNA quantification

The cell proliferation was measured using DNA quantification (Fig. 3). The lowest number of cells was shown in group PHB-soap/PLA-SF 24 hours after adding of the extract. Cell number in group PHB/PCL-SF was comparable with the control on day 3. The results of the assay were influenced by high variance in measured values and high standard deviations.

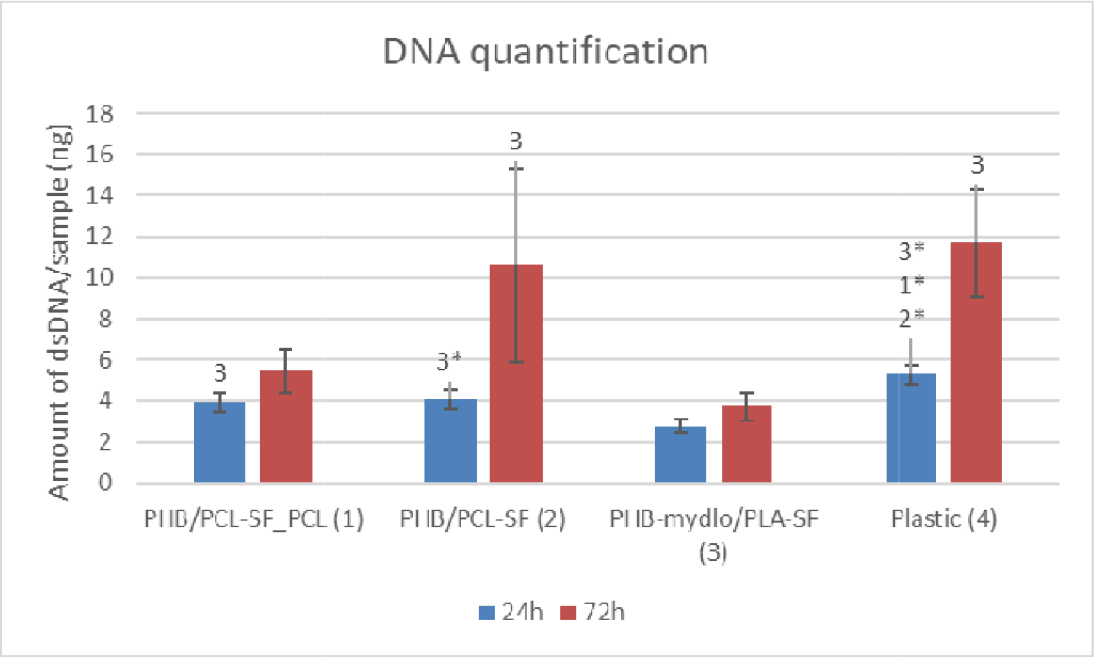

Fig. 3: *Cell proliferation was measured using dsDNA quantification. Numbers above the columns sign statistical significance ($p<0,05$, $*p<0,001$).*

Conclusion

Sample PHB/PCL-SF was found to be biocompatible. The samples PHB/PCL-SF-TCP and PHB-soap/PLA-SF are cytotoxic.

Evaluation of cell adhesion on different surfaces

10 samples with 5 different surface morphologies from 2 different materials sterilized using ethylene oxide were delivered from VUT. Samples were seeded with Saos-2 osteosarcoma cell line. Metabolic activity and cell proliferation were measured. Cells adhesion on scaffolds was visualized using confocal microscopy.

Tested samples:

1 – 2.1 Placka	6 – 2.4 Placka
2 – 2.1 0 µm oko	7 – 2.4 0 µm oko
3 – 2.1 50 µm oko	8 – 2.4 50 µm oko
4 – 2.1 150 µm oko	9 – 2.4 150 µm oko
5 – 2.1 250 µm oko	10 – 2.4 250 µm oko

11 – Contr: Saos-2 cells seeded on tissue culture plastic were used as a control (It serves as a control of cells condition. Tissue culture plastic is optimized for cell adhesion and growth, so, it is normal, when values measured on samples are the same, or lower). 2.1 = PHB/PLA-SF_2020, 2.4 = PHB/PLA-SF-TCP_2020

1. Methods

1.1 Scaffold seeding

Scaffolds with diameter of 6 mm in 96-well plates were seeded with Saos-2 cells. Cells were seeded with 5×10^3 in 20 µL of the culture medium (McCoy's Medium enriched by 15 % of fetal bovine serum and 1 % of antibiotics (100 U/mL penicillin and 100 µg/mL streptomycin). After 2-hours adhesion of cells, 230 µl of medium was added. This procedure was used to increase the efficiency of the cell adhesion. The low cell seeding density was used because of better visualization of cells adhesion by confocal microscopy. Cell-seeded scaffolds were cultured in humidified incubator at 5 % of CO_2 and 37 °C.

1.2 Cell viability analysis

MTS assay (CellTiter 96® AQueous One Solution Cell Proliferation Assay; Promega) was used to probe cell metabolic activity. Samples were transferred to clean 96-wells to avoid measurement of cells growing on the bottom of the well. MTS solution (20 µL) and 100 µL of the fresh medium was added to the wells with scaffolds or with the control cells seeded on the bottom of the well. The microplate was incubated at 37 °C for 2 hours. The MTS substrate is metabolized by mitochondrial enzymes to violet formazan, which absorbs light at 490 nm. The absorbance of the solution (100 µL) was read in clean microplates using microplate reader (Infinite M200 PRO, Tecan, Switzerland) at 490 nm and reference wavelength 690 nm. The absorbance of scaffold without cells incubated with MTS substrate was subtracted from the values.

1.3 Analysis of cell proliferation

Quantification of DNA was used to determine of cellular proliferation. The samples were analyzed using Quant-iT™ dsDNA Assay Kit (Life Technologies). The scaffolds after MTS measurement were put in 200 µL of cell lysis solution (0.2 % v/v Triton X-100, 10 mM Tris (pH 7.0), and 1 mM EDTA) and lysed by freeze-thawing (3 cycles with rough vortexing). For analysis, 20 µL of cell lysate from samples was added to 200 µL of reagent solution, which is bind to double strand DNA of cells and emit florescence signal. The fluorescence intensity was recorded on multimode fluorescence reader (Infinite M200 PRO, Tecan, Switzerland; λ_{ex} = 485 nm, λ_{em} = 523 nm). The florescence of the scaffolds incubated without cells was subtracted from the measured values. Results were evaluated using the calibration curve of the standards in the kit.

1.4 Statistics

MTS assay and DNA quantification were performed on 6 independently prepared samples. Because of the variability of the measured results, margin values were not included. Nevertheless, at least 4 samples were used for the statistic evaluation. Quantitative data are presented as mean values ± standard deviation (SD). Results were evaluated statistically using SigmaStat 12.0, Systat. If the data passed the normality test and the test of equality of variances, statistical significance between a pair of groups was determined by ANOVA test and Tukey's comparative test for post-hoc analysis. If the data were without normal distribution, statistical significance between a pair of groups was determined using Kruskal-Wallis One Way Analysis of Variance on Ranks and Dunn's multiple comparisons test for post hoc analysis. All results were considered statistically significant if p was <0.05.

2. Results

We used low cell seeding density because of visualization of cell adhesion on scaffolds using confocal microscopy. Independently adhered cells are necessary for visualization of focal adhesions.

2.1 Measurement of metabolic activity

The metabolic activity of cells on all tested samples was very low (Fig. 1). The values even decrease on day 3. There were no statistical differences between the samples. It suggests cytotoxicity of the samples.

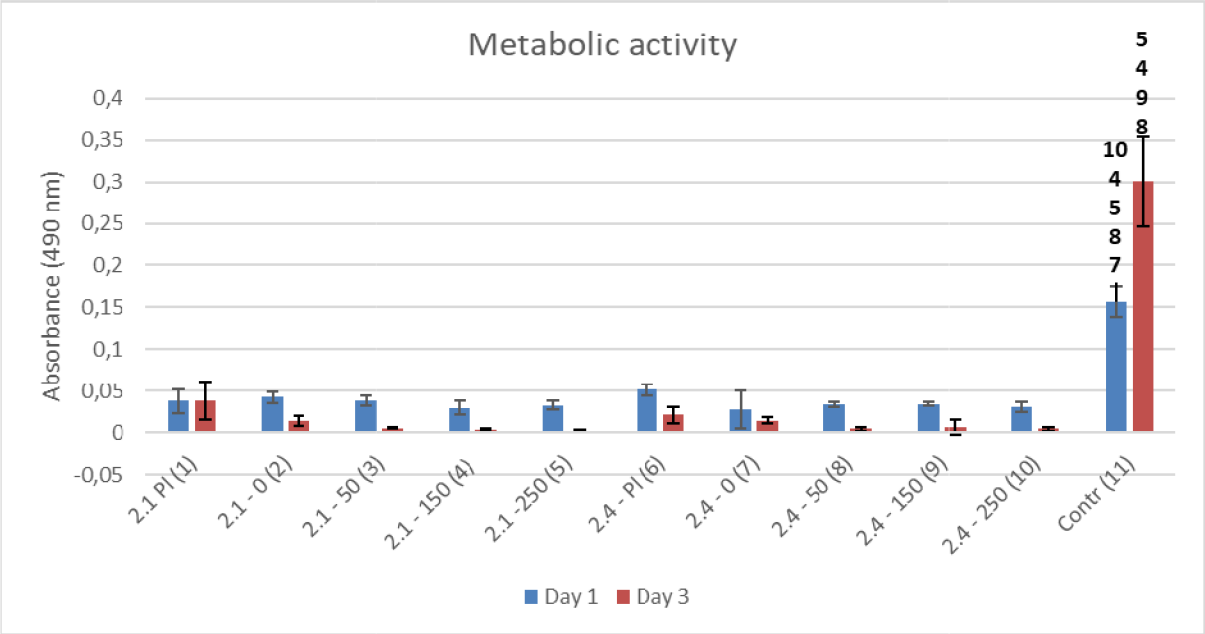

Fig. 1: *Metabolic activity of the cells cultured on samples measured using MTS analysis. Saos-2 cells cultured on tissue culture plastic were used as a control (Contr). Numbers above the columns sign statistical significance $p<0.05$.*

2.2 Measurement of cell proliferation using DNA quantification

The cell proliferation was measured using DNA quantification (Fig.2). The measured cell adhesion was low on all samples. The lowest cell number was detected on sample 6 on day 1. There were no statistical differences between the samples on day 3. Interestingly, the cell number was low even on control, where high metabolic activity was measured. The reason may lie in insufficient lysis of cells cultured on tissue cultured plastic. The method of lysis was different from samples.

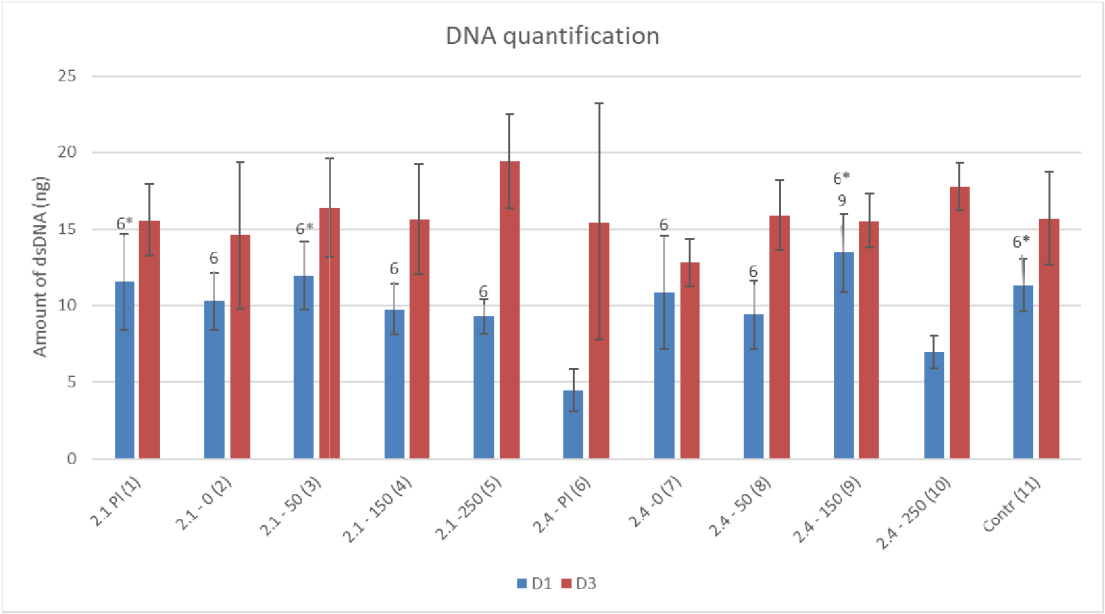

Fig. 2: *Cell proliferation was measured using DNA quantification. Numbers above the columns sign statistical significance, black numbers - $p<0.05$, red numbers – $p<0.001$.*

2.3 Visualization of cell distribution on scaffolds

Day 1

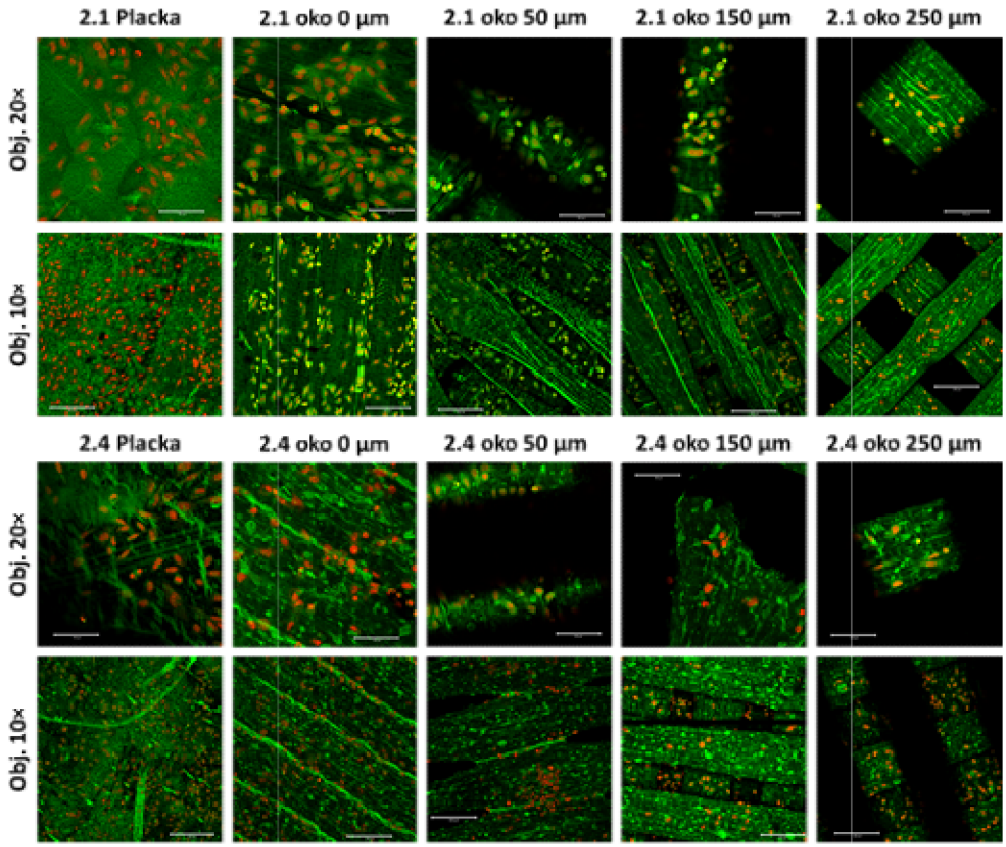

Day 3

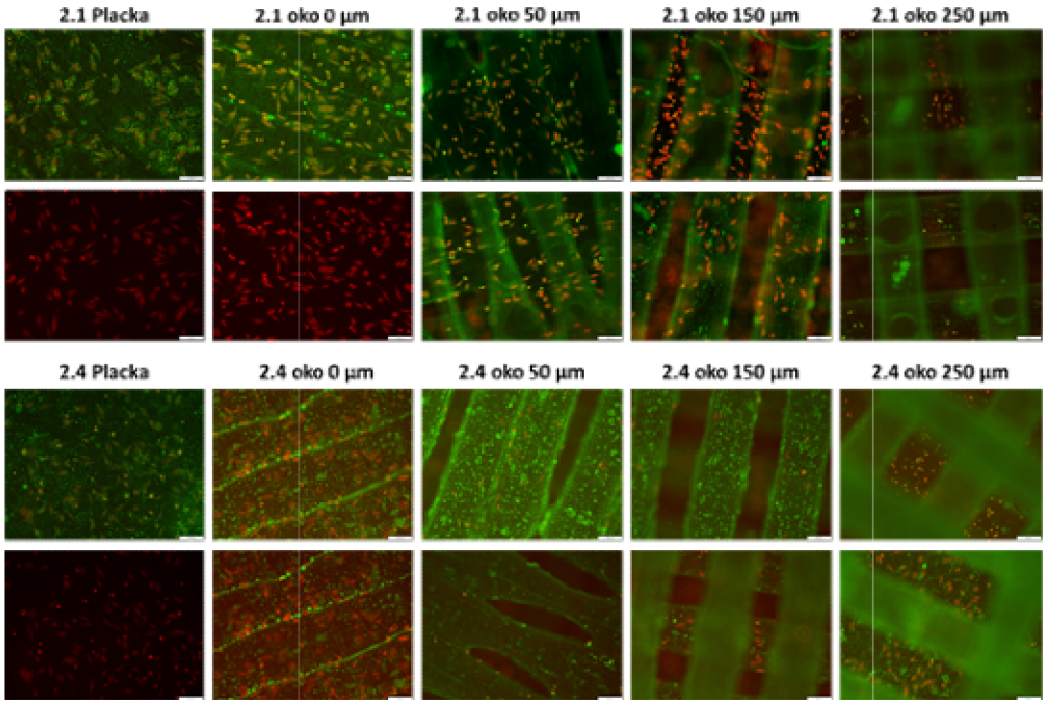

Conclusion

The metabolic activity assay shows very low values, what means that samples are cytotoxic. The values measured using DNA quantification were low and did not show any differences between the samples and the control. The reason can be insufficient lysis of control cells cultured on tissue cultured plastic. Moreover, the assay detects dsDNA, which is stable in solution for some days. It means that even apoptotic cells can be included.

Report of cytotoxicity measurement – 4/22

15 types of samples were delivered from VUT in the end of March, sterilized using ethylenoxide:

1. PHB/PCL-SF_NOVÉ
2. PHB/PCL-SF_STARÉ
3. PHB/PCL-SF/TCP_NOVÉ
4. PHB/PCL-SF/TCP_STARÉ
5. PHB-mýdlo_NOVÉ
6. PHB-mýdlo_STARÉ
7. RP7_BIOMASA
8. 2.1 STARÉ
9. 2.1 REF
10. 2.4 STARÉ
11. 2.4 REF

12/30 PHB/2394_PRÁŠEK
13/30 PHB/MÝDLO/PRÁŠEK
14/30 TCP NOVÉ_PRÁŠEK
15/30 TCP STARÉ_PRÁŠEK
12/100 PHB/2394_PRÁŠEK
13/100 PHB/MÝDLO/PRÁŠEK
14/100 TCP NOVÉ_PRÁŠEK
15/100 TCP STARÉ_PRÁŠEK
Control – cells seeded on tissue culture plastic in the same density were used as a control

1. Methods

1.1 Infusion preparation

Samples were incubated in culture medium: DMEM (Sigma Aldrich) supplemented with 10 % of fetal bovine serum and 1 % of antibiotics (Penicilin/Streptomycin) at 10 % CO_2, 37 °C for 48 hod, 250 µL/sample, in the case of powder it was either 30 mg or 100 mg of the powder /250 µL of culture medium. The powder samples were centrifuged after incubation at 2200 rpm for 5 min.

1.2 Cell seeding and culture

3T3 mice fibroblasts were seeded in the density 5×10^3 cells per well of 96-well plate in culture medium. After 24 hours, 200 µL of extract of the groups 1-11, 14/30, 15/30 and control. In the groups 12, 13, 14 and 15 there were not enough powder to prepare extract of concentration 100 mg/250 µl. For that reason, lower amount of extract was added. 120 µL of extract was added for the group 14/100 and 160 µL of extract for the groups 13/30 and 15/100. In the group 12, there was not enough powder to prepare extract of concentration 100 µg/250 µl. Group 13/100 – the extract contained the powder. The extract from solid samples was possible to aspirate without spinning. Extracts from powders was possible to aspirate after centrifugation (2200 rpm, 5 min). Cells were cultured in extracts for 24 and 72 hours at 37 °C and 10 % CO_2.

1.3 Visualization of cells using optical microscopy

Cells cultured in extracts were visualized using optical microscopy 24 and 72 hours after seeding (microscope Olympus IX73, camera Olympus DP80).

1.4 Measurement of metabolic activity

MTS assay (CellTiter 96® AQueous One Solution Cell Proliferation Assay; Promega) was used to probe cell metabolic activity. Cells were incubated in MTS solution (20 μL) and 100 μL of the fresh culture medium at 37 °C for 2 hours. The MTS substrate is metabolized by mitochondrial enzymes to violet formazan, which absorbs light at 490 nm. The absorbance of the solution (100 μL) was read in clean microplates using microplate reader (Infinite M200 PRO, Tecan, Switzerland) at 490 nm and reference wavelength 690 nm. The absorbance of the pure medium with MTS substrate was subtracted from the values.

1.5 Statistics

MTS assay and DNA quantification were performed on 6 independently prepared samples. Because of the variability of the measured results, margin values were not included. Nevertheless, at least 4 samples were used for the statistic evaluation. Quantitative data are presented as mean values ± standard deviation (SD). Results were evaluated statistically using SigmaStat 12.0, Systat. If the data passed the normality test and the test of equality of variances, statistical significance between a pair of groups was determined by ANOVA test and Student-Newman-Keuls test for post-hoc analysis. If the data were without normal distribution, statistical significance between a pair of groups was determined using Kruskal-Wallis One Way Analysis of Variance on Ranks and Dunn's multiple comparisons test for post hoc analysis. All results were considered statistically significant if p was <0.05.

2. Results:

Samples 4, 5 and 8 had slightly lower pH noticed when extracts were added to the cells.

2.1 Cell visualization using optical microscopy

The cells of control group cultured in normal medium were in good condition and their amount was increasing till day 3 (Fig. 1). Cells cultured in extracts of groups 1, 2, 3, 4, 7, 8, 9, 10, and 11 showed good cell morphology and formed confluent layer after 72-hour cultivation. The lower amount of cells compared to these groups was visible in group 5. The cells cultured in extracts of group 6 underwent apoptosis. Cytotoxic effect of the extracts was visible for groups 12 and 13. The cell cultured in extract of group 14 did not proliferate, but showed good cell morphology. The extracts of the group 15 were not cytotoxic even for concentration 100 mg/250 μL of culture medium.

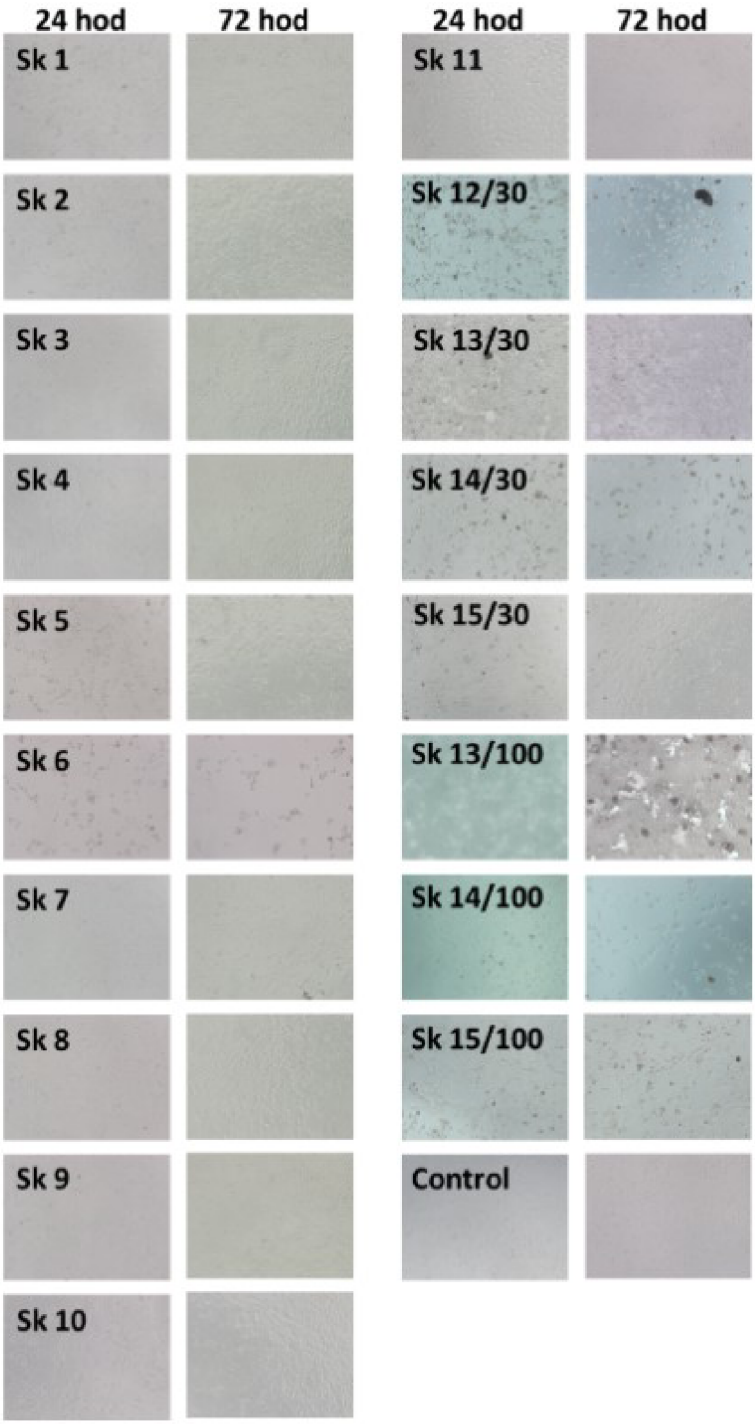

Fig. 1: *Optical microscopy of cells cultured in extracts for 24 and 72 hours. Magnification 100 ×.*

2.2 Measurement of metabolic activity

The cell metabolic activity was measured using MTS test 24 and 72 hours after adding of the extracts (Fig. 2). Cell metabolic activity was similar on all tested groups, including control, except groups 12/300, 13/30 and 13/100. Lower metabolic activity was also detected on group 6 but without statistical significance. 72 hours after seeding was visible lower metabolic activity also on groups 6, 14/30 and 14/100. The results correspond well with the optical microscopy visualization.

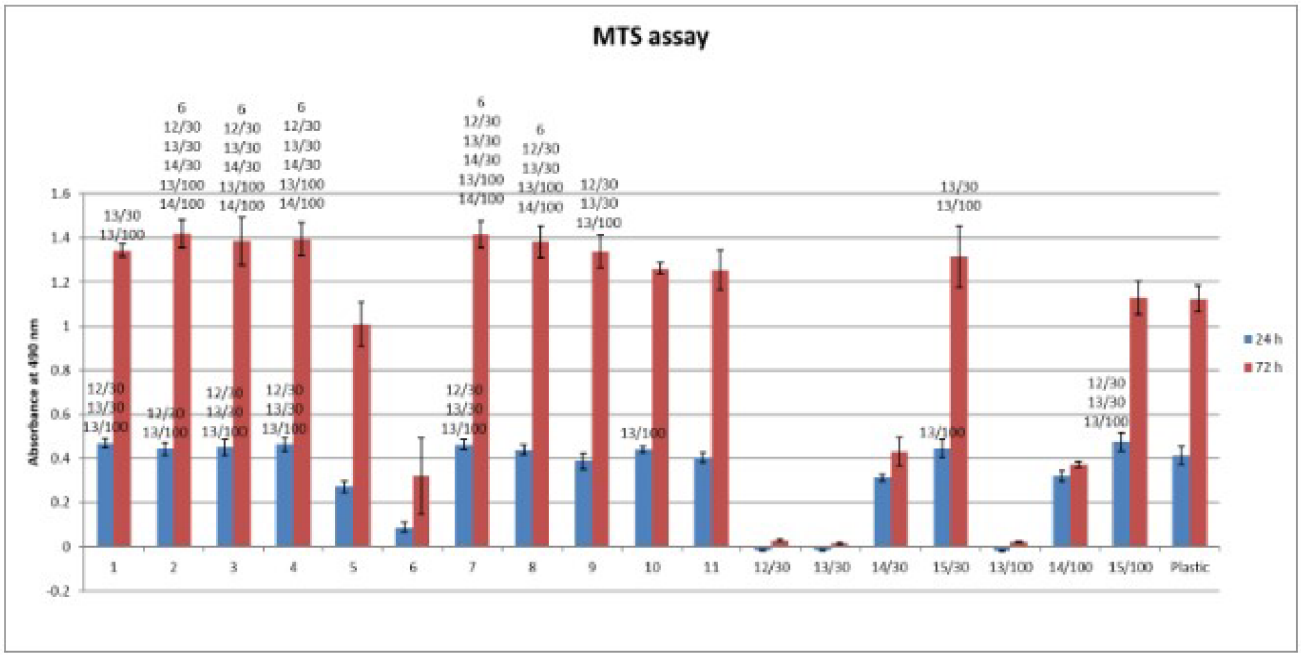

Fig. 2: *Metabolic activity of 3T3 fibroblasts cultured in extracts measured using MTS test 24 and 72 hours after seeding. 3T3 fibroblasts cultured in growth medium were used as a control (Contr). The numbers above the columns sign statistical significance ($p<0,05$).*

Conclusion

Most of the solid samples were fully biocompatible. The sample 6 was shown to be cytotoxic (PHB-mýdlo_STARÉ). The extracts from the powder 12, 13 and 14 was cytotoxic (PHB/2394_PRÁŠEK, PHB/MÝDLO/PRÁŠEK, TCP NOVÉ_PRÁŠEK). The powder 15 (TCP STARÉ_PRÁŠEK) was biocompatible even in concentration 100 mg/ 250 µl of medium.